



STRUCTURAL ANALYSIS OF A KINETIC STEEL SCULPTURE

Lappeenranta–Lahti University of Technology LUT

Master's Programme in Mechanical Engineering

2022

Mikael Ekholm

Examiner(s): Prof. Timo Björk

D.Sc. (Tech.) Antti Ahola

M.Sc. (Tech) Petja Lindström

ABSTRACT

Lappeenranta–Lahti University of Technology LUT

LUT School of Energy Systems

Mechanical Engineering

Mikael Ekholm

Structural analysis of a kinetic steel sculpture

Master's thesis

2022

116 pages, 121 figures, 24 tables and 8 appendices

Examiner(s): Prof. Timo Björk

M.Sc. (Tech) Petja Lindström

Keywords: sculpture, structural analysis, fatigue, Hot Spot, Eurocode 1, Eurocode 3

In this master's thesis the structural analysis of a kinetic steel sculpture is performed. The sculpture will be built into the new residential area called Asemanranta in Hämeenlinna. Sculpture consists of a ring with a diameter of 6.8 m which is supported by posts made of steel. The ring is attached to the posts with the shafts and when the sculpture is operating the ring is rotating around 1.4 revolutions per minute.

The structural analysis is performed by using FE-analysis, Hot Spot -method and guidelines of the Eurocode. All dimensioning and load determinations are performed according to SFS-EN 1991 and SFS-EN 1993.

The main goal of the master's thesis is to make sure that the sculpture can carry its self-weight and it can operate in circumstances it has been designed to. Determined circumstances take into account local wind, snow, and thermal loads that may lead to the yielding, unstableness or vibrating of structural members. Fatigue assessment is also performed to ensure that sculpture could operate the designed lifetime in normal predictable conditions.

The result of the analysis is that the sculpture fulfils the specified requirements, and the structure can resist all predictable load cases that may occur during its lifetime.

TIIVISTELMÄ

Lappeenrannan–Lahden teknillinen yliopisto LUT

LUT Energiajärjestelmät

Konetekniikka

Mikael Ekholm

Liikkuvan teräsveistoksen rakenneanalyysi

Konetekniikan diplomityö

2022

116 sivua, 121 kuvaa, 24 taulukkoa ja 8 liitettä

Tarkastaja(t): Prof. Timo Björk

DI Petja Lindström

Avainsanat: teräsveistos, rakenneanalyysi, väsyminen, Hot Spot, Eurokoodi 1, Eurokoodi 3

Tässä diplomityössä tutkitaan liikkuvan teräsveistoksen rakenteellista kestävyyttä. Teräsveistos tullaan sijoittamaan uudelle asuinalueelle nimeltään Asemanranta, joka sijaitsee Hämeenlinnassa. Teräsveistos koostuu halkaisijaltaan 6,8 metrin kehästä, joka on tuettu teräspilareilla. Kehä on liitetty pilareihin akseleilla ja teräsveistoksen ollessa toiminnassa, kehä pyörii akseleiden ympäri noin 1,4 kierrosta minuutissa.

Rakenneanalyysi suoritetaan käyttämällä FE-analyysiä, Hot Spot -menetelmää ja Eurokoodin ohjeistuksia. Kaikki mitoitukset ja kuormitusten määrittämiset tehdään standardien SFS-EN 1991 ja SFS-EN 1993 vaatimusten mukaisesti.

Diplomityön päätavoite on varmistaa, että teräsveistos kykenee kannattelemaan oman painonsa ja, että se kykenee toimimaan olosuhteissa, joihin se on suunniteltu. Määritetyt olosuhteet ottavat huomioon tuuli-, lumi- ja lämpötilakuormat, jotka voivat johtaa rakenneosien myötäämiseen, epästabiiliuuteen tai värähtelyyn. Rakenteelle suoritetaan myös väsymistarkastelu, jotta voidaan varmistaa, että teräsveistos kykenee toimimaan suunnitellun toiminta-ajan normaaleissa ennustettavissa olosuhteissa.

Rakenneanalyysin tuloksena voidaan todeta, että teräsveistos täyttää sille annetut vaatimukset ja veistos kestää kaikki ennustettavat kuormitustilanteet, jotka voivat ilmetä sen toiminta-ajan aikana.

ALKUSANAT

Haluan kiittää Hefmec Engineering Oy:tä loistavan diplomityöaiheen tarjoamisesta sekä ohjauksesta ja tuesta koko diplomityöprosessin aikana. Ilman jatkuvaa tukea (ja painostusta) diplomityön valmistuminen olisi varmasti venynyt hyvinkin pitkälle tulevaisuuteen, sillä pakottavaa tarvetta valmistumiselle ei tämän diplomityön tekoaikaan varsinaisesti ollut. Diplomityön tekemiseen annettu tuki on kuitenkin vain pieni osa niistä eväistä, jotka olen Hefmeciltä saanut suunnittelijan työurani aloitukseen, ja siitä haluankin antaa erityiskiitoksen koko Hefmecin työyhteisölle.

Haluan kiittää myös LUT-yliopistoa, TkT Antti Aholaa ja Prof. Timo Björkiä sekä totta kai muuta henkilökuntaa kattavasta ja riittävän syvällisestä teräsrakennesuunnitteluun liittyvästä opetuksesta. Monet syväluotaavat detaljit saattoivat tuntua opintojen aikana turhalta työelämän kannalta, mutta niin vain niihin törmäsi jo ensimmäisen työvuoden aikana. Tästä hauskana esimerkkinä lujuusopin laminaattirakenteet ja eri aineista yhdistetyt palkit.

Erityiskiitokset annan Koneenrakennuskilta ry:lle loistavista tapahtumista sekä muille läheisille kiltalaisille ja etenkin *pojat-pilalla* -porukalle, joiden kanssa koettiin vauhdikkaita hetkiä, niin opintojen kuin vapaa-ajankin merkeissä.

Mikael Ekholm

Riihimäellä 2.8.2022

SYMBOLS AND ABBREVIATIONS

A	Altitude above Sea Level	[m]
a	Throat thickness of the weld	[mm]
a_G	Factor of galloping instability	
A_{ref}	Reference area of the structure or structural element	[m ²]
A_s	Tensile stress area of a bolt	[mm ²]
A_{SL}	Total area where the snow load is affected	[m ²]
$A_{ }$	Total area of the surfaces parallel to wind direction	[m ²]
A_{\perp}	Total area of the surfaces perpendicular to wind direction	[m ²]
b	Reference width of the cross-section where the vortex shedding occurs	[m]
$B_{p,Rd}$	Design punching shear resistance at ultimate limit state	[N]
c_0	Terrain orography factor	
c_{dir}	Directional factor	
C_e	Exposure coefficient	
c_f	Force coefficient for the specific structure or structural element	
c_{lat}	Lateral force coefficient	
$c_{lat,0}$	Basic lateral force coefficient	
$c_{lat,single}$	Lateral force coefficient for a single structural element	
$c_s c_d$	Structural factor	
c_{season}	Season factor	
C_t	Thermal coefficient	

d	Inwind depth that is measured perpendicularly between plate and torsional axis	[m]
d_o	Nominal diameter of the ring	[m]
d_2	Pitch diameter of a bolt	[mm]
D_{km}	Diameter of contact area between head and plate	[mm]
d_m	Bolt head diameter	[mm]
d_{ring}	Diameter of ring	[m]
FAT	Fatigue class according to SFS-EN 1993-1-9	[MPa]
$F_{b,Rd}$	Design bearing resistance at ultimate limit state	[N]
$F_{p,C}$	Preloading force	[N]
F_R	Resultant force applied to the weld	[N]
F_{SL}	Total snow load force	[N]
$F_{s,Rd,ser}$	Design slip resistance of the bolted joint at serviceability state	[N]
$F_{t,Ed}$	Design tensile force at ultimate limit state	[N]
$F_{t,Rd}$	Design tensile resistance at ultimate limit state	[N]
f_u	Ultimate tensile strength of the weakest part joined	[MPa]
f_{ub}	Ultimate strength of a bolt	[MPa]
$F_{v,Ed}$	Design shear force at ultimate limit state	[N]
$F_{v,Ed,ser}$	Design shear force at serviceability state	[N]
$F_{v,Rd}$	Design shear resistance at ultimate limit state	[N]
F_w	Resultant wind force	[N]
$F_w(s)$	Load caused by vortex shedding	[N]
$F_{w,Ed}$	Design value for the force per unit length applied to a weld	[N]
$F_{w,Rd}$	Design weld resistance per unit length	[N/mm]

h	Height of the structural element	[m]
I_v	Wind turbulence intensity	
K	Mode shape factor	
k_2	Factor that is depending on the shape of the bolt	
k_1	Turbulence factor	
k_r	Terrain factor	
k_s	Factor for slip resistance of bolted joint	
K_w	Effective correlation length factor	
l	Length or height of the structure or structural element	[m]
l_w	Length of a weld	[mm]
m	Factor for fatigue analyses	
M_B	Torque that is loading the mounting bracket of the electric motor	[Nm]
$m(s)$	Vibrating mass per unit length	[kg/m]
$m_{i,e}$	Equivalent mass of the fundamental mode per unit length	[kg/m]
m_{total}	Total mass of structure or structural element	[kg]
n	Number of friction surfaces	
N	Fatigue life obtained by using Hot Spot -method	
$n_{1,y}$	First cross-wind mode frequency of structure	[Hz]
$n_{i,y}$	Natural frequency of the structure	[Hz]
N_R	Number of cycles	
P	Pitch of thread	[mm]
$q_p(z_e)$	Peak velocity pressure at reference height z_e	[N/m ²]
Re	Reynolds number	
s	Snow load in persistent or transient circumstances	[N/m ²]

Sc	Scruton number	
s_k	Characteristic value of the snow load on the ground	[N/m ²]
St	Strouhal number of the structural element	
T	Lifetime of structure in seconds	[s]
t_p	Thickness of plate in a bolted joint	[mm]
ν	Kinematic viscosity of the air	[m ² /s]
ν_0	$\sqrt{2}$ times modal value of the Weibull distributed wind velocity	[m/s]
ν_b	Basic wind velocity	[m/s]
$\nu_{b,0}$	Fundamental value for the basic wind	[m/s]
ν_{CG}	Critical galloping wind velocity	[m/s]
$\nu_{crit,I}$	Critical wind velocity for vibration mode i	[m/s]
$y_{F,max}$	Maximum displacement over time of the point where the mode	[m]
ν_m	Mean wind velocity	[m/s]
Z	Zone number for snow load	
z_0	Roughness length	[m]
$z_{0,II}$	Roughness factor for terrain category II	[m]
z_e	Reference height	[m]
z_g	Height from the ground	[m]
α_{st}	Linear expansion coefficient of steel	
α_v	Factor that depends on the strength class of a bolt	
β_w	Correlation factor	
γ_{M2}	Partial safety factor	
γ_{M3}	Partial safety factor	
$\gamma_{M3,ser}$	Partial safety factor	

ΔT	Temperature change	[K]
$\Delta \tau_R$	Shear stress range	[MPa]
$\Delta \tau_C$	Shear fatigue class	[MPa]
$\Delta \tau_L$	Cut off limit	[MPa]
δ_s	Structural damping as the logarithmic decrement	
ε_0	Bandwidth factor	
ζ	Factor for specific structural element	
λ	Factor for correlation length calculations	
μ	Slip factor	
μ_G	Friction coefficient of threads	
μ_i	Snow load shape coefficient	
μ_K	Friction coefficient of bolt's head	
ρ	Air density	[kg/m ³]
$\sigma_{0,4t}$	Nodal stress at distance of 0,4 times plate thickness from weld toe	[MPa]
$\sigma_{1,0t}$	Nodal stress at distance of 1,0 times plate thickness from weld toe	[MPa]
σ_b	Bending stress	[MPa]
σ_{hs}	Hot Spot -stress (structural stress)	[MPa]
σ_m	Membrane stress	[MPa]
σ_s	Structural stress	[MPa]
$\Phi_{i,y}$	Mode shape of the structural element	

Abbreviations

HS-method Hot Spot -method, structural stress method

VIV Vortex induced vibration

Table of contents

Abstract

Acknowledgements

Symbols and abbreviations

1	Introduction	10
1.1	Daily Mirror -kinetic steel sculpture	10
1.2	Objectives.....	13
2	Load conditions	14
2.1	Wind load	14
2.1.1	Wind force	14
2.1.2	Friction force.....	19
2.1.3	Vortex shedding.....	21
2.1.4	Galloping	29
2.1.5	Divergence and flutter	29
2.2	Snow load.....	30
2.3	Thermal load	34
3	Theory and research methods.....	37
3.1	Hot Spot -method (structural stress)	37
3.2	Static analysis.....	41
3.3	Natural frequency and vibration.....	53
3.4	Fatigue analysis.....	55
3.5	Bolted joints	62
3.5.1	Static capacity	62
3.5.2	Tightening torque.....	68
3.5.3	Fatigue of bolts	68
3.6	Welds.....	69
4	Results	72
4.1	Static analysis.....	72
4.2	Natural frequency and vibration.....	89

4.3	Fatigue.....	92
4.4	Bolted joints	105
4.4.1	Static capacity	105
4.4.2	Preload force and tightening torque.....	107
4.4.3	Shear fatigue of bolts	107
4.5	Welds.....	108
5	Conclusions	109
5.1	Further research.....	114
	References.....	115

Appendices

Appendix 1. Wind load calculations

Appendix 2. Snow load calculations

Appendix 3. Thermal action calculations

Appendix 4. Analytical calculations for bolt forces

Appendix 5. Bolt forces determined by FE-analysis (23 m/s storm wind)

Appendix 6. Fatigue assessment for the most critical welded joints

Appendix 7. Shear fatigue of bolts

Appendix 8. Design forces and resistances of welds

1 Introduction

In this master's thesis the structural analysis of Daily Mirror -kinetic steel sculpture will be carried out. The project is performed in cooperation of Hefmec Engineering Oy, artist Johanna Rope and city of Hämeenlinna. The main goal of the study is to determine required structural members, joints and optimize the structure so that it doesn't lose its stability in any excepted situation. Eurocodes 1 and 3 are utilized to examine requirements that are set for outdoor constructions and the structure is analysed in respect of these requirements. These requirements are for example snow loads, wind actions and natural frequency aspects.

1.1 Daily Mirror -kinetic steel sculpture

Daily mirror is a kinetic steel sculpture that will be built to the city of Hämeenlinna. It will be located in a new residential area called Asemanranta and the general shape is designed by artist Johanna Rope. Hefmec Engineering Oy is taking care of mechanical design and structural analysis.

The Daily Mirror sculpture consists of two posts that are bolted to the concrete foundation and between the posts there is 6.8 meters wide ring that is rotating around. The motion is created with an electrical motor. The basic operation of the sculpture is presented in Figure 1.

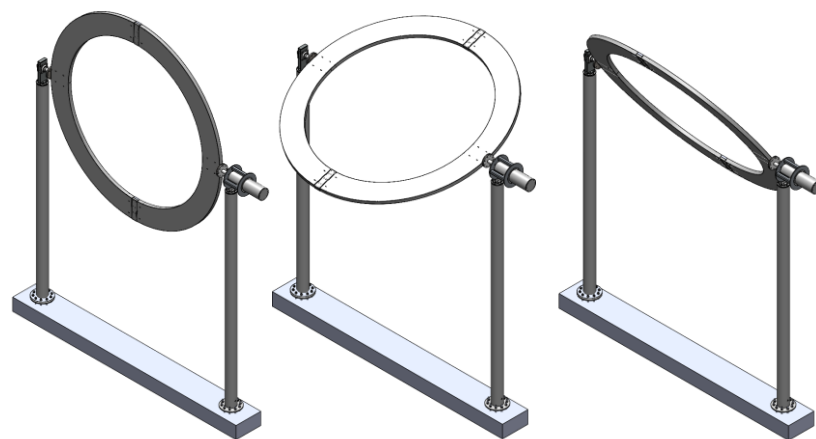


Figure 1. The operating sculpture

The sculpture is supposed to operate for 15 years, and the electric motor is controlled with twilight switch so that the ring starts to rotate at the dawn and stops before sundown. After 15 years the sculpture will be locked to upwards position, and it will be converted to static sculpture.

The ring is supported to the posts with shafts made of 1.4401 stainless steel and SKF FYJ 100 TF flange bearings, and the rotational motion is created with Kraftmek IEC90S B5 electric motor. The motor is bolted to the end of the post with mounting bracket. Between the ring shaft and electric motor is flexible coupling that allows a slight movement and misalignment between the components. The ring is attached to the ring shafts with bolted flanges. The main dimensions of the sculpture are presented in Figure 2 and section view in Figure 3.

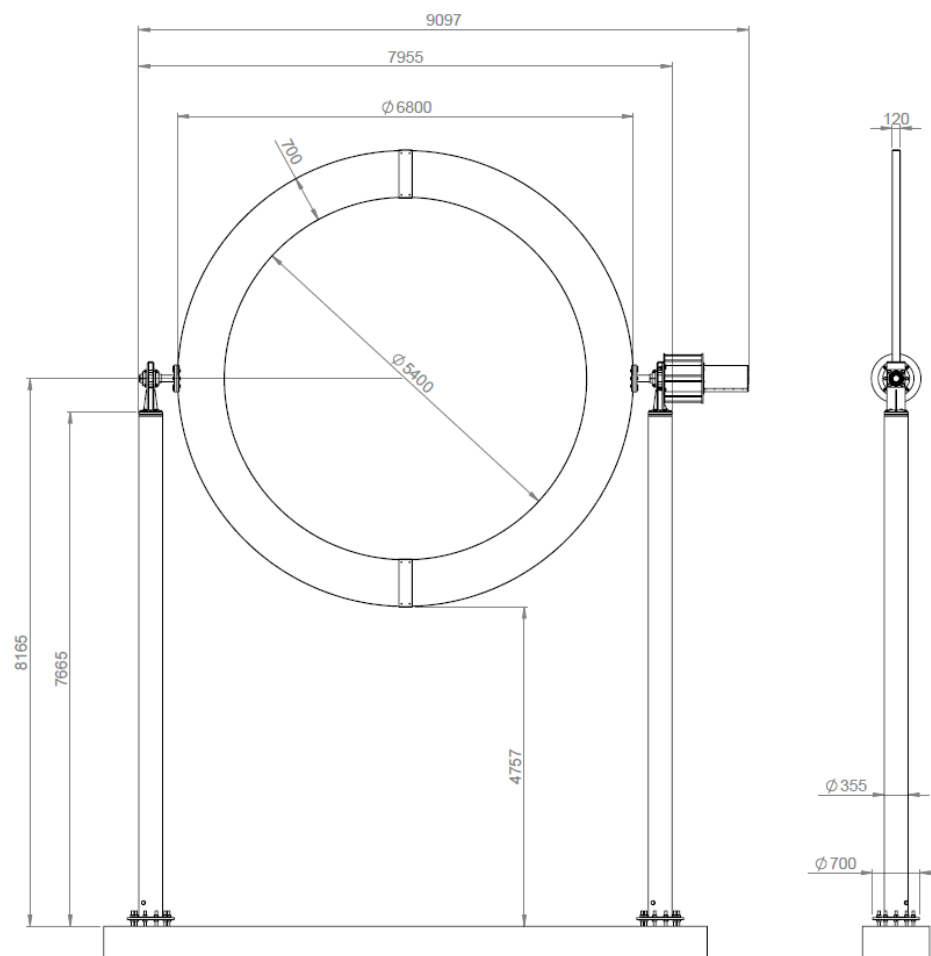


Figure 2. The main dimensions of the Daily Mirror -sculpture

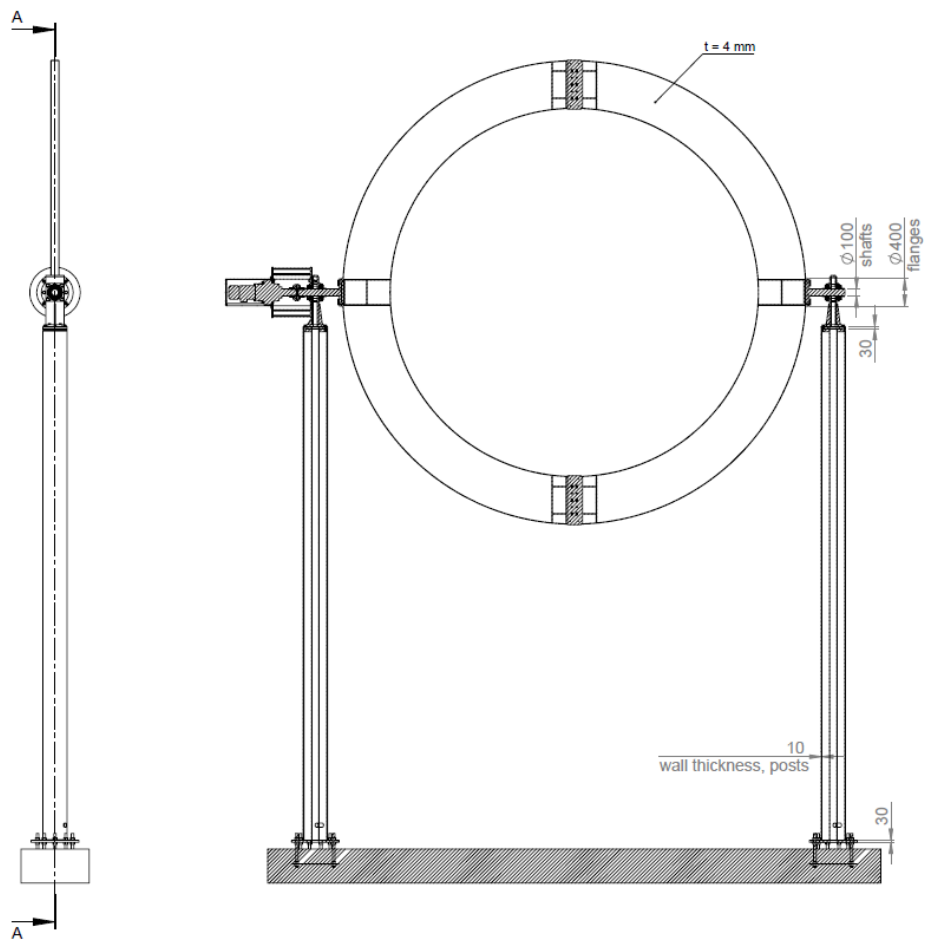


Figure 3. The section view of the preliminary structure

Dimensions and materials of the structural members and joints are estimated during the mechanical design process, and these can be changed during the study if needed. Changes need to be done so that the general shape and design of the structure are not critically changed. Materials used in the preliminary structure are presented in Table 1.

Table 1. Materials used in the preliminary structure.

Component	Type	Dimensions			Material
		Outer \emptyset	Inner \emptyset	Thickness	
Plates for foundation bolts	Plate	700 mm		30 mm	S355J2+N
Posts	Hollow bar	355 mm	335 mm	10 mm	S355J2+N
Shaft flanges, bearing flanges and end caps	Plate			20 mm	S355J2+N
Ring	Plate			4 mm	S355J2+N
Ring shafts	Rod			100 mm	X5CrNiMo17 1.4401

Ring shafts are made of stainless steel to prevent corrosion damages on machined surfaces which can make maintenance more complicate and shorten the lifetime of bearings.

1.2 Objectives

In this master's thesis the structural analysis of kinetic sculpture excluding buckling analysis will be performed. Also, the fatigue analysis is performed for the main joints of the structure and the fatigue analyses of other joints are excluded from the thesis. In addition, detailed mechanical designing or the design of the concrete foundation are not included in the scope of the study. Component selection criteria and automation will be designed individually after strength analysis. The strength analysis is mainly performed by using numerical methods (FEM) therefore the analytical methods of the analyses performed are not presented in this thesis.

The goal of the study is to ensure the strength of the structure so that it can operate through the planned life cycle. Outdoor sculptures are affected on wind, snow and temperature loads and the effects of those are examined with static analysis including ultimate capacity and stability as well as fatigue and vibration analysis. Load conditions are determined according to SFS-EN 1991-1.

2 Load conditions

Load conditions are determined according to Eurocode 1 SFS-EN 1991-1-3, -1-4 and -1-5 standards.

2.1 Wind load

SFS-EN 1991-1-4 gives instructions how to determine wind actions that must be taken account when designing outdoor structures such as buildings and civil engineering structures up to height of 200 m. Wind actions consists of actual wind force that is parallel to wind direction, friction force, vortex shedding that is perpendicular to wind direction and galloping, divergence, and flutter phenomena. (SFS-EN 1991-1-4).

2.1.1 Wind force

The wind force stands for a resultant force that is parallel to wind direction and tries to deform the structure along the wind direction. Load case and deformation direction are presented in Figure 4.

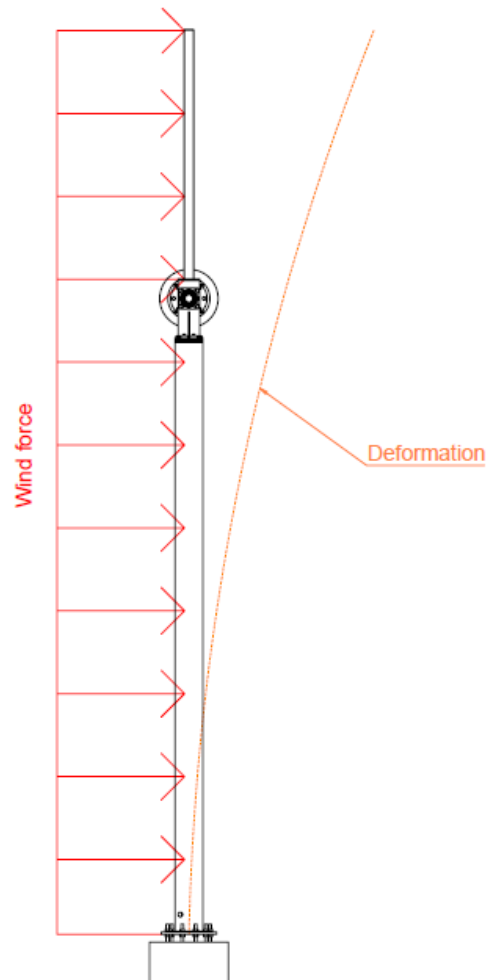


Figure 4. Deformation caused by wind force

Resultant wind force can be calculated using force coefficients or using surface pressure theory (SFS-EN 1991-1-4 p. 44). In this case the wind force is calculated by using local force coefficients. The resultant wind force F_w can be calculated by equation:

$$F_w = c_s c_d c_f \cdot q_p(z_e) \cdot A_{ref} \quad (1)$$

Where $c_s c_d$ is the structural factor, c_f is the force coefficient for the specific structure or structural element, $q_p(z_e)$ is the peak velocity pressure at reference height z_e and A_{ref} is the reference area of the structure or structural element under study (SFS-EN 1991-1-4 p. 45-46).

For structures with a height less than 15 meters the value for the structural factor $c_s c_d$ can be taken as 1.0 (SFS-EN 1991-1-4 p. 48). When determining the force coefficient c_f , the sculpture is considered as a large signboard. The value for the force coefficient c_f may be taken as 1,80 when following expression is valid:

$$z_g > \frac{h}{4} \quad (2)$$

where z_g and h are heights presented in Figure 5. (SFS-EN 1991-1-4 p. 108). Corresponding values for factors z_g and h are presented in Figure 6.

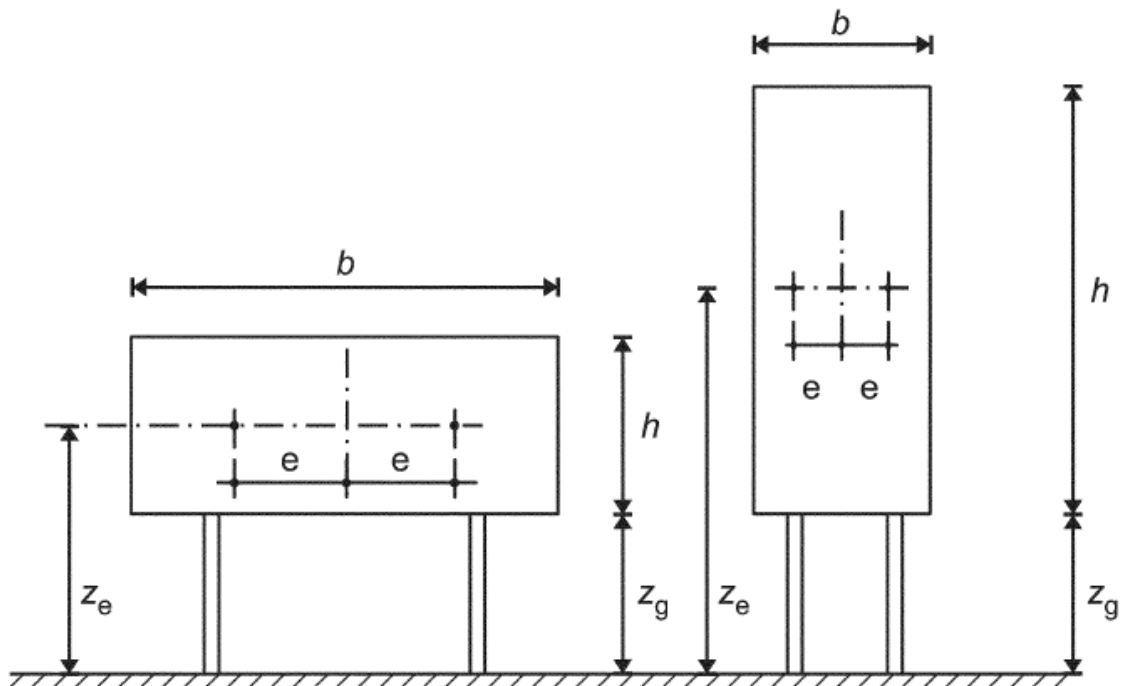


Figure 5. Dimensions of a signboard (SFS-EN 1991-1-4 p. 110)

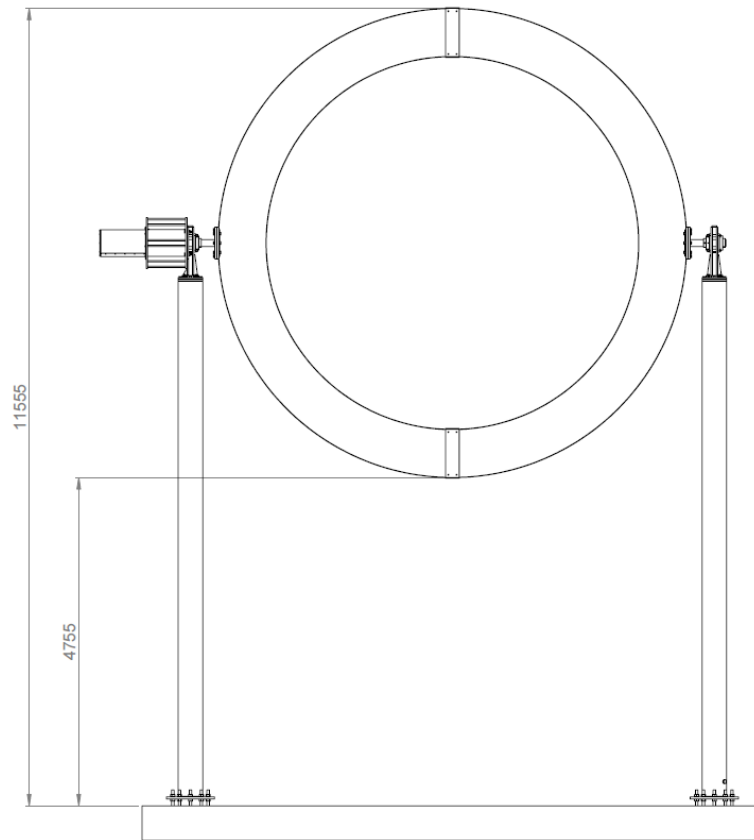


Figure 6. Dimensions of the sculpture

The peak velocity pressure $q_p(z_e)$ can be determined by equation:

$$q_p(z_e) = \frac{[1 + 7I_v(z_e)] \cdot \rho \cdot v_m^2(z_e)}{2} \quad (3)$$

where $I_v(z)$ is wind turbulence intensity, ρ is the air density (1.25 kg/m^3) and v_m is mean wind velocity. (SFS-EN 1991-1-4 p. 40).

The wind turbulence intensity $I_v(z_e)$ may be calculated by equation:

$$I_v(z_e) = \frac{k_I}{c_0(z) \cdot \ln\left(\frac{z}{z_0}\right)} \quad (4)$$

where k_I is the turbulence factor, $c_0(z)$ is the terrain orography factor and z_0 is the roughness length. Recommended value for the turbulence factor k_I is 1.0. (SFS-EN 1991-1-4 p. 38).

The terrain orography factor c_0 is taken account if the orography of the area is increasing wind velocity more than 5 % (SFS-EN 1991-1-4 p. 38). In this case there are not hills, cliffs or mountains near the structure so the value for the factor c_0 may be taken as 1.0 (SFS-EN 1991-1-4 p. 35).

The roughness length z_0 can be determined from Figure 7. The structure will be place on urban area so the value for the roughness length is 0.3 m.

Terrain category	z_0 m	z_{min} m
0 Sea or coastal area exposed to the open sea	0,003	1
I Lakes or flat and horizontal area with negligible vegetation and without obstacles	0,01	1
II Area with low vegetation such as grass and isolated obstacles (trees, buildings) with separations of at least 20 obstacle heights	0,05	2
III Area with regular cover of vegetation or buildings or with isolated obstacles with separations of maximum 20 obstacle heights (such as villages, suburban terrain, permanent forest)	0,3	5
IV Area in which at least 15 % of the surface is covered with buildings and their average height exceeds 15 m	1,0	10

NOTE: The terrain categories are illustrated in A.1.

Figure 7. Values for the roughness length z_0 (SFS-EN 1991-1-4 p. 36).

The mean wind velocity v_m may be calculated by equation:

$$v_m(z) = c_r(z) \cdot c_0(z) \cdot v_b \quad (5)$$

where c_r is the roughness factor and v_b is the basic wind velocity (SFS-EN 1991-1-4 p. 34).

The roughness factor can be calculated by equation:

$$c_r(z) = k_r \cdot \ln\left(\frac{z}{z_0}\right) \quad (6)$$

where k_r is the terrain factor depending on the roughness length and can be calculated by equation:

$$k_r = 0.19 \left(\frac{z_0}{z_{0,II}}\right)^{0.07} \quad (7)$$

where $z_{0,II}$ is the roughness factor for terrain category II presented in Figure 7. (SFS-EN 1991-1-4 p. 34)

The basic wind velocity v_b may be calculated by using equation:

$$v_b = c_{dir} \cdot c_{season} \cdot v_{b,0} \quad (8)$$

where c_{dir} is the directional factor, c_{season} is the season factor and $v_{b,0}$ is the fundamental value for the basic wind. The recommended values for c_{dir} and c_{season} is 1.0. (SFS-EN 1991-1-4 p. 32). The recommended value for the basic wind velocity $v_{b,0}$ is 23 m/s. (SFS-EN 1991-1-4 p. 144).

2.1.2 Friction force

Wind velocity may cause friction forces that acts on the surfaces that are parallel compared to wind direction. The force is caused by friction between air and parallel surfaces. The friction forces may be ignored if the total area of parallel surfaces is less than 4 times of the total area of perpendicular surfaces. (SFS-EN 1991-1-4 p. 46). In this case, the expression mentioned before is valid and friction forces can be ignored. Total areas of parallel and perpendicular surfaces are presented in Figure 8 and Figure 9.

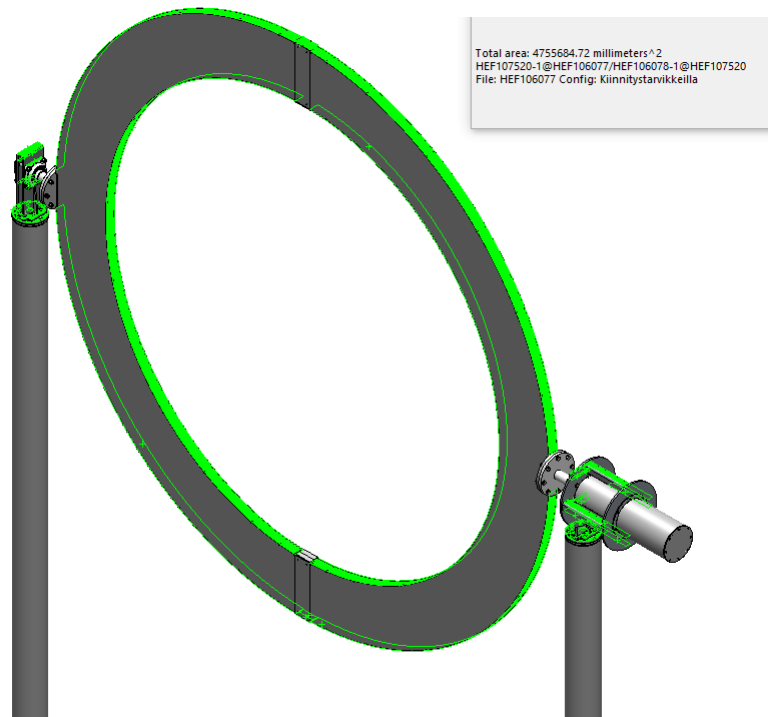


Figure 8. Total area of the surfaces parallel to wind direction ($A_{\parallel} = 4.8 \text{ m}^2$)

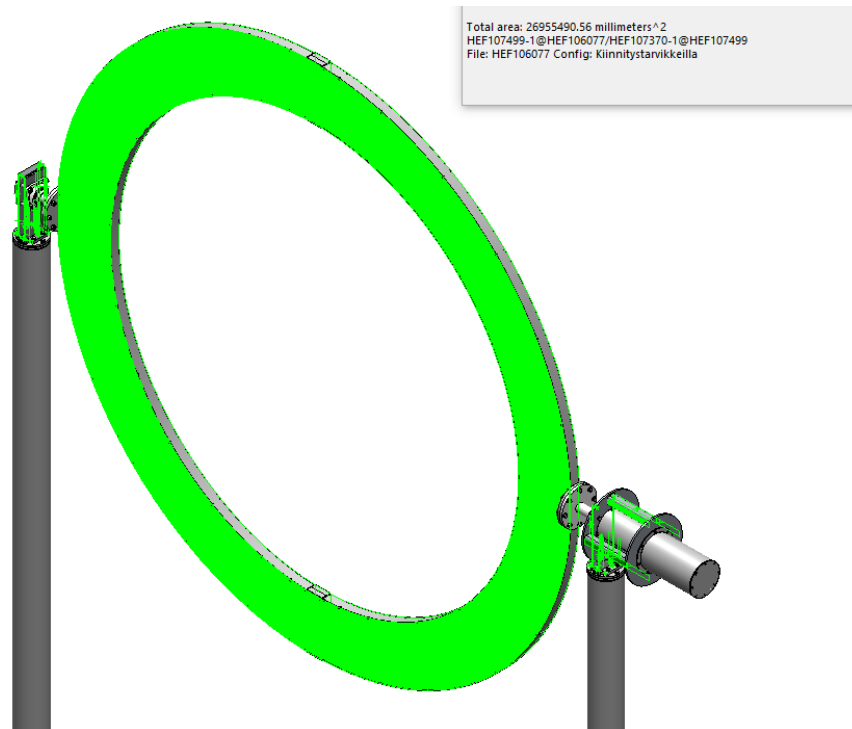


Figure 9. Total area of the surfaces perpendicular to wind direction ($A_{\perp} = 26.9 \text{ m}^2$)

$$\text{Ratio of surfaces} = \frac{A_{\parallel}}{A_{\perp}} = 0.17 < 4 \quad (9)$$

2.1.3 Vortex shedding

Wind or every kind of flow past cylinder shaped element can cause vortex shedding and as a result the structural element experiences variable aerodynamic forces that can cause vortex induced vibration (VIV). Under certain circumstances VIV can cause the vortex shedding frequency to match with the natural frequency of the structure and lead to synchronization of frequencies. (Singh & Mattal 2005 p. 1085). The vortex shedding is illustrated in Figure 10.

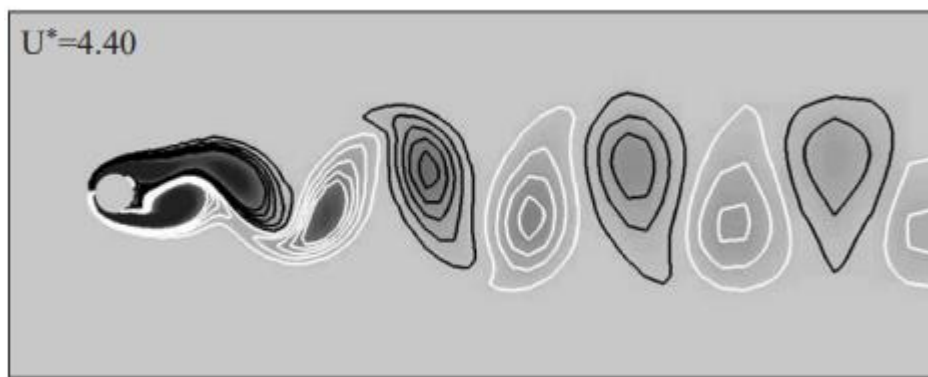


Figure 10. Vortex shedding phenomena (Singh & Mittal 2005 p. 1094).

The effect of vortex shedding must be examined when the following expression is valid:

$$v_{\text{crit},i} > 1.25 \cdot v_m \quad (10)$$

where $v_{\text{crit},i}$ is a critical wind velocity for vibration mode i . The critical wind velocity is typically normal or frequent wind velocity and because of that the fatigue effects and therefore number of cycles of vibrating must be examined. (SFS-EN 1991-1-4 p. 196).

The critical wind velocity $v_{\text{crit},i}$ may be calculated by using equation:

$$v_{\text{crit},i} = \frac{b \cdot n_{i,y}}{St} \quad (11)$$

where b is the reference width of the cross-section where the vortex shedding occurs, $n_{i,y}$ is the natural frequency of the structure and St is Strouhal number of the structural element. (SFS-EN 1991-1-4 p. 196).

The natural frequency is determined by finite element analysis and Strouhal number may be determined from Figure 11.


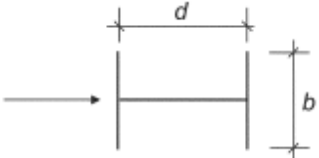
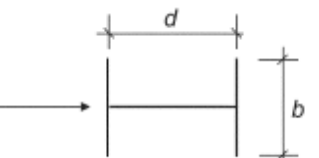
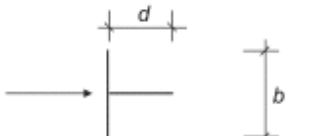
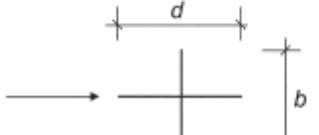
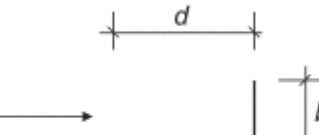
Poikkileikkaus	St
 <p>kaikilla Reynoldsin luvun arvoilla</p>	0,18
 <p>$0,5 \leq d/b \leq 10$</p>	kuvasta E.1
 <p>lineaarinen interpolointi</p>	$db = 1$ 0,11 $db = 1,5$ 0,10 $db = 2$ 0,14
 <p>lineaarinen interpolointi</p>	$db = 1$ 0,13 $db = 2$ 0,08
 <p>lineaarinen interpolointi</p>	$db = 1$ 0,16 $db = 2$ 0,12
 <p>lineaarinen interpolointi</p>	$db = 1,3$ 0,11 $db = 2,0$ 0,07
HUOM. Strouhalin luvun arvojen ekstrapolointi suhteen d/b funktiona ei ole sallittua.	

Figure 11. Strouhal numbers for different structural elements (SFS-EN 1991-1-4 p. 200).

The load caused by vortex shedding may be calculated by equation:

$$F_w(s) = m(s) \cdot (2\pi \cdot n_{i,y})^2 \cdot \Phi_{i,y}(s) \cdot y_{F,max} \quad (12)$$

where $m(s)$ is vibrating mass per unit length, $\Phi_{i,y}$ is the mode shape of the structural element normalised to values of 1.0 at the location of maximum displacement and $y_{F,max}$ is the maximum displacement over time of the point where the mode shape is equal to 1.0. (SFS-EN 1991-1-4 p. 204).

The normalised mode shape of the structure $\Phi_{i,y}$ may be determined by equation:

$$\Phi_{i,y}(z) = \left(\frac{z}{h}\right)^\zeta \quad (13)$$

where factor ζ may be determined from Table 2. (SFS-EN 1991-1-4 p. 244).

Table 2. Determining of the factor ζ (SFS-EN 1991-1-4 p. 244-245).

ζ	Structure or structural element
0,6	Slender frame structures without load sharing wall or clad
1,0	Structures with a central core, peripheral columns, and shear bracings
1,5	Slender cantilever buildings or building with concrete core
2,0	Towers and chimneys
2,5	Towers with steel supports (lattice)

The maximum displacement $y_{F,max}$ may be calculated by using equation:

$$\frac{y_{F,max}}{b} = \frac{1}{St^2} \cdot \frac{1}{Sc} \cdot K \cdot K_w \cdot c_{lat} \quad (14)$$

where b is width of the structure (perpendicular to the wind direction), Sc is the Scruton number, K is the mode shape factor, K_w is the effective correlation length factor and c_{lat} is the lateral force coefficient. (SFS-EN 1991-1-4 p. 204).

Scruton number can be determined from the equation:

$$Sc = \frac{2 \cdot \delta_s \cdot m_{i,e}}{\rho \cdot b^2} \quad (15)$$

where δ_s is the structural damping as the logarithmic decrement and $m_{i,e}$ is the equivalent mass of the fundamental mode per unit length. (SFS-EN 1991-1-4 p. 202). The structural damping can be determined from Figure 12.

Structural type		structural damping, δ_s
reinforced concrete buildings		0,10
steel buildings		0,05
mixed structures concrete + steel		0,08
reinforced concrete towers and chimneys		0,03
unlined welded steel stacks without external thermal insulation		0,012
unlined welded steel stack with external thermal insulation		0,020
steel stack with one liner with external thermal insulation ^a	$h/b < 18$	0,020
	$20 \leq h/b < 24$	0,040
	$h/b \geq 26$	0,014
steel stack with two or more liners with external thermal insulation ^a	$h/b < 18$	0,020
	$20 \leq h/b < 24$	0,040
	$h/b \geq 26$	0,025
steel stack with internal brick liner		0,070
steel stack with internal gunite		0,030
coupled stacks without liner		0,015
guyed steel stack without liner		0,04
steel bridges + lattice steel towers	welded	0,02
	high resistance bolts	0,03
	ordinary bolts	0,05
composite bridges		0,04
concrete bridges	prestressed without cracks	0,04
	with cracks	0,10
Timber bridges		0,06 - 0,12
Bridges, aluminium alloys		0,02
Bridges, glass or fibre reinforced plastic		0,04 - 0,08
cables	parallel cables	0,006
	spiral cables	0,020
NOTE: The values for timber and plastic composites are indicative only. In cases where aerodynamic effects are found to be significant in the design, more refined figures are needed through specialist advice (agreed if appropriate with the competent Authority). [AC> deleted text <AC]		
^a For intermediate values of h/b , linear interpolation may be used		

Figure 12. Values for logarithmic decrements of structural damping (SFS-EN 1991-1-4 p. 252).

In this case the structure is considered as a mixture of steel and concrete (posts, $\delta_s = 0.08$) and steel building (ring, $\delta_s = 0.05$).

The equivalent mass of fundamental mode $m_{i,e}$ may be calculated by equation:

$$m_{i,e} = \frac{\int_0^l m(s) \cdot \Phi_i^2(s) ds}{\int_0^l \Phi_i^2(s) ds} \quad (16)$$

where $m(s)$ is mass per unit length and l is length or height of the structure or structural element. (SFS-EN 1991-1-4 p. 248).

The mass per unit length can be expressed as:

$$m(s) = \frac{m_{total}}{l} \cdot s \quad (17)$$

where m_{total} is the total mass of structure or structural element and s is:

$$0 < s \leq l \quad (18)$$

The correlation length factor K_w may be determined by using equation:

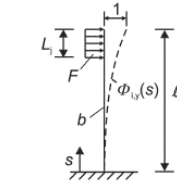
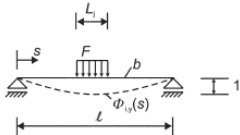
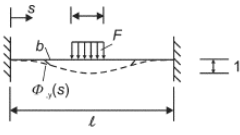
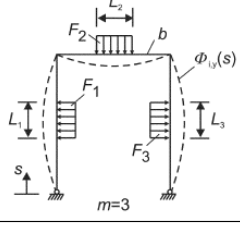
$$K_w = 3 \cdot \frac{L_j}{\lambda} \cdot \left(1 - \frac{L_j}{\lambda} + \frac{1}{3} \cdot \left(\frac{L_j}{\lambda} \right)^2 \right) \quad (19)$$

where m is determined from Figure 13, L_j is the distance between two node points (Figure 13) and λ is calculated by using equation:

$$\lambda = \frac{l}{b} \quad (20)$$

where l is length of the structure or structural element. (SFS-EN 1991-1-4 p. 211-212).

The mode shape factor K can also be determined from Figure 13.

Structure	mode shape $\Phi_{1,y}(s)$	K_W	K
	see F.3 with $\zeta = 2,0$ $n = 1$; $m = 1$	$3 \cdot \frac{L_1/b}{\lambda} \cdot \left[1 - \frac{L_1/b}{\lambda} + \frac{1}{3} \cdot \left(\frac{L_1/b}{\lambda} \right)^2 \right]$	0,13
	see Table F.1 $n = 1$; $m = 1$	$\cos \left[\frac{\pi}{2} \cdot \left(1 - \frac{L_1/b}{\lambda} \right) \right]$	0,10
	see Table F.1 $n = 1$; $m = 1$	$\frac{L_1/b}{\lambda} + \frac{1}{\pi} \cdot \sin \left[\pi \cdot \left(1 - \frac{L_1/b}{\lambda} \right) \right]$	0,11
	modal analysis $n = 3$ $m = 3$	$\frac{\sum_{i=1}^n \int_{L_i} \phi_{1,y}(s) ds}{\sum_{i=1}^m \int_{l_i} \phi_{1,y}(s) ds}$	0,10

NOTE 1 The mode shape, $\Phi_{1,y}(s)$, is taken from F.3. The parameters n and m are defined in Expression |AC> (E.8) <AC| and in Figure E.3

NOTE 2 $\lambda = l/b$

Figure 13. Factors for correlation length factor calculations (SFS-EN 1991-1-4 p. 212).

The lateral force coefficient c_{lat} may be determined in the respect of the basic lateral force coefficient $c_{lat,0}$. The formula is presented in Figure 14.

Critical wind velocity ratio	c_{lat}
$\frac{V_{crit,i}}{V_{m,Lj}} \leq 0,83$	$c_{lat} = c_{lat,0}$
$0,83 \leq \frac{V_{crit,i}}{V_{m,Lj}} < 1,25$	$c_{lat} = \left(3 - 2,4 \cdot \frac{V_{crit,i}}{V_{m,Lj}} \right) \cdot c_{lat,0}$
$1,25 \leq \frac{V_{crit,i}}{V_{m,Lj}}$	$c_{lat} = 0$

where:

- $c_{lat,0}$ is the basic value of c_{lat} as given in Table E.2 and, for circular cylinders, in Figure E.2
- $V_{crit,i}$ |AC> is the critical wind velocity (see E.1.3.1) <AC|
- $V_{m,Lj}$ |AC> is the mean wind velocity (see 4.3.1) in the centre of the effective correlation length as defined in Figure E.3 <AC|

Figure 14. Lateral force coefficient compared to basic value in the respect of critical wind velocity (SFS-EN 1991-1-4 p. 208).

The basic lateral force coefficient $c_{lat,0}$ can be determined from Figure 15.

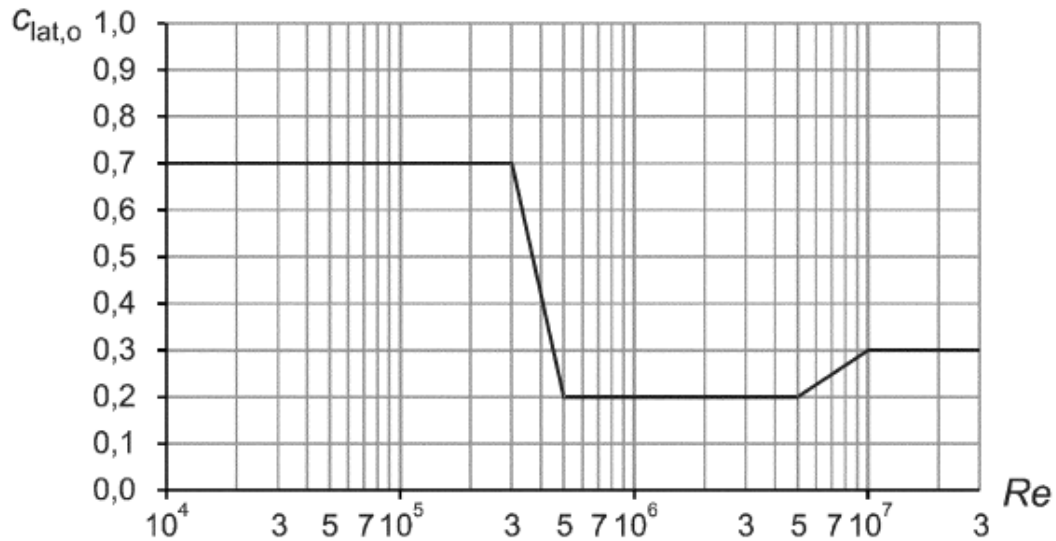


Figure 15. Basic value of the lateral force coefficient in respect of Reynolds number Re (SFS-EN 1991-1-4 p. 208).

The Reynolds number of structural element can be calculated by equation:

$$Re(v_{crit,i}) = \frac{b \cdot v_{crit,i}}{v} \quad (21)$$

where v is the kinematic viscosity of the air ($v \approx 15 \times 10^{-6} \text{ m}^2/\text{s}$). (SFS-EN 1991-1-4 p. 202).

The lateral coefficient factor can be modified in conditions where vertical cylinders are placed in a row or grouped arrangement. Different configurations are presented in Figure 16. (SFS-EN 1991-1-4 p. 215). In sculpture, posts are forming grouped structure so the posts may be investigated as a system of structural elements.

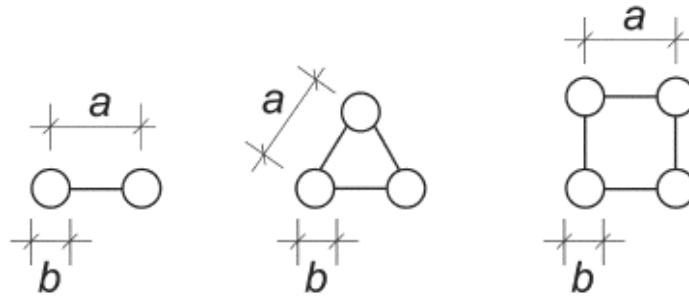


Figure 16. In-line and grouped system of cylinders (SFS-EN 1991-1-4 p. 216).

The lateral coefficient factor may be modified by using following equations:

$$c_{lat} = 1,5 \cdot c_{lat,single} \quad \text{when} \quad 1 \leq \frac{a}{b} < 10 \quad (22)$$

$$c_{lat} = c_{lat,single} \quad \text{when} \quad \frac{a}{b} \geq 15 \quad (23)$$

The lateral coefficient factor c_{lat} may be linearly interpolated when the ratio of distances a and b has value between 10 and 15. For fatigue assessment the total amount of load cycles caused by vortex shedding can be determined by using the following expression:

$$N = 2 \cdot T \cdot n_{y,i} \cdot \varepsilon_0 \cdot \left(\frac{v_{crit,i}}{v_0} \right)^2 \cdot \exp \left(- \left(\frac{v_{crit,i}}{v_0} \right)^2 \right) \quad (24)$$

where T is the lifetime of structure in seconds, ε_0 is bandwidth factor that describes the band of wind velocities with VIV and v_0 is $\sqrt{2}$ times modal value of the Weibull distributed wind velocity. (SFS-EN 1991-1-4 p. 214). To simplify calculations, the wind velocity v_0 may be taken as (SFS-EN 1991-1-4 p. 214, note 2):

$$v_0 = 0.2 \cdot v_m \quad (25)$$

The bandwidth factor ε_0 can be taken as the value of 0.3 (SFS-EN 1991-1-4 p. 214, note 3).

2.1.4 Galloping

Another phenomenon that can cause instability behaviour of the structure is galloping. Galloping means a self induces vibration of a relatively flexible structure. The structure may experience galloping when deformation occurs in cross wind bending mode. Usually, non-circular cross sections like L-, I-, U-, T- and C-profiles are prone to galloping. In galloping the vibration starts at a critical galloping wind velocity v_{CG} and the amplitude of motion increases rapidly with increasing wind velocity. (SFS-EN 1991-1-4 p. 220).

The critical galloping wind velocity v_{CG} may be calculated by equation:

$$v_{CG} = \frac{2 \cdot Sc}{a_G} \cdot n_{1,y} \cdot b \quad (26)$$

where a_G is the factor of galloping instability, $n_{1,y}$ is the first cross-wind mode frequency of structure. For a_G the value of 10 can be used if the factor is unknown. (SFS-EN 1991-1-4 p. 220-222).

2.1.5 Divergence and flutter

Divergence and flutter are phenomena that can cause instabilities in flexible plate-like structures for example signboards or bridges. In SFS-EN 1991-1-4, there are mentioned three different criteria for plate-like structures that are prone to divergence or flutter. All these criteria must be satisfied before divergence or flutter phenomena must be investigated. (SFS-EN 1991-1-4 p. 231). The criteria are:

1. The structure or part of it has elongated cross-section with b/d ratio less than 0,25.
2. The torsional axis of structure is parallel to plane of the plate and perpendicular to the wind direction. Also, the centre of torsion must be at least $d/4$ downwind of the windward edge of the plate. Factor d is the inwind depth that is measured perpendicularly between plate and torsional axis.
3. The lowest natural frequency of the structure is the same as in the torsional mode or the lowest torsional frequency is less than 2 times the lowest translational frequency. (SFS-EN 1991-1-4 p. 232).

In this case the criteria number two is not valid since the distance between windward plane and torsional axis is only 60 mm. Because of that the structure is not prone to divergence or flutter and the phenomenon can be ignored. The structure is presented in Figure 17.

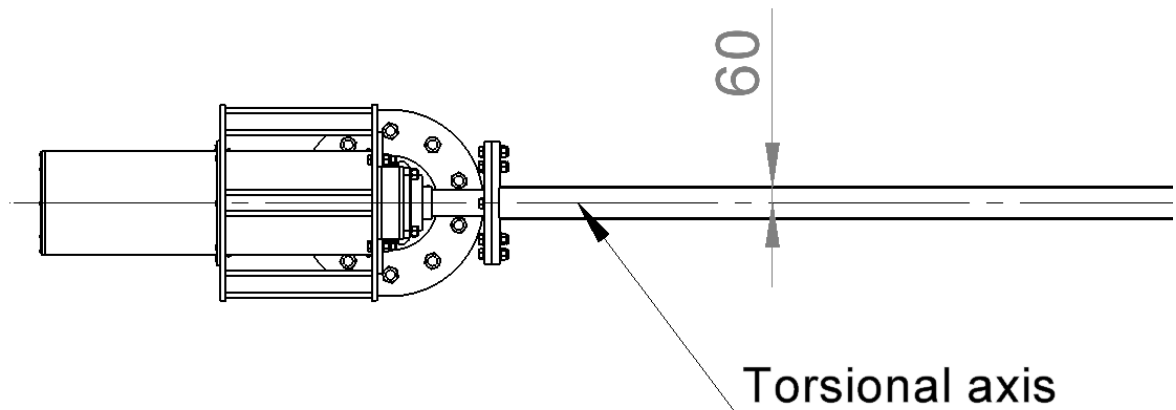


Figure 17. The distance between windward plane and torsional axis.

2.2 Snow load

Snow load can be determined based on SFS-EN 1991-1-3. Snow loads are divided to two different types which are drifted and undrifted snow load. Drifted snow load describes situation where snow has been moved from one location to another for example by the action of wind. Undrifted snow load describes equally distributed snow load that is only affected by the shape of the plane of supporting structure. (SFS-EN 1991-1-3 p. 16-28). In this case, the ring of the sculpture is always either rotating or stopped into position where it is perpendicular compared to ground level, so the drifted snow load is not possible in normal circumstances.

Snow load in persistent or transient circumstances s [kN/m²] may be calculated by using equation:

$$s = \mu_i \cdot C_e \cdot C_t \cdot s_k \quad (27)$$

where μ_i is the snow load shape coefficient, C_e is the exposure coefficient, C_t is the thermal coefficient and s_k is the characteristic value of the snow load on the ground. (SFS-EN 1991-1-3 p. 28).

The snow load shape coefficient can be determined from Figure 18. The recommended value for μ_1 (0°) in the National Annex is 0.8.

Angle of pitch of roof α	$0^\circ \leq \alpha \leq 30^\circ$	$30^\circ < \alpha < 60^\circ$	$\alpha \geq 60^\circ$
$\mu_1(\alpha)$	$\mu_1(0^\circ) \geq 0,8$	$\mu_1(0^\circ) \frac{(60^\circ - \alpha)}{30^\circ}$	0,0
$\mu_2(\alpha)$	0,8	$0,8 \frac{(60^\circ - \alpha)}{30^\circ}$	0,0
$\mu_3(\alpha)$	$0,8 + 0,8 \alpha/30^\circ$	1,6	--

Figure 18. The shape coefficients for snow load (SFS-EN 1991-1-3 p. 32).

The exposure coefficient may be determined from Figure 19.

Topography	C_e
Windswept ^a	0,8
Normal ^b	1,0
Sheltered ^c	1,2

^a *Windswept topography*: flat unobstructed areas exposed on all sides without, or little shelter afforded by terrain, higher construction works or trees.
^b *Normal topography*: areas where there is no significant removal of snow by wind on construction work, because of terrain, other construction works or trees.
^c *Sheltered topography*: areas in which the construction work being considered is considerably lower than the surrounding terrain or surrounded by high trees and/or surrounded by higher construction works.

Figure 19. Recommended values for C_e in different topographies (SFS-EN 1991-1-3 p. 30).

The thermal coefficient C_t considers circumstances where the heat leakages of the building decrease the snow load on the roof. This may happen for example when using glass roofs which thermal transmittance is relatively large ($> 1 \text{ W/m}^2\text{K}$). For all other cases the factor C_t can be taken as 1.0. (SFS-EN 1991-1-3 p. 30).

The expression for the characteristic value for snow load s_k can be determined from the Figure 20.

Climatic Region	Expression
Alpine Region	$s_k = (0,642Z + 0,009) \left[1 + \left(\frac{A}{728} \right)^2 \right]$
Central East	$s_k = (0,264Z - 0,002) \left[1 + \left(\frac{A}{256} \right)^2 \right]$
Greece	$s_k = (0,420Z - 0,030) \left[1 + \left(\frac{A}{917} \right)^2 \right]$
Iberian Peninsula	$s_k = (0,190Z - 0,095) \left[1 + \left(\frac{A}{524} \right)^2 \right]$
Mediterranean Region	$s_k = (0,498Z - 0,209) \left[1 + \left(\frac{A}{452} \right)^2 \right]$
Central West	$s_k = (0,164Z - 0,082) + \frac{A}{966}$
Sweden, Finland	$s_k = (0,790Z + 0,375) + \frac{A}{336}$
UK, Republic of Ireland	$s_k = (0,140Z - 0,1) + \frac{A}{501}$

Figure 20. Snow load in respect of altitude (SFS-EN 1991-1-3 p. 64).

In Finland, the equation below is used:

$$s_k = (0.790 \cdot Z + 0.375) + \frac{A}{336} \quad (28)$$

where Z is the zone number given in Figure 21 and A is the altitude above sea level.

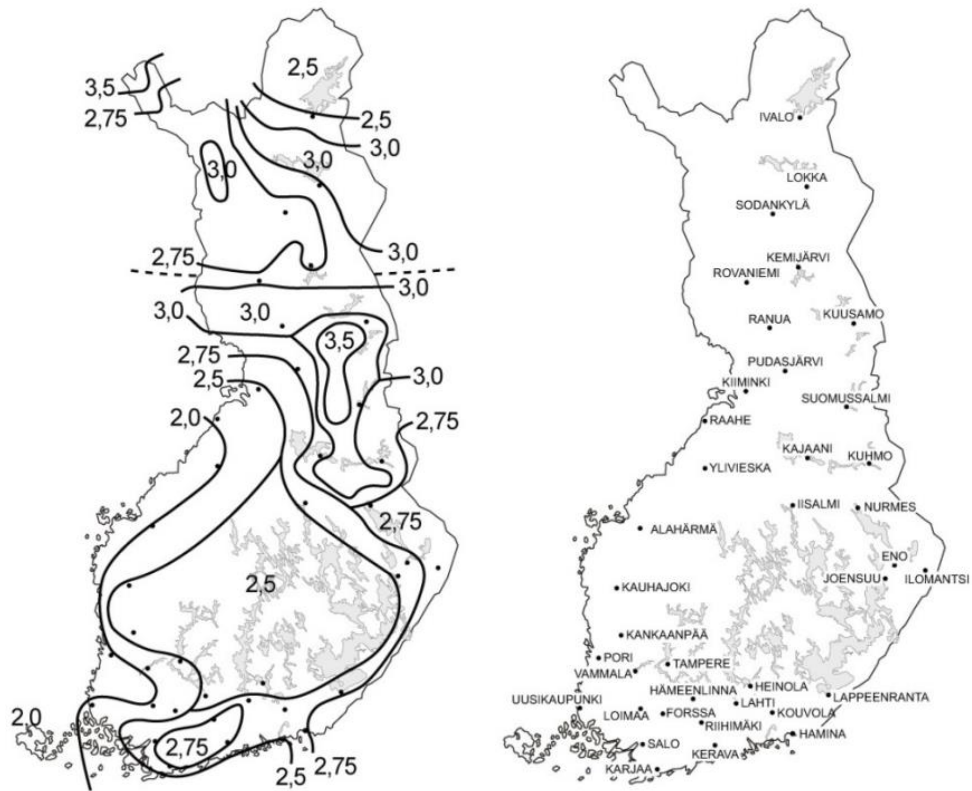


Figure 21. Snow load on ground level [kN/m²] (Bergman 2019 p. 15).

The total snow load force F_{SL} may be calculated by equation:

$$F_{SL} = s \cdot A_{SL} \quad (29)$$

where A_{SL} is the total area where the snow load is affected.

2.3 Thermal load

Thermal loads describe the actions that occurs when the temperature of structure get higher or lower within a specified time interval. Thermal actions must be investigated especially when designing loadbearing structure to ensure that thermal actions and movement will not cause detrimental stress concentrations at the weak points. The effect of thermal loads can be eliminated by joints that allow movement or by including increased local stresses in the design. (SFS-EN 1991-1-5 p. 22).

The maximum and minimum shadow temperature can be determined from Figure 22 and Figure 23.

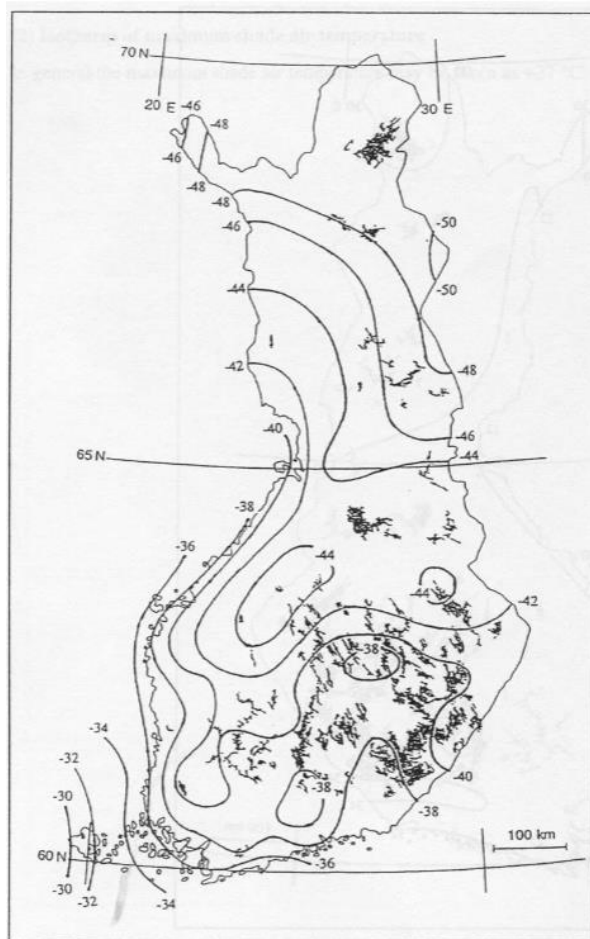


Figure 22. The minimum shadow temperature (SFS-EN 1991-1-5 Annex 6 p. 3)

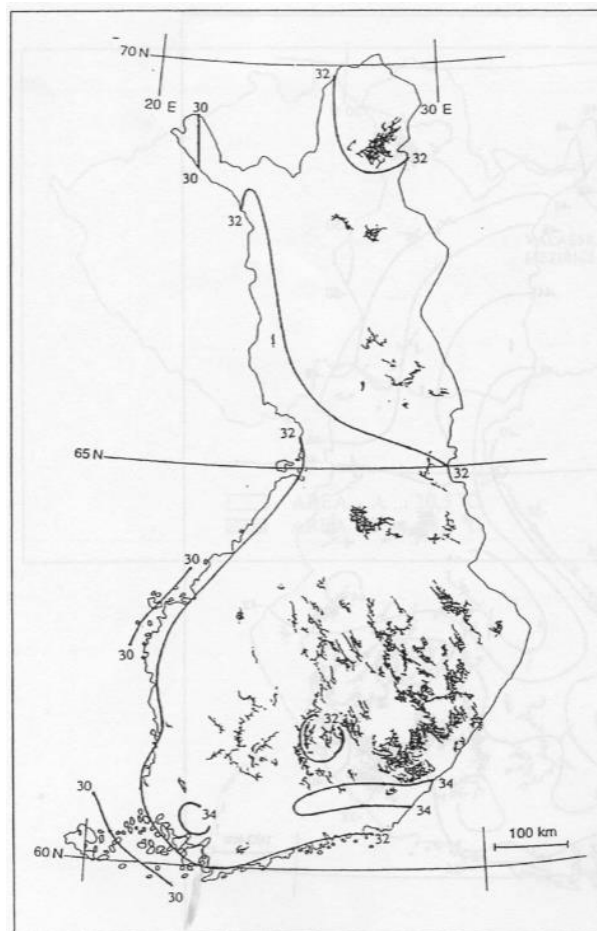


Figure 23. The maximum shadow temperature (SFS-EN 1991-1-5 Annex 6 p. 4)

The maximum value may be modified to take account solar radiation effect. The expression is presented in Figure 24.

Season	Significant factor	Temperature T_{out} in °C	
Summer	Relative absorptivity depending on surface colour	0,5 bright light surface	$T_{max} + T_3$
		0,7 light coloured surface	$T_{max} + T_4$
		0,9 dark surface	$T_{max} + T_5$
Winter		T_{min}	

NOTE: Values of the maximum shade air temperature T_{max} , minimum shade air shade temperature T_{min} , and solar radiation effects T_3 , T_4 , and T_5 may be specified in the National Annex. If no data are available for regions between latitudes 45 °N and 55 °N the values $T_3 = 0$ °C, $T_4 = 2$ °C, and $T_5 = 4$ °C are recommended, for North-East facing elements and $T_3 = 18$ °C, $T_4 = 30$ °C, and $T_5 = 42$ °C for South-West or horizontal facing elements.

Figure 24. The effect of solar radiation (SFS-EN 1991-1-5 p. 28)

In this case the sculpture is considered as dark surface and T_5 is taken as a value of 42 °C since the installation direction is unknown.

The most critical part for thermal actions in the sculpture is the ring and its bearing flanges. That is why thermal actions in the ring are calculated. Thermal effect on the diameter of ring Δd_{ring} can be calculated by equation:

$$\Delta d_{ring} = \alpha_{st} \cdot d_o \cdot \Delta T \quad (30)$$

where α_{st} is the linear expansion coefficient of steel (Figure 25), d_o is the nominal diameter of the ring and ΔT is the change in temperature.

Material	α_T ($\times 10^{-6}/^{\circ}\text{C}$)
Aluminium, aluminium alloy	24
Stainless steel	16
Structural steel, wrought or cast iron	12 (see Note 6)
Concrete except as under	10
Concrete, lightweight aggregate	7
Masonry	6-10 (see Notes)
Glass	(see Note 4)
Timber, along grain	5
Timber, across grain	30-70 (see Notes)
NOTE 1 For other materials special advice should be sought.	
NOTE 2 The values given should be used for the derivation of thermal actions, unless other values can be verified by tests or more detailed studies.	
NOTE 3 Values for masonry will vary depending on the type of brickwork; values for timber across the grain can vary considerably according to the type of timber.	
NOTE 4 For more detailed information see:	
EN 572-1: <i>Glass in Building – Basic soda lime silicate glass – Part 1: Definitions and general physical and mechanical properties</i> ;	
prEN 1748-1-1: <i>Glass in Building – Special basic products – Part 1-1: Borosilicate glass – Definition and description</i> ;	
prEN 1748-2-1: <i>Glass in Building – Special basic products – Part 1-1: Glass ceramics – Definition and description</i> ;	
prEN 14178-1: <i>Glass in Building – Basic alkaline earth silicate glass products – Part 1: Float glass</i>	
NOTE 5 For some materials such as masonry and timber other parameters (e.g. moisture content) also need to be considered. See EN 1995 - EN 1996.	
NOTE 6 For composite structures the coefficient of linear expansion of the steel component may be taken as equal to $10 \times 10^{-6}/^{\circ}\text{C}$ to neglect restraining effects from different α_T -values.	

Figure 25. Coefficients of linear expansion (SFS-EN 1991-1-5 p. 62)

3 Theory and research methods

Theory and research methods used in this thesis are presented in this chapter. Static analysis and natural frequency of the structure is analysed by using FE-analysis by Solidworks - software and its Simulation -add-in. Fatigue assessment is mainly conducted with Hot Spot -method however nominal stresses is used in assessments where using the Hot Spot -method is not possible. Fatigue assessment is conducted according to SFS-EN 1993-1-9. Bolted joints and welds are analysed according to SFS-EN 1993-1-8.

3.1 Hot Spot -method (structural stress)

Typically fatigue assessment of welded components is conducted by using nominal stresses and fatigue classes that defines properties of different joint types. The problem in the nominal stress method is that it ignores dimensional variations of different welded joints. In addition, welded structures are usually so complex that exact values for nominal stresses are hard to determinate. (Niemi, Fricke & Maddox 2018 p. 1).

Using Hot Spot -method or structural stress method (*HS-method*, abbreviation will be used later in this thesis) is worthwhile in structures where potential fatigue crack growth will appear on the upper or lower weld toe. When using HS-method the actual dimensions of detail will be taken into consideration. Structural stress includes the stress concentration that is caused by detail itself but not the local non-linear stress peak. The local non-linear stress peak is caused by the notch effect at the weld toe. (Niemi, Fricke & Maddox 2018 p. 1). The potential crack initiation points are presented in Figure 26.

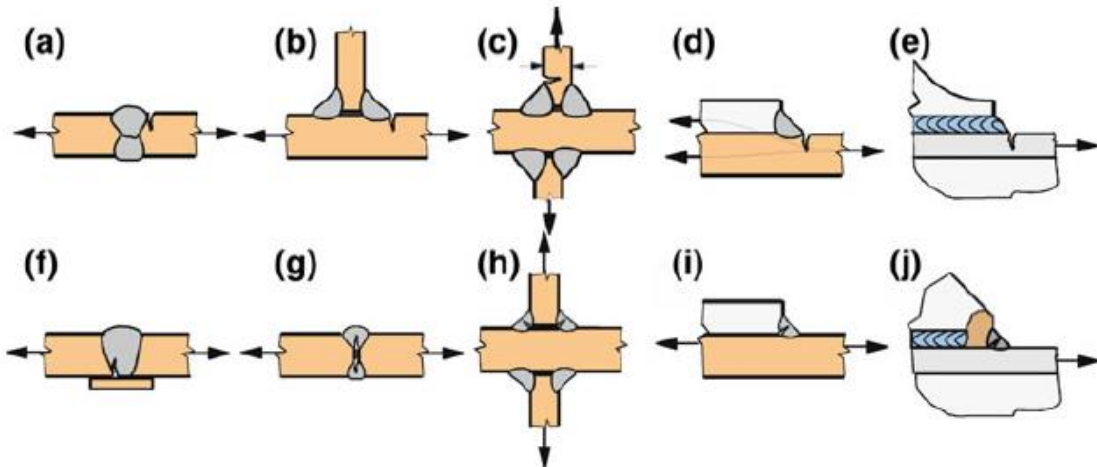


Figure 26. Potential fatigue crack initiation points in welded structures (Niemi, Fricke & Maddox 2018 p. 6).

Hot Spot -stress or structural stress includes membrane and shell bending stresses but does not take account non-linear stress peak that is caused by the geometrical properties of weld toe. Expression of Hot Spot -stress is illustrated in Figure 27.

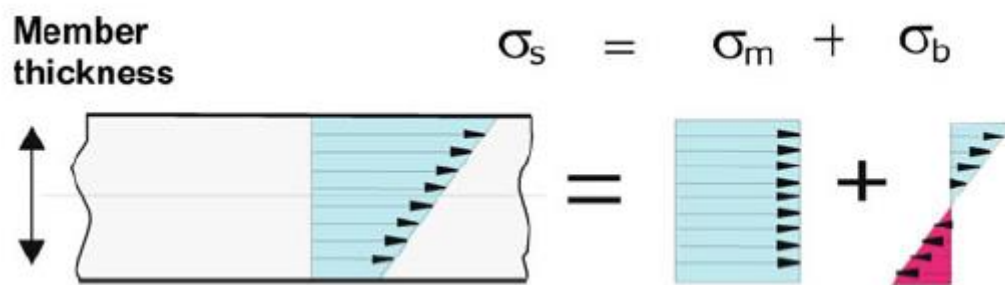


Figure 27. Structural stress as the sum of membrane and bending stresses (Niemi, Fricke & Maddox 2018 p. 7)

Definition of Hot Spot -stress can be divided into two different types that depend on the location of critical weld toe. In type *a*, the critical weld toe is located on the surface of plate and in type *b* on the edge of plate. (Niemi, Fricke & Maddox 2018 p. 6) The difference between types *a* and *b* is presented in Figure 28.

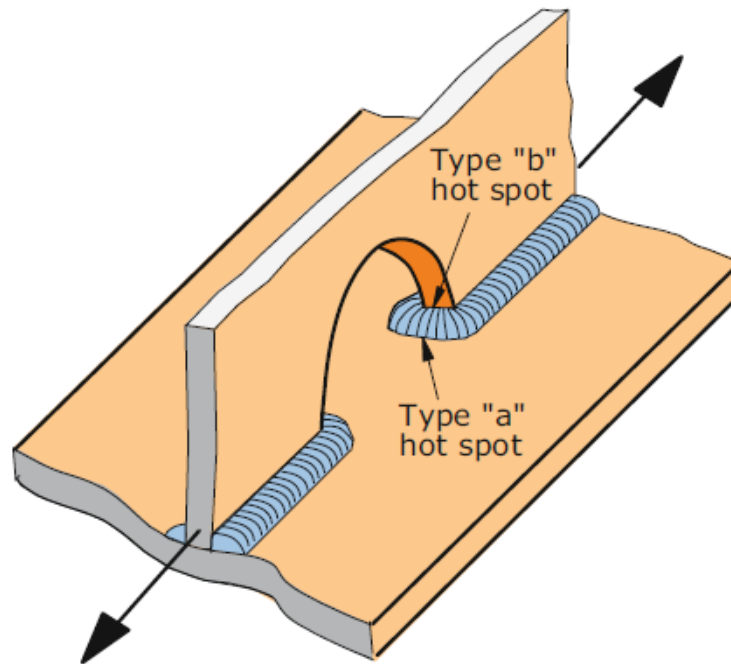


Figure 28. Difference between two Hot Spot -types (Niemi, Fricke & Maddox 2018 p. 6)

Hot Spot -stress can be determined by using linear surface extrapolation (LSE) which means that nodal stresses are determined from the stress plot and those are used to calculate actual Hot Spot -stress by equation:

$$\sigma_{hs} = 1,67 \cdot \sigma_{0,4t} - 0,67 \cdot \sigma_{1,0t} \quad (31)$$

where $\sigma_{0,4t}$ and $\sigma_{1,0t}$ are nodal stresses at distances of 0,4- and 1,0-times plate thickness from the weld toe. (Niemi, Fricke & Maddox 2018 p. 29). The points where nodal stresses are determined are presented in Figure 29.

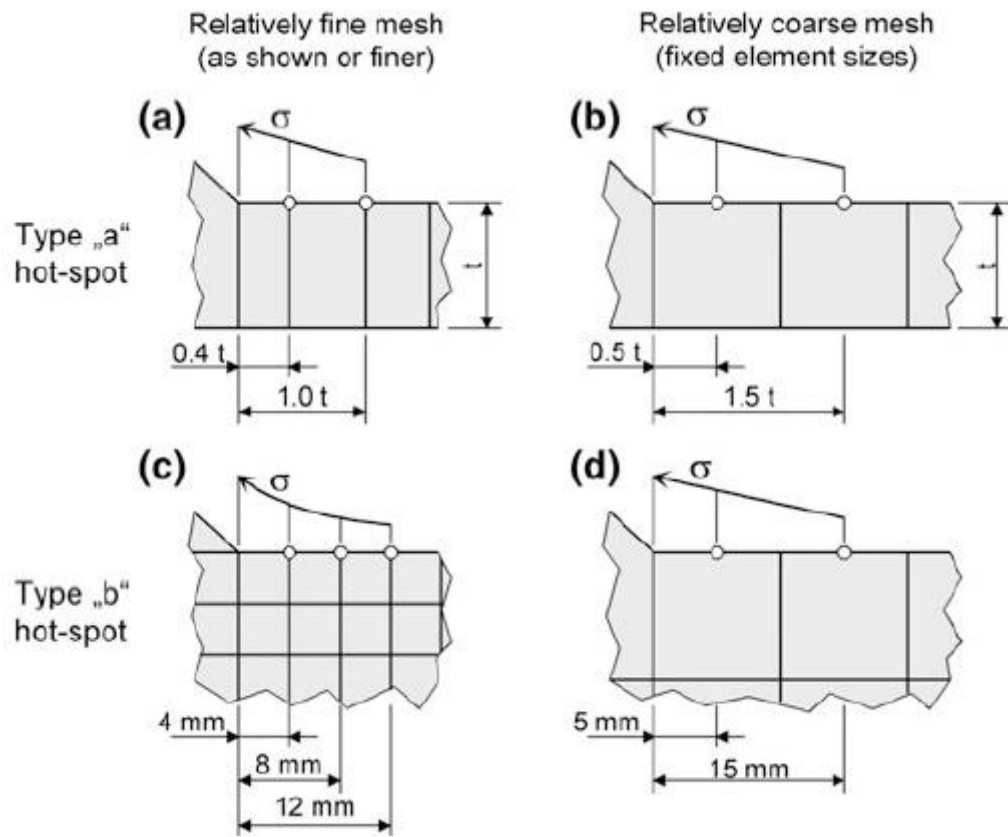


Figure 29. Nodal stress points for linear stress extrapolation (Niemi, Fricke & Maddox 2018 p. 23).

Nodal stresses are determined by using FE-analysis. Welded joint is modelled in FE-model and meshed so that examined nodes are at the correct distance from the weld toe (Figure 29). International Institute of Welding (IIW) has given guideline for the element sizes that may be used in FE-model when obtaining Hot Spot -stresses. Recommended element sizes are presented in Figure 30.

Types of model and weld toe:		Relatively coarse models		Relatively fine models	
		Type a	Type b	Type a	Type b
Element Length × Width	Shells:	$\leq t \times t$ and $t \times w/2^a$	10 mm × 10 mm	$\leq 0.4t \times t$ and $0.4t \times w/2^a$	≤ 4 mm × 4 mm
	Solids:	$\leq t \times t$ and $t \times w^a$	10 mm × 10 mm	$\leq 0.4t \times t$ and $0.4t \times w/2^a$	≤ 4 mm × 4 mm
Extrapol. Points	Shells:	$0.5t/1.5t$ (mid-side pts.) ^b	5 mm/15 mm (mid-side points)	$0.4t/1.0t$ (nodal points)	4 mm/8 mm/12 mm (nodal points)
	Solids:	$0.5t/1.5t$ (surface centre)	5 mm/15 mm (surface centre)	$0.4t/1.0t$ (nodal points)	4 mm/8 mm/12 mm (nodal points)

Figure 30. Recommended element sizes for Hot Spot -model (Niemi, Fricke & Maddox 2018 p. 22).

3.2 Static analysis

The structure is analysed with finite element method by using Solidworks- CAD-software and its Simulation -add-in. Linear analysis and Intel Direct Sparse solver are used in all cases. In static analyses following aspects are considered:

1. Static capacity of the structure (Von Mises -stress compared to the yield stress of material)
2. Displacement that occurs with the specific load case
3. Bolt forces

The analyses are performed in nine different load cases and configurations. Cases 1-8 are performed by analysing the whole structure and in the case number nine, the electric motor bracket is examined. The wind loads are calculated based on the equations presented in chapter 2.1.1 and snow loads based on the equations presented in chapter 2.2. Wind load is also calculated with the mean annual wind velocity and the value for that is 5 m/s (Ilmatieteenlaitos 2022). The effect of concrete core of the posts is only considered in configurations three and five and in other case the concrete core is ignored to simplify the analysis process. That way of analysis is on the safe side and the strength of the structure is not depending on the concrete core. Load cases and configurations are presented in Table 3.

Table 3. Load cases and configurations considered in static analyses

Number	Load case	Configuration	Loads applied
1	Gravity only	The ring perpendicular compared to ground, without concrete core in the posts	Gravity: 9.81 m/s ²
2	Wind load, mean wind velocity in Hämeenlinna (5 m/s)	The ring perpendicular compared to ground, without concrete core in the posts	Gravity: 9.81 m/s ² Force: 4 350 N
3	Wind load, maximum operating wind velocity (10 m/s)	The ring perpendicular compared to ground, without concrete core in the posts	Gravity: 9.81 m/s ² Force: 8 650 N
4	Wind load, maximum operating wind velocity (10 m/s)	The ring perpendicular compared to ground, with concrete core in the posts	Gravity: 9.81 m/s ² Force: 8 650 N
5	Wind load, storm wind (23 m/s)	The ring perpendicular compared to ground, without concrete core in the posts	Gravity: 9.81 m/s ² Force: 19 800 N
6	Wind load, storm wind (23 m/s)	The ring perpendicular compared to ground, with concrete core in the posts	Gravity: 9.81 m/s ² Force: 19 800 N
7	Snow load	The ring perpendicular compared to ground, without concrete core in the posts	Gravity: 9.81 m/s ² Force: 2 700 N
8	Snow load	The ring parallel compared to ground, without concrete core in the posts	Gravity: 9.81 m/s ² Force: 27 800 N
9	Wind load, storm wind (23 m/s)	Electric motor bracket	Torque caused by wind load when the ring is locked = 16 830 Nm

The material models used in the analyses are presented in Table 4. Mechanical properties of used material are determined according to SFS-EN 10025-2, SFS-EN 10088-3 and guidelines of Finnish Transport Infrastructure Agency. S355 plates are mostly 20-30 mm thick so the reduced yield strength 345 MPa is used (SFS-EN 10025-2 p. 24).

Table 4. Material models used in the FE-analyses (SFS-EN 10025-2 p. 24) (SFS-EN 10088-3 p. 20) (Finnish Transport Infrastructure Agency 2000 p. 10)

Material	Model type	Elastic modulus	Poisson's ratio	Yield strength	Tensile strength	Mass density
S355J2+N	Linear Elastic Isotropic	210 GPa	0.3	345 MPa	490 MPa	7850 kg/m ³
X5CrNiMo 17 1.4401	Linear Elastic Isotropic	193 GPa	0.29	200 MPa	500 MPa	8000 kg/m ³
Concrete C20/25	Linear Elastic Isotropic	22 GPa	0.2	-	1.03 MPa	2500 kg/m ³

The structure is modelled by using shell- and solid-elements. Components modelled with shell-elements are presented as highlighted in Figure 31. Shell-element are modelled so that the bottom sides of the elements are facing outwards (agreed way in Hefmec Engineering, easier define shells in case the model has a lot of shell elements).

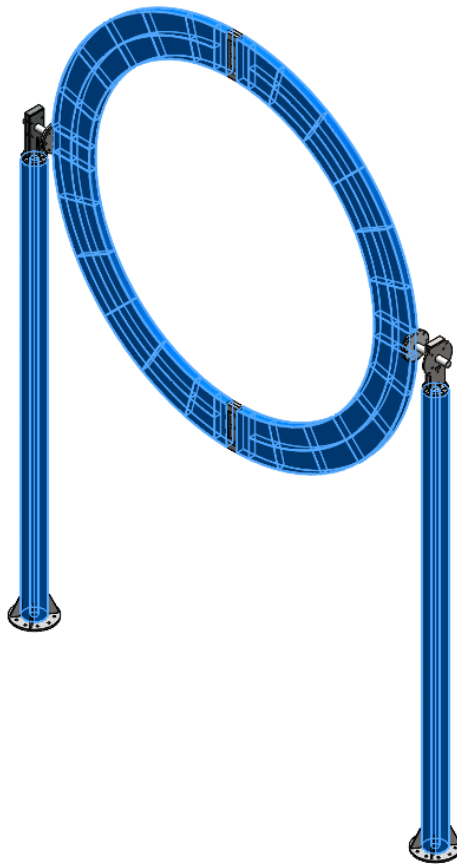


Figure 31. The components that are modelled with shell-elements.

Virtual wall -boundary condition is applied to the bottom face of the posts' foundation plates and plates are attached to virtual wall with *foundation bolt* -fixtures. Bolted joints are modelled with *bolted connection* -interaction. Strength data is applied to the foundation bolts and bolted connections to analyse strength of the joint. M36-foundation bolts are presented in Figure 32 and bolted connections in Figure 33.

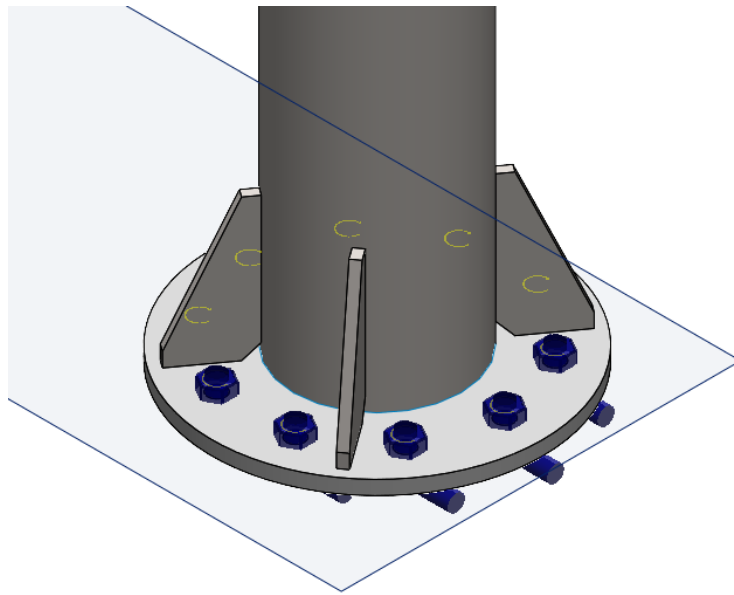


Figure 32. Foundation bolt -fixtures applied to attaching plate.

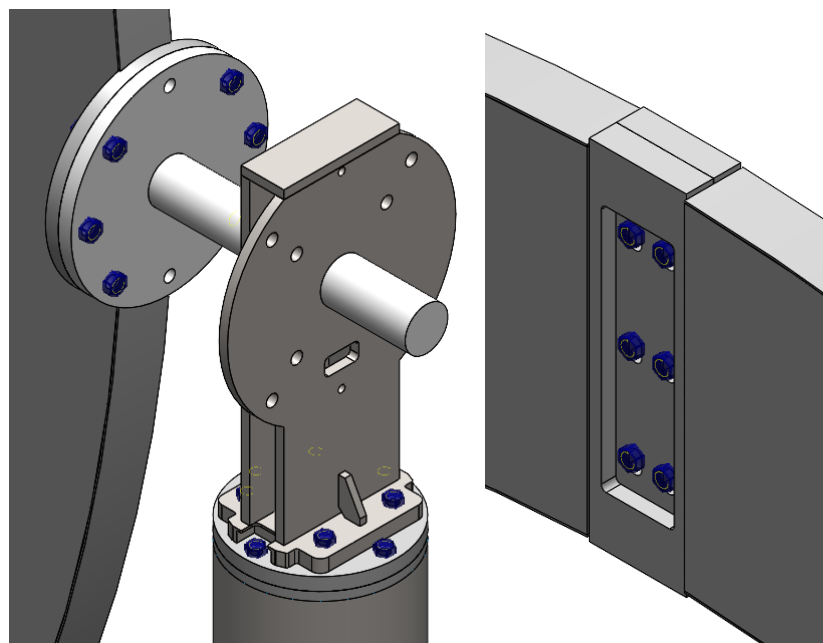


Figure 33. Bolted connections used in the FE-model.

To stabilize the ring and prevent the rotation of the model, a rigid connection is placed between the end face of the ring shaft and shaft carrier. The rigid connection is presented in Figure 34.

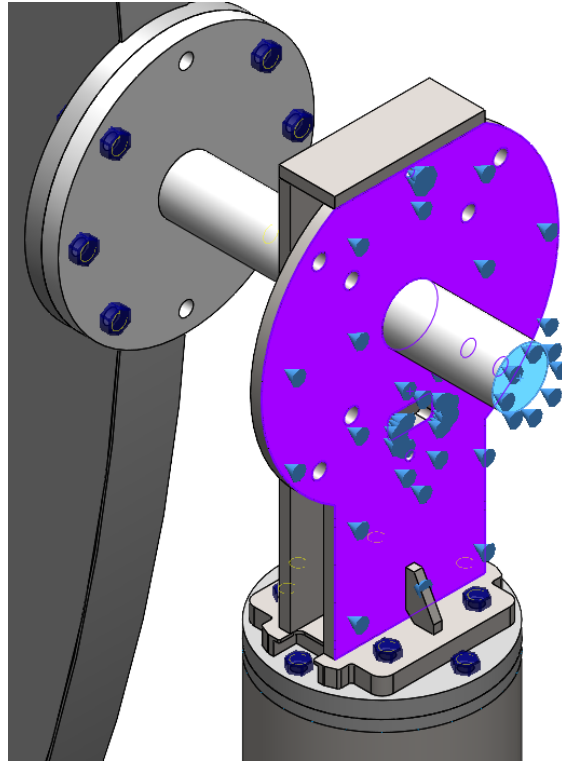


Figure 34. The rigid connection between the ring shaft and the shaft carrier

The contact interactions are applied between components that are not welded together. *No penetration* -contacts without friction are used. *No penetration* -contacts are also applied between concrete core and surfaces of the posts when analysing the effect of concrete core. Interactions used in the FE-model are presented in Figure 35 - Figure 38.

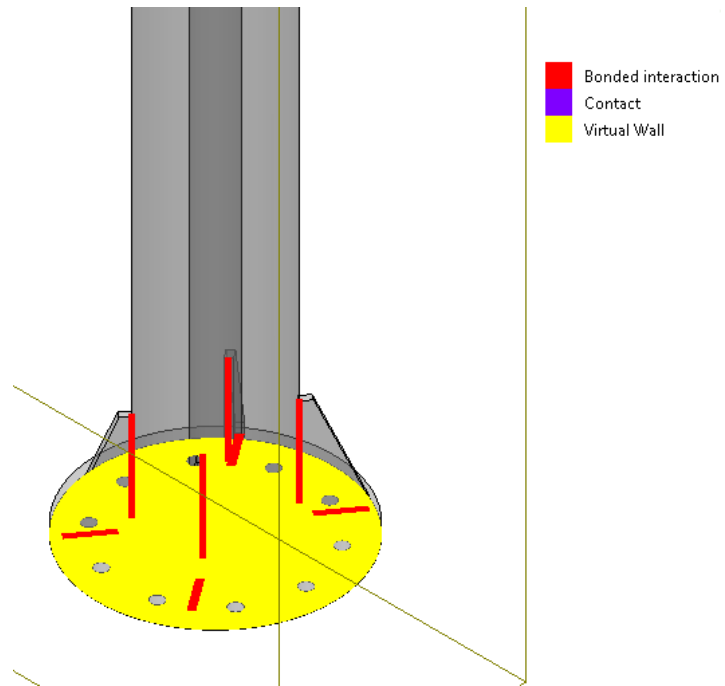


Figure 35. Interactions used in posts' attaching plates

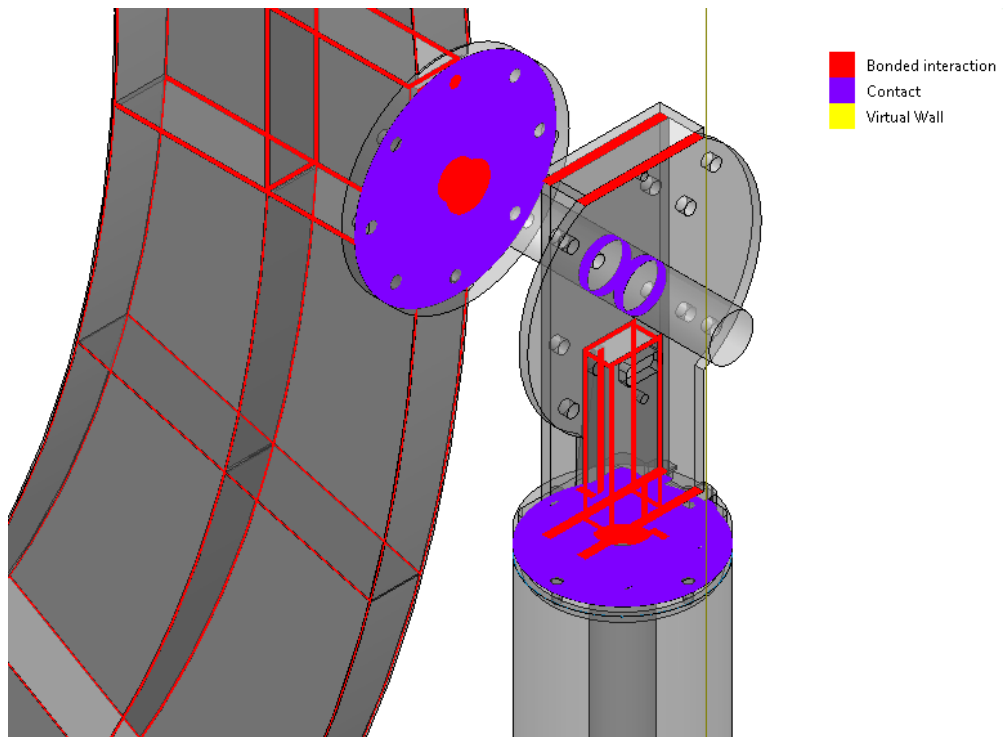


Figure 36. Interactions used in endcaps, shaft carriers and shafts.

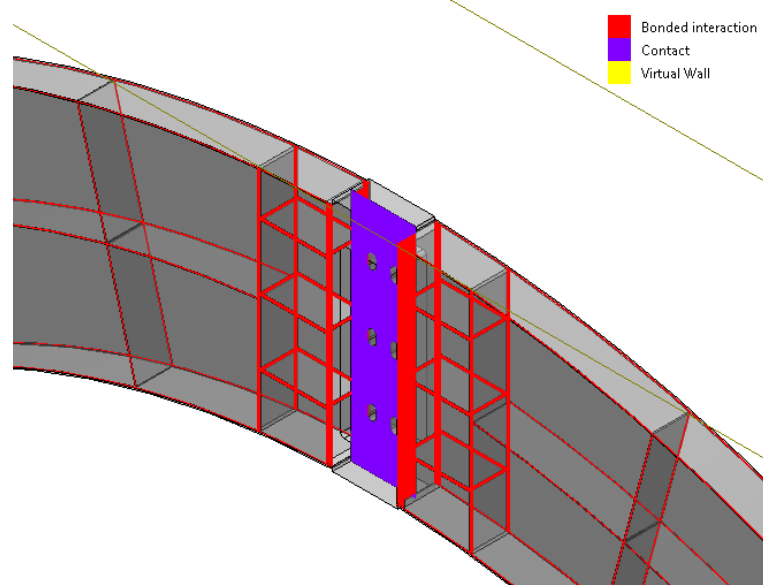


Figure 37. Interactions used the joint of ring halves.

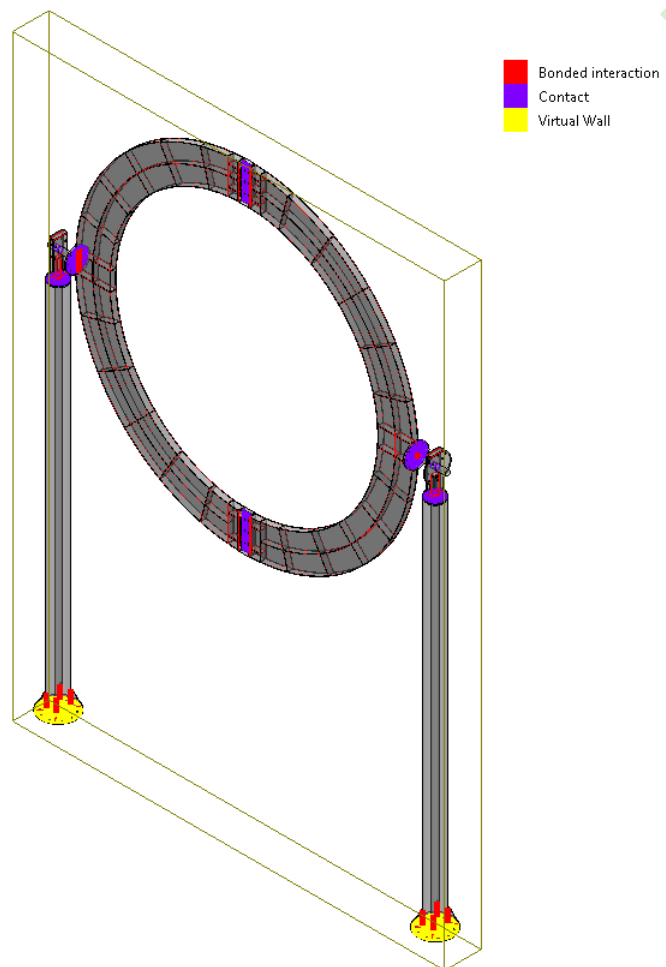


Figure 38. Interactions of the whole structure.

Wind load, snow load and gravity are applied to the ring like presented in Figure 39 and Figure 40.

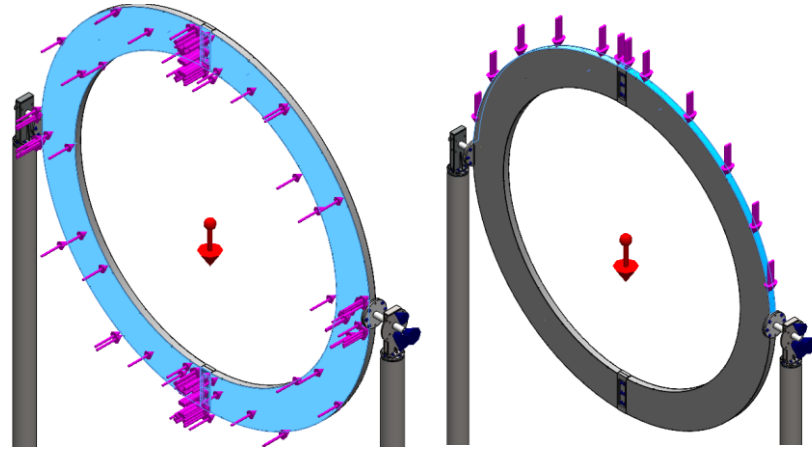


Figure 39. Forces applied to FE-model

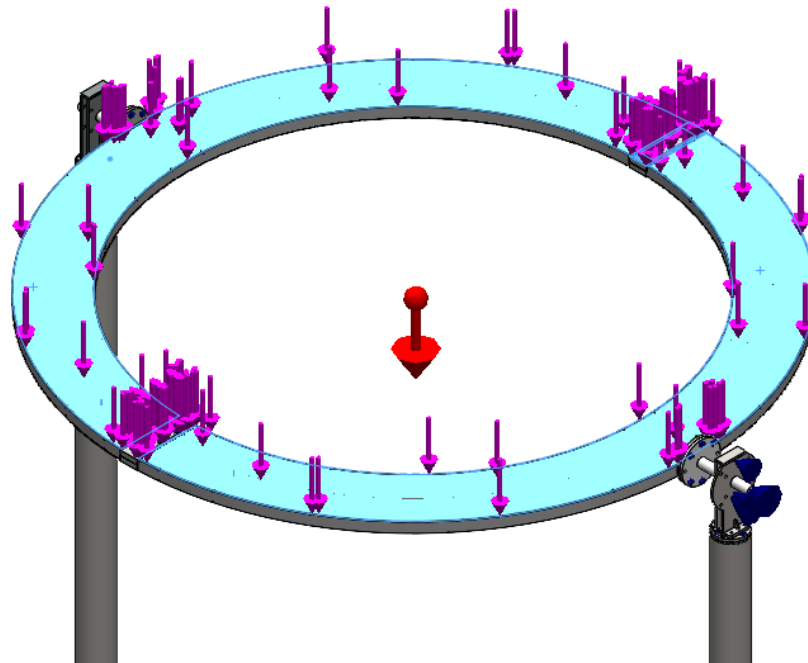


Figure 40. Forces applied to FE-model

The FE-model is meshed by using automatic meshing tool in Solidworks Simulation. Mesh control is applied to parts that are modelled by using solid elements except the concrete core. Mesh properties are presented in Table 5 and meshed model in Figure 41.

Table 5. Mesh properties used in FE-model

Element type	Mesher	Maximum element size	Minimum element size
Shell	Blended curvature-based mesh	50 mm	7.5 mm
Solid	Blended curvature-based mesh	15 mm	7.5 mm
Solid (concrete core)	Blended curvature-based mesh	50 mm	7.5 mm

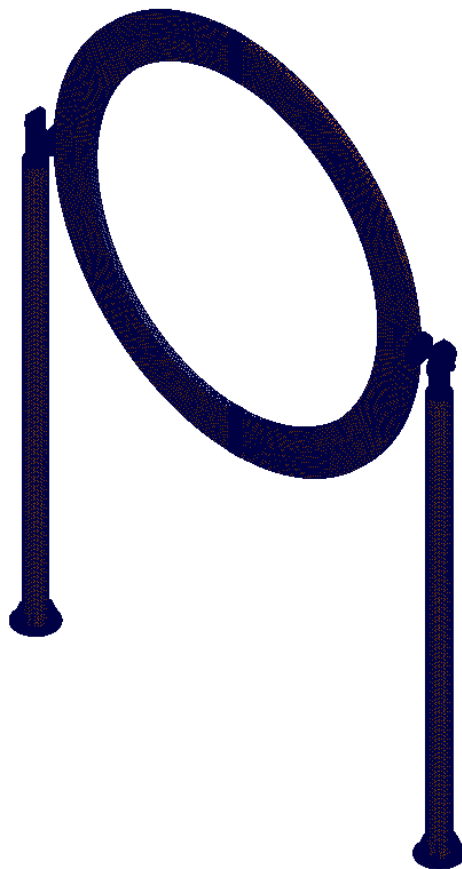


Figure 41. Meshed model used in load cases 1-8. Orange color indicates the bottom side of shell elements.

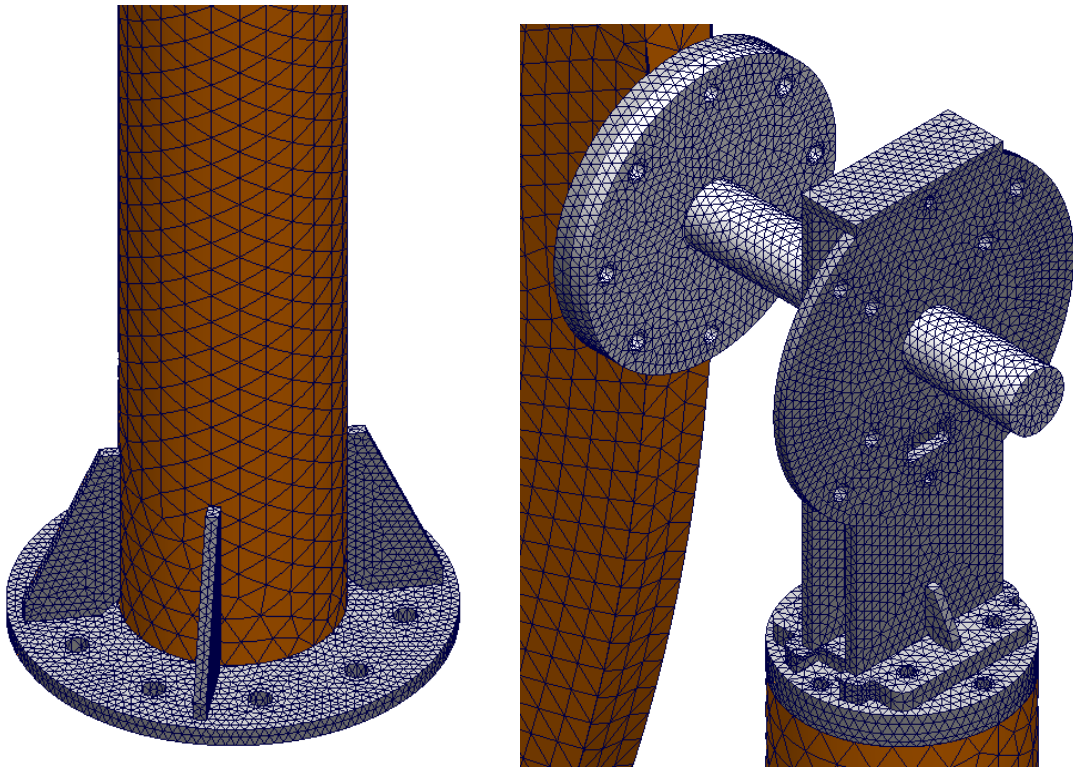


Figure 42. Element mesh at bottom and top end of the posts. Orange color indicates the bottom side of shell elements.

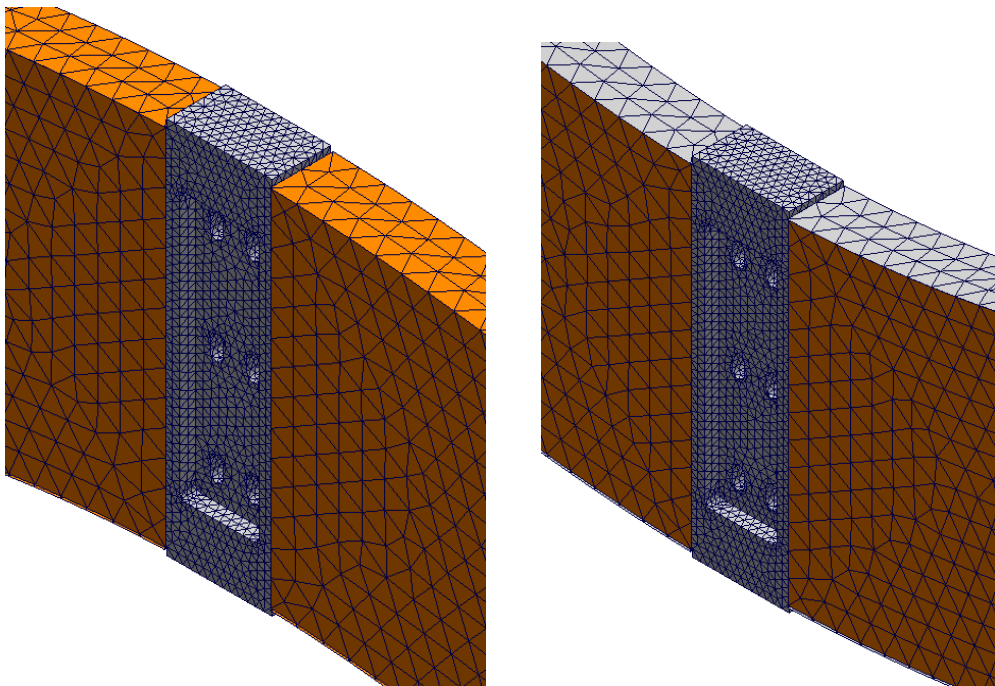


Figure 43. Element mesh at the joints of ring halves. Orange color indicates the bottom side of shell elements.

The mounting bracket for electric motor is also analyzed to ensure that it can resist the torque caused by storm wind when the ring is locked. Bracket is modelled with blended-curvature based mesher with 10 mm maximum and 5 mm minimum element size. Hollow section beams are modelled with shell elements and plates with solid elements. The FE-model is fixed to virtual wall with M24-foundation bolts and additional geometry is placed to present the electric motor. That additional geometry is connected to bracket with 18 M12-bolted connections. Torque force is applied to the outer surface of the additional geometry and the value for that is calculated with equation:

$$M_B = \frac{1}{2} F_{R,wind} \cdot 1700 \text{ mm} = 16\,830 \text{ Nm} \quad (32)$$

Values used in the equation are presented in Figure 44, used FE-model in Figure 45 and meshed FE-model in Figure 46.

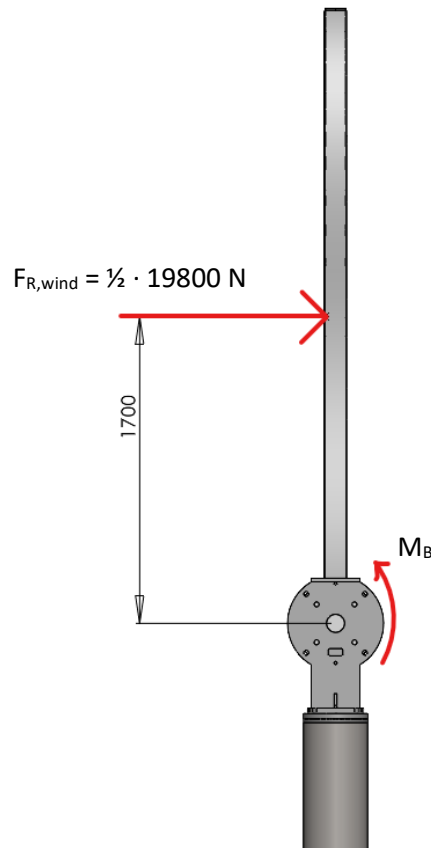


Figure 44. Expression for the torque affecting in the mounting bracket

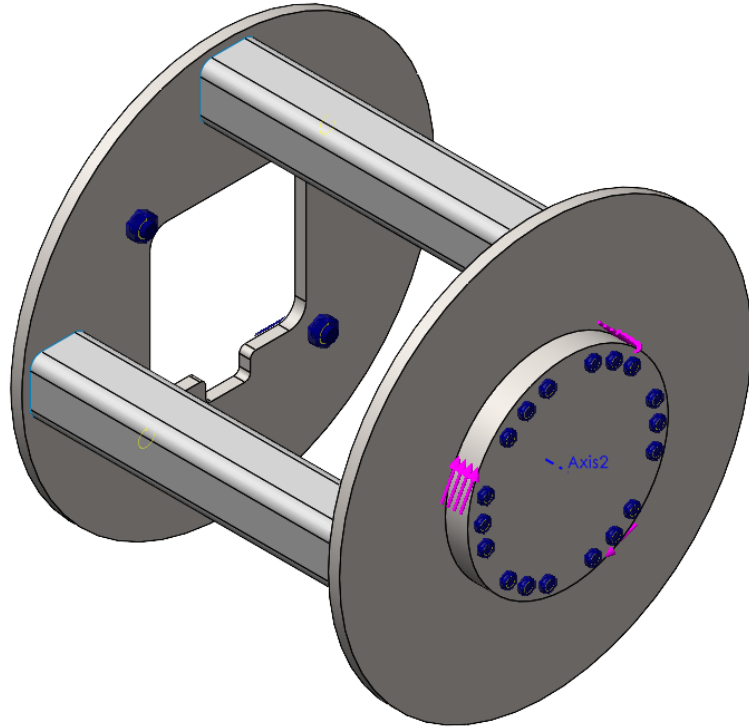


Figure 45. Forces and boundary conditions used in the analysis

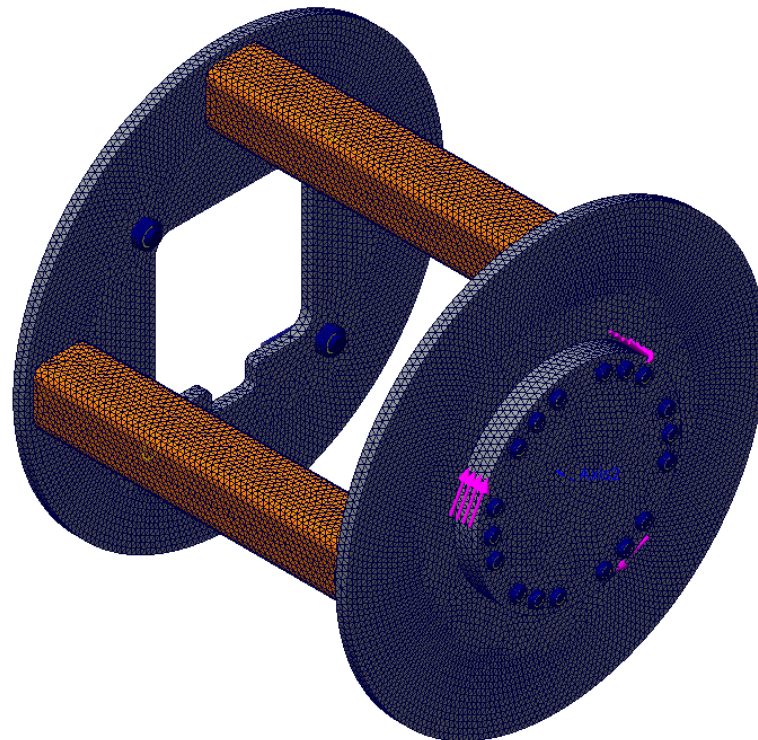


Figure 46. Meshed FE-model for mounting bracket analysis. Orange color indicates the bottom side of shell elements.

3.3 Natural frequency and vibration

Natural frequency analysis is performed by using Solidworks Simulation -add-in. Analysis is performed as a frequency analysis and by using Intel Direct Sparse -solver. In frequency analysis no penetration contacts cannot be used so all the joints are bonded together hence the bolted connections are not used. FE-model is meshed with same element sizes than in static analysis and same material models are used. Global motion of the structure is restrained with *fixed*-boundary condition that is place to the bottom end of the posts. Fixed boundary condition is presented in Figure 47 and global interactions in Figure 48.

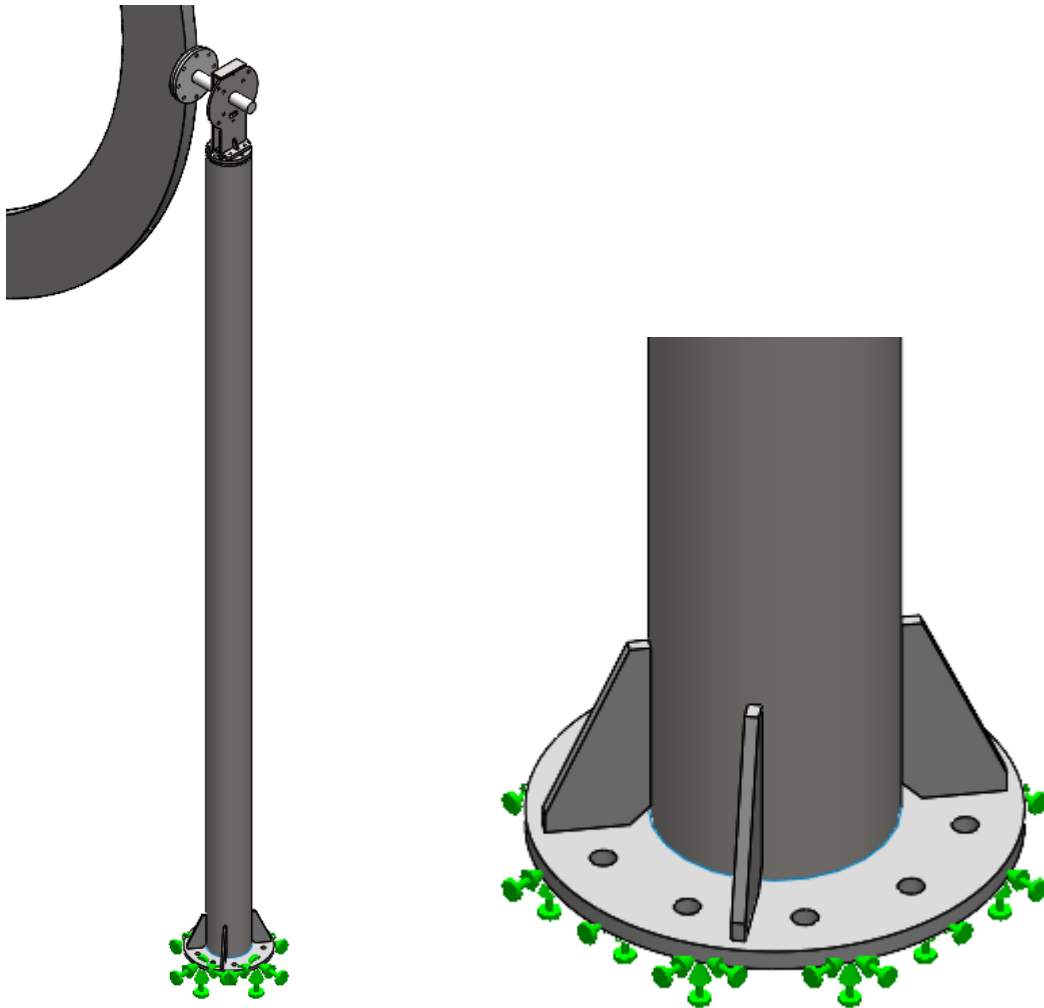


Figure 47. Fixed boundary condition at the bottom face of the posts.

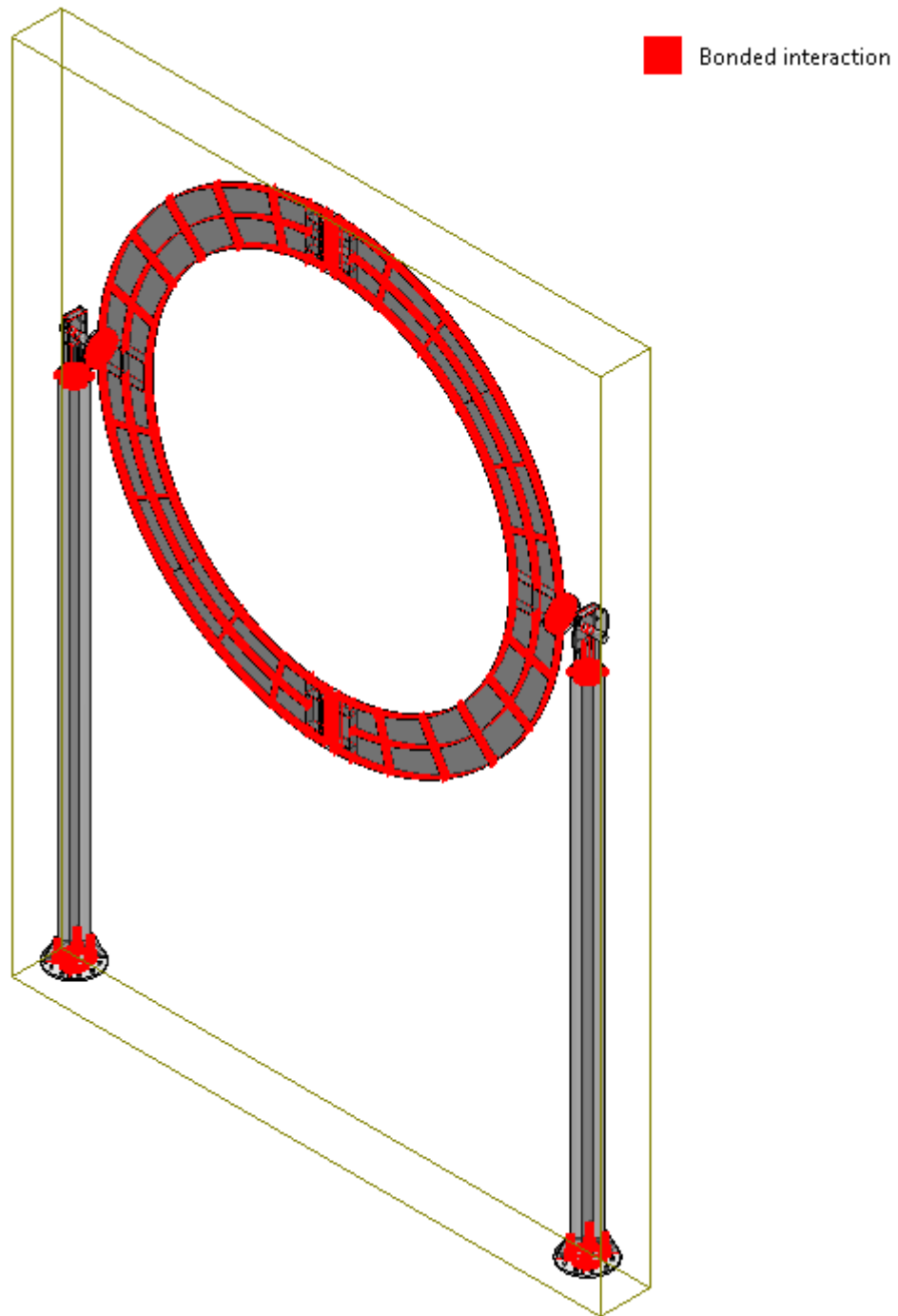


Figure 48. Global interactions of the FE-model

3.4 Fatigue analysis

Vibration that is caused by vortex shedding may cause fatigue crack initiation in the structure. Therefore, the lateral forces and number of cycles that occurs by vortex shedding in different natural frequencies are calculated based on the equations presented in chapter 2.1.3. Vortex shedding may occur on the surface of the posts or the ring therefore both cases are examined. Calculated forces and number of cycles are used in fatigue assessment and fatigue life is examined for different welded details using Hot Spot -method. Fatigue assessment is also conducted with the wind load that is caused by mean wind velocity (5 m/s) in Hämeenlinna area. Forces caused by vortex shedding, number of cycles and critical wind velocities are presented in Table 6 and Table 7.

Table 6. Forces caused by vortex shedding and number of cycles on the surface of the posts and critical wind velocities.

<i>Natural frequency [Hz]</i>	<i>Lateral force [N]</i>	<i>Displacement [mm] (only mode shape 1)</i>	<i>Number of cycles</i>	<i>Critical wind velocity [m/s]</i>
2.0	204.7	0.3208	210 029 559	3.9
2.4	297.7	-	243 094 796	4.7
3.0	465.1	-	224 618 221	5.9
3.3	562.8	-	193 198 739	6.5
6.6	2250.91	-	815 453	13.0
14.0	10128.1	-	1	27.6
14.4	10715.1	-	0	28.4
15.8	12899.9	-	0	31.1
16.2	13561.3	-	0	31.9
16.9	14758.6	-	0	33.3
21.2	23224.3	-	0	41.8
25.8	34396.2	-	0	50.8

Table 7. Forces caused by vortex shedding and number of cycles on the surface of the ring and critical wind velocities.

<i>Natural frequency [Hz]</i>	<i>Lateral force [N]</i>	<i>Displacement [mm] (only mode shape 1)</i>	<i>Number of cycles</i>	<i>Critical wind velocity [m/s]</i>
2.0	3.8	0.016	122 852 469	2.2
2.4	5.5	-	189 317 101	2.6
3.0	8.6	-	292 840 327	3.3
3.3	10.4	-	340 191 680	3.6
6.6	41.4	-	259 109 246	7.2
14.0	186.2	-	42 427	15.4
14.4	197	-	20 380	15.8
15.8	237.2	-	1 284	17.3
16.2	249.4	-	551	17.8
16.9	271.4	-	118	18.6
21.2	427	-	1	23.3
25.8	632.4	-	0	28.4

To simplify the analysis process, the Hot Spot -models are analysed with 1000 N reference force and stresses at critical points are determined. After that, the stresses in cases presented in Table 6 and Table 7 are extrapolated from the reference stresses.

Hot Spot -stress may be calculated by using equation 31 and local stresses $\sigma_{0.4t}$ and $\sigma_{1.0t}$ are determined by using FE-analysis. After the Hot Spot -stress is determined, the fatigue life may be determined by using equation (Niemi, Fricke & Maddox 2018 p. 72):

$$N = 2 \cdot 10^6 \cdot \frac{FAT^3}{\Delta\sigma_{hs}^3} \quad (33)$$

where FAT is the fatigue class of the welded detail and $\Delta\sigma_{hs}$ is the calculated Hot Spot -stress. The value of FAT is taken as 90 MPa in load-carrying fillet welds and 100 MPa in non-load carrying welds (Niemi, Fricke & Maddox 2018 p. 41).

Fatigue assessment is performed for the most critical details of the structure. These details are presented Figure 49. Hot Spot -models are modelled by using the requirements presented in chapter 3.1.

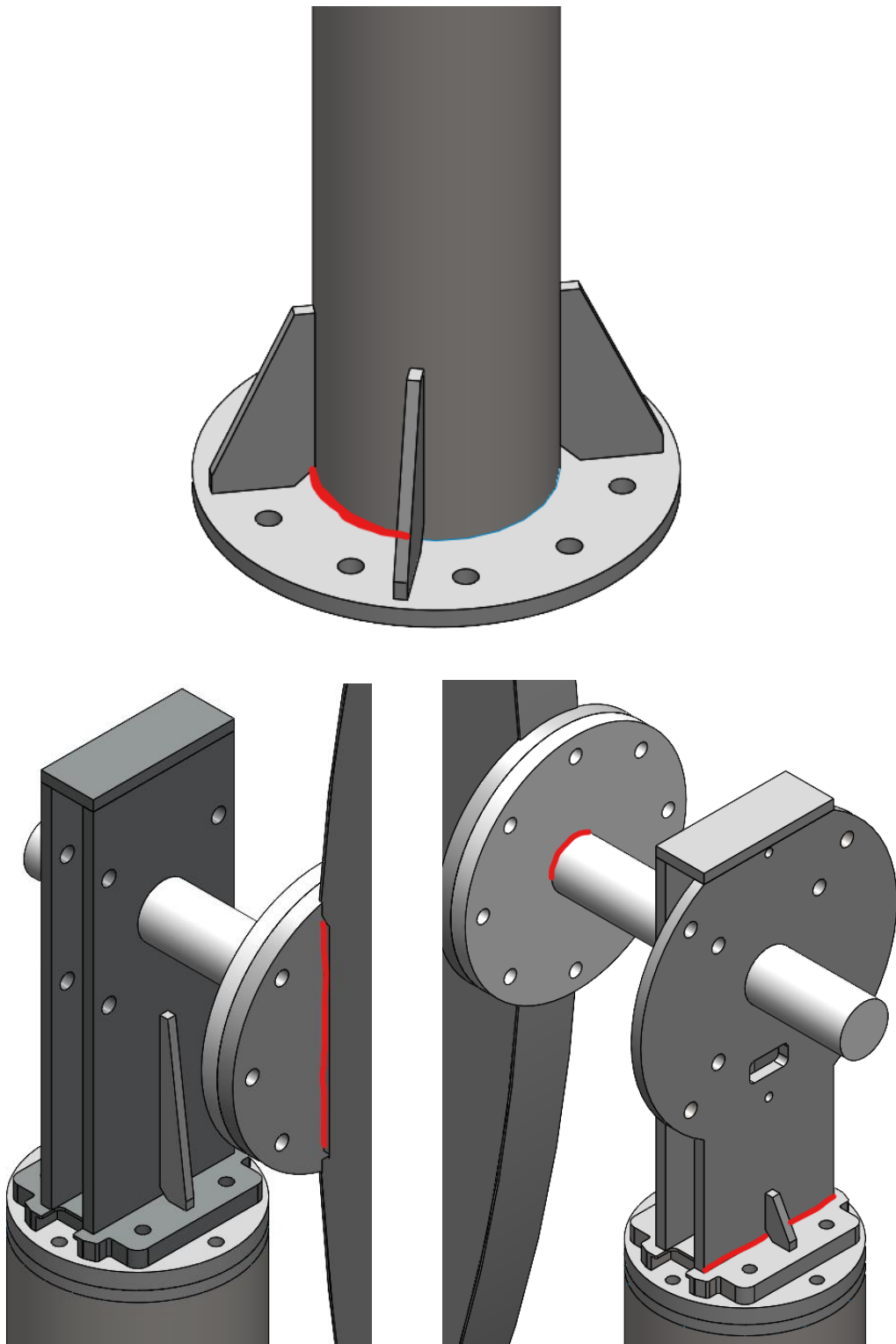


Figure 49. Welded details that are the most critical for fatigue crack initiation. Possible crack initiation location is presented with the red line. In the posts and in the shaft carrier the upper weld toes are critical, in the shafts both weld toes are examined and, in the ring, the lower weld toe is critical.

Element mesh is created so that nodes are located at distance of $0.4t$ and $1.0t$ from the weld toe and blended curvature based mesher is used. Mesh control is applied to the areas where the Hot Spot -stresses will be obtained. In those areas the maximum element size is 2 mm and minimum 1.5 mm. No penetration contacts are applied to the joints that are not welded together. Hot Spot -models with boundary conditions and forces are presented in Figure 50 - Figure 52 and meshed models in Figure 53 - Figure 55.

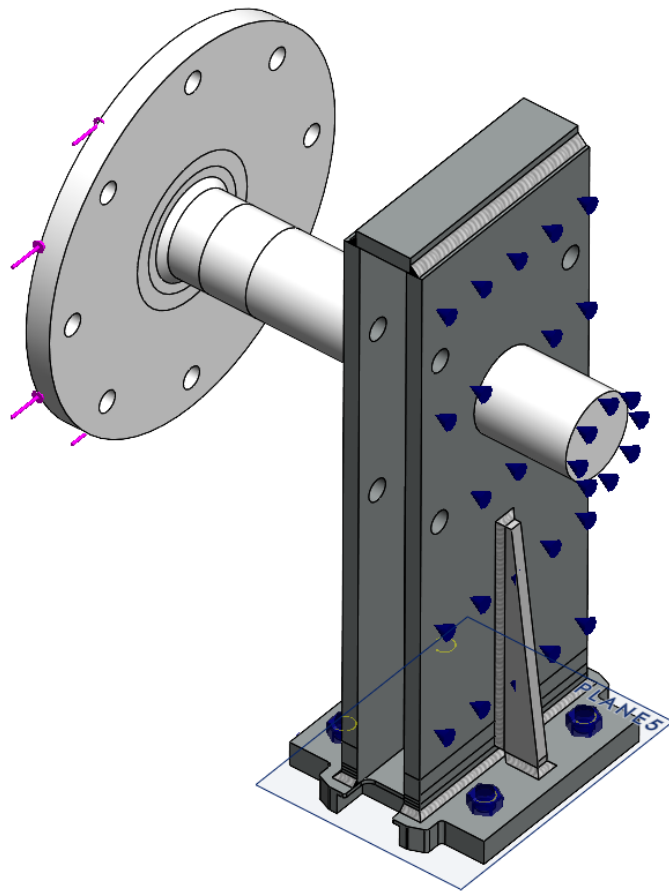


Figure 50. Hot Spot -model of the shaft and the shaft carrier. Reference force 1000 N is applied to the end of the ring attaching plate.

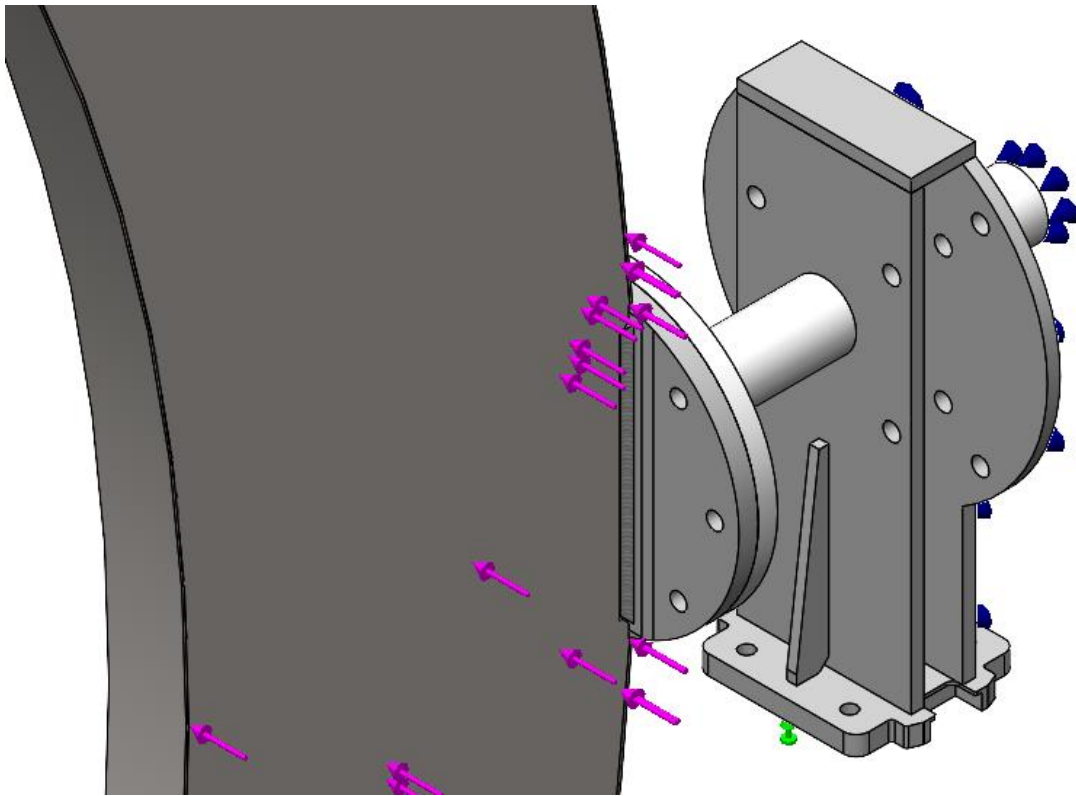


Figure 51. Hot Spot -model of the ring. Reference force 1000 N is applied to the face of the ring.

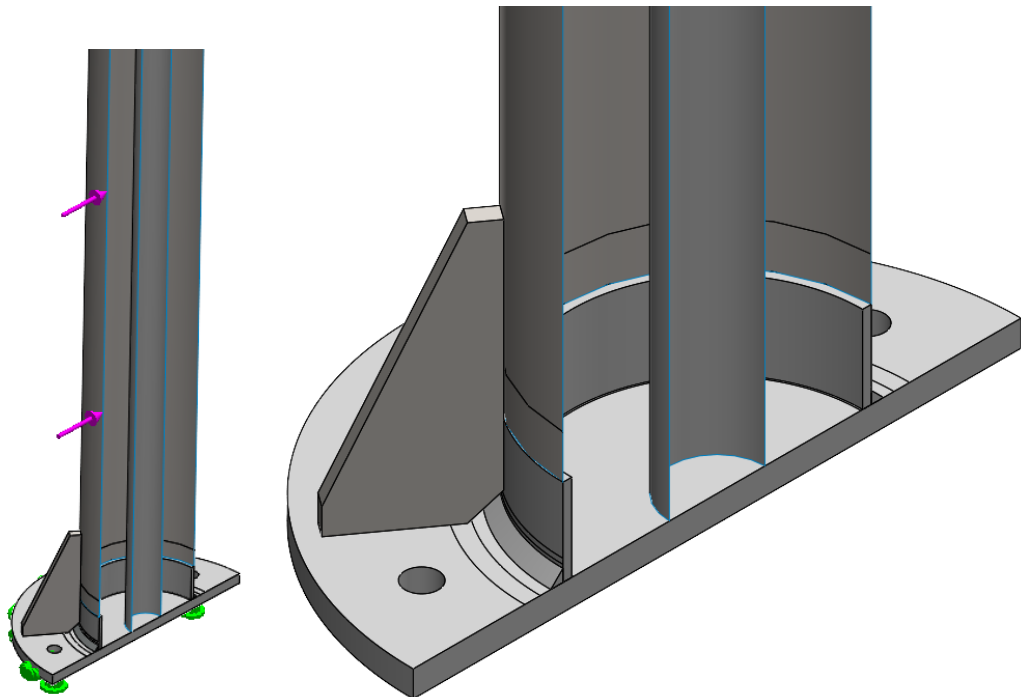


Figure 52. Symmetric Hot Spot -model of the post. Reference force 1000 N is applied to the face of the post.

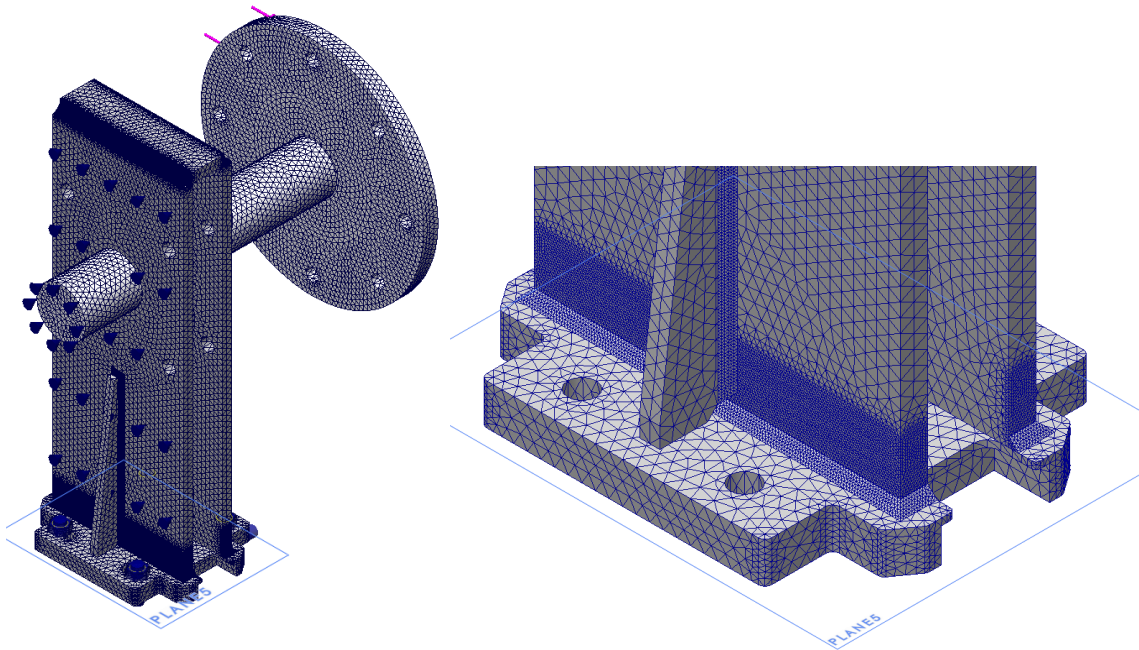


Figure 53. Meshed Hot Spot -model of shaft and shaft carrier. Maximum global element size is 10 mm and minimum 0.5 mm. Mesh control is added to Hot Spot -areas and the maximum value for element size is 2 mm and minimum 1.5 mm.

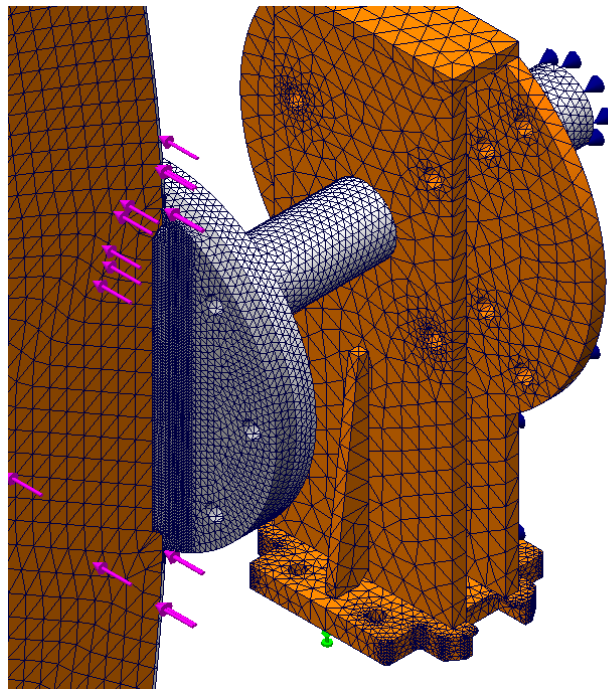


Figure 54. Meshed Hot Spot -model of the ring. Maximum global element size is 30 mm and minimum 3.6 mm. Mesh control is added to Hot Spot -areas and the maximum value for element size is 2 mm and minimum 1.5 mm.

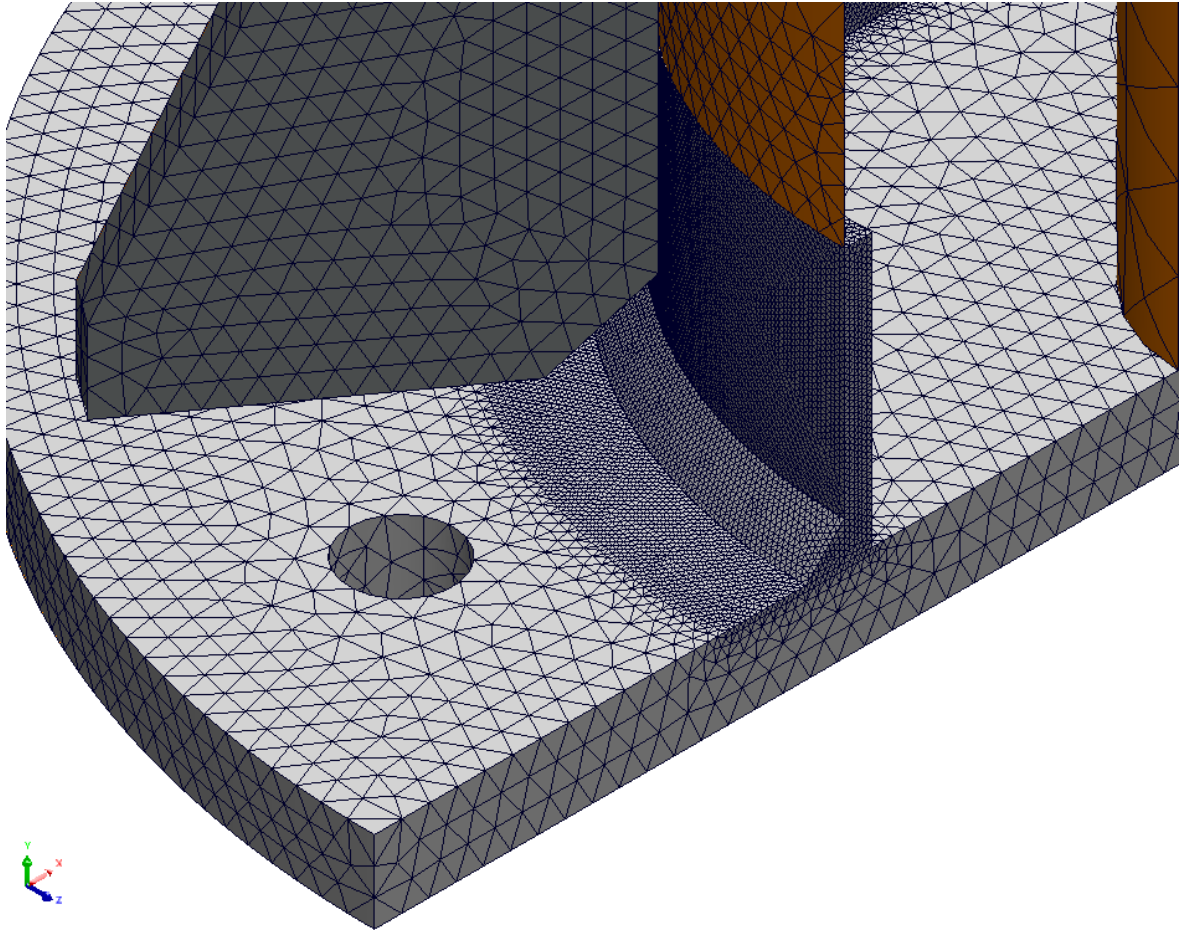


Figure 55. Meshed symmetric Hot Spot -model of the ring. Maximum global element size is 30 mm and minimum 1.0 mm. Hot Spot -area is modelled with solid elements and the rest of the post is modelled with shell elements. Mesh control is added to Hot Spot -areas and the maximum value for element size is 2 mm and minimum 1.5 mm.

3.5 Bolted joints

Capacity of the bolted joints is determined analytically according to SFS-EN 1993-1-8 and numerically by using FE-method. Fatigue assessment of the bolts is performed analytically according to SFS-EN 1993-1-9 with the loads determined by FE-method.

3.5.1 Static capacity

Capacity of bolted joints is determined according to SFS-EN 1993-1-8. Bolted joints are divided into five different categories that depend on the required properties of the joint (SFS-EN 1993-1-8 p. 21). Categories are presented in Figure 56.

Category	Criteria	Remarks
Shear connections		
A bearing type	$F_{v,Ed} \leq F_{v,Rd}$ $F_{v,Ed} \leq F_{b,Rd}$	No preloading required. Bolt classes from 4.6 to 10.9 may be used.
B slip-resistant at serviceability	$F_{v,Ed,ser} \leq F_{s,Rd,ser}$ $F_{v,Ed} \leq F_{v,Rd}$ $F_{v,Ed} \leq F_{b,Rd}$	Preloaded 8.8 or 10.9 bolts should be used. For slip resistance at serviceability see 3.9.
C slip-resistant at ultimate	$F_{v,Ed} \leq F_{v,Rd}$ $F_{v,Ed} \leq F_{b,Rd}$ $F_{v,Ed} \leq N_{net,Rd}$	Preloaded 8.8 or 10.9 bolts should be used. For slip resistance at ultimate see 3.9. $N_{net,Rd}$ see 3.4.1(1) c).
Tension connections		
D non-preloaded	$F_{t,Ed} \leq F_{t,Rd}$ $F_{t,Ed} \leq B_{p,Rd}$	No preloading required. Bolt classes from 4.6 to 10.9 may be used. $B_{p,Rd}$ see Table 3.4.
E preloaded	$F_{t,Ed} \leq F_{t,Rd}$ $F_{t,Ed} \leq B_{p,Rd}$	Preloaded 8.8 or 10.9 bolts should be used. $B_{p,Rd}$ see Table 3.4.
The design tensile force $F_{t,Ed}$ should include any force due to prying action, see 3.11. Bolts subjected to both shear force and tensile force should also satisfy the criteria given in Table 3.4.		

Figure 56. Categories for bolted connections (SFS-EN 1993-1-8 p. 22)

In this case, bolted joints should be slip-resistant at serviceability state and bolts are preloaded when the sculpture is installed. Therefore, the categories B and D are examined. Based on the Figure 56 the requirements for the joints are:

$$F_{v,Ed,ser} \leq F_{s,Rd,ser} \quad (34)$$

$$F_{v,Ed} \leq F_{v,Rd} \quad (35)$$

$$F_{v,Ed} \leq F_{b,Rd} \quad (1)$$

$$F_{t,Ed} \leq F_{t,Rd} \quad (2)$$

$$F_{t,Ed} \leq B_{p,Rd} \quad (3)$$

where $F_{v,Ed,ser}$ is the design shear force at the serviceability limit state, $F_{s,Rd,ser}$ is the design slip resistance at the serviceability limit state, $F_{v,Ed}$ is the design shear force at the ultimate limit state, $F_{s,Rd}$ is the design slip resistance at the ultimate state, $F_{b,Rd}$ is the design bearing resistance, $F_{t,Ed}$ is the design tensile force at the ultimate limit state, $F_{t,Rd}$ is the design tension resistance and $B_{p,Rd}$ is the design punching shear resistance. (SFS-EN 1993-1-8 p. 22)

There are also maximum and minimum values for the positioning and spacing of holes for bolts. These values are presented in Figure 57 and Figure 58.

Distances and spacings, see Figure 3.1	Minimum	Maximum ^{1) 2) 3)}		
		Structures made from steels conforming to EN 10025 except steels conforming to EN 10025-5		Structures made from steels conforming to EN 10025-5
		Steel exposed to the weather or other corrosive influences	Steel not exposed to the weather or other corrosive influences	Steel used unprotected
End distance e_1	$1,2d_0$	$4t + 40$ mm		The larger of $8t$ or 125 mm
Edge distance e_2	$1,2d_0$	$4t + 40$ mm		The larger of $8t$ or 125 mm
Distance e_3 in slotted holes	$1,5d_0$ ⁴⁾			
Distance e_4 in slotted holes	$1,5d_0$ ⁴⁾			
Spacing p_1	$2,2d_0$	The smaller of $14t$ or 200 mm	The smaller of $14t$ or 200 mm	The smaller of $14t_{min}$ or 175 mm
Spacing $p_{1,0}$		The smaller of $14t$ or 200 mm		
Spacing $p_{1,i}$		The smaller of $28t$ or 400 mm		
Spacing p_2 ⁵⁾	$2,4d_0$	The smaller of $14t$ or 200 mm	The smaller of $14t$ or 200 mm	The smaller of $14t_{min}$ or 175 mm

Figure 57. Minimum and maximum dimensions of holes for bolts (SFS-EN 1993-1-8 p. 23)

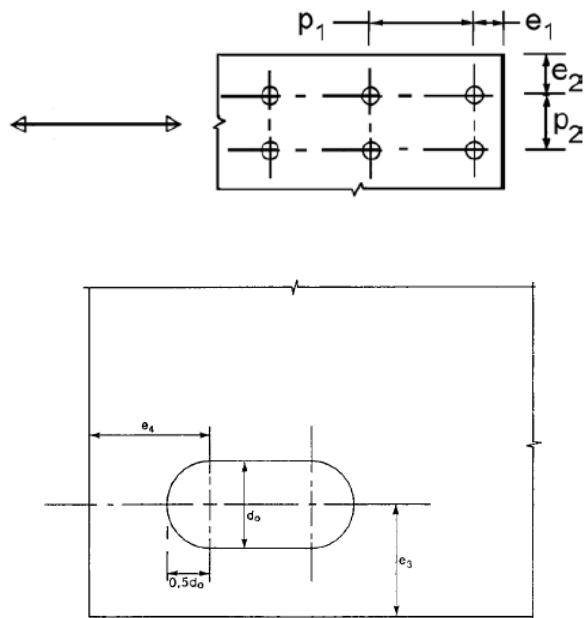


Figure 58. Symbols for edge distances, end distances and spacing of bolts (SFS-EN 1993-1-8 p. 24)

The shear resistance of the bolt may be calculated by using equation:

$$F_{v,Rd} = \frac{\alpha_v \cdot f_{ub} \cdot A_s}{\gamma_{M2}} \quad (39)$$

where factor α_v is factor that depends on the strength class of a bolt, f_{ub} is ultimate strength of a bolt, A_s is the tensile stress area of the bolt and γ_{M2} is the partial safety factor of the joint. (SFS-EN 1993-1-8 p. 27). Factor α_v can be determined from Table 8, ultimate strength of the bolt f_{ub} from Figure 59, tensile stress area A_s from Table 9 and partial safety factor γ_{M2} from Figure 60. Recommended values for partial safety factors are presented in Table 10.

Table 8. Values for factor α_v (SFS-EN 1993-1-8 p. 27).

Bolt class	Factor α_v
4.6, 5.6 or 8.8	0,6
4.8, 5.8, 6.8 or 10.9	0,5

Bolt class	4.6	4.8	5.6	5.8	6.8	8.8	10.9
f_{yb} (N/mm ²)	240	320	300	400	480	640	900
f_{ub} (N/mm ²)	400	400	500	500	600	800	1000

Figure 59. Nominal values for the yield and ultimate strength for bolts (SFS-EN 1993-1-8 p. 20).

Table 9. Tensile stress areas of M20-, M24- and M36-bolts. (Björk et al. 2014 p. 134)

	Size		
	M20	M24	M36
Tensile stress area A_s	245 mm ²	353 mm ²	817 mm ²

Resistance of members and cross-sections	γ_{M0} , γ_{M1} and γ_{M2} see EN 1993-1-1
Resistance of bolts	γ_{M2}
Resistance of rivets	
Resistance of pins	
Resistance of welds	
Resistance of plates in bearing	
Slip resistance - at ultimate limit state (Category C) - at serviceability limit state (Category B)	γ_{M3} $\gamma_{M3,ser}$
Bearing resistance of an injection bolt	γ_{M4}
Resistance of joints in hollow section lattice girder	γ_{M5}
Resistance of pins at serviceability limit state	$\gamma_{M6,ser}$
Preload of high strength bolts	γ_{M7}
Resistance of concrete	γ_c see EN 1992

Figure 60. Partial safety factors of bolted joints (SFS-EN 1993-1-8 p. 18).

Table 10. Recommended values for partial safety factors (SFS-EN 1993-1-8 p. 18).

Safety factor	γ_{M2}	γ_{M3}	$\gamma_{M3,ser}$	γ_{M4}	γ_{M5}	$\gamma_{M6,ser}$	γ_{M7}
Value	1.25	1.25	1.1	1.0	1.0	1.0	1.1

The tension resistance $F_{t,Rd}$ of the bolt may be determined by using equation:

$$F_{t,Rd} = \frac{k_2 \cdot f_{ub} \cdot A_s}{\gamma_{M2}} \quad (40)$$

where k_2 is a factor that depends on the shape of the bolt. For countersunk bolts k_2 is taken as the value of 0.63 and otherwise the value of 0.9 is used. (SFS-EN 1993-1-8 p. 27).

The bearing resistance $F_{b,Rd}$ can be determined by using equation:

$$F_{b,Rd} = \frac{k_1 \cdot \alpha_b \cdot f_{ub} \cdot d \cdot t}{\gamma_{M2}} \quad (41)$$

where k_1 for edge bolts is the smallest of;

$$k_1 = 2.8 \cdot \frac{e_2}{d_0} - 1.7 \quad \text{or} \quad 2.5 \quad (42)$$

Factor k_1 for inner bolts is the smallest of;

$$k_1 = 1.4 \cdot \frac{p_2}{d_0} - 1.7 \quad \text{or} \quad 2.5 \quad (43)$$

Factor α_b for single holes is the smallest of;

$$\alpha_b = \frac{f_{ub}}{f_u} \quad \text{or} \quad 1.0 \quad (44)$$

and in the direction of load transfer;

$$\text{End bolts:} \quad \alpha_b = \frac{e_1}{3d_0} \quad (45)$$

$$\text{Inner bolts:} \quad \alpha_b = \frac{p_1}{3d_0} - \frac{1}{4} \quad (46)$$

(SFS-EN 1993-1-8 p. 27).

The punching shear resistance may be calculated by using expression:

$$B_{p,Rd} = \frac{0.6\pi \cdot d_m \cdot t_p \cdot f_u}{\gamma_{M2}} \quad (47)$$

where d_m is the bolt head diameter and t_p is the thickness of plate. (SFS-EN 1993-1-8 p. 27).

The design slip resistance $F_{s,Rd}$ can be determined by following equation:

$$F_{s,Rd} = \frac{k_s n \mu}{\gamma_{M3}} \cdot F_{p,C} \quad (48)$$

where k_s is the factor given in Figure 61, n is the number of friction surfaces, μ is the slip factor given in Figure 62 and $F_{p,C}$ is the preloading force that should be taken as (SFS-EN 1993-1-8 p. 30):

$$F_{p,C} = 0.7 f_{ub} \cdot A_s \quad (49)$$

Description	k_s
Bolts in normal holes.	1,0
Bolts in either oversized holes or short slotted holes with the axis of the slot perpendicular to the direction of load transfer.	0,85
Bolts in long slotted holes with the axis of the slot perpendicular to the direction of load transfer.	0,7
Bolts in short slotted holes with the axis of the slot parallel to the direction of load transfer.	0,76
Bolts in long slotted holes with the axis of the slot parallel to the direction of load transfer.	0,63

Figure 61. Values for factor k_s (SFS-EN 1993-1-8 p. 30).

Class of friction surfaces (see 1.2.7 Reference Standard: Group 7)	Slip factor μ
A	0,5
B	0,4
C	0,3
D	0,2

Figure 62. Values for slip factor μ (SFS-EN 1993-1-8 p. 31).

For a category B joints the slip resistance $F_{s,Rd,ser}$ should be taken as:

$$F_{s,Rd,ser} = \frac{k_s \cdot n \cdot \mu \cdot (F_{p,C} - 0.8F_{t,Ed,ser})}{\gamma_{M3,ser}} \quad (50)$$

where $F_{t,Ed,ser}$ is the design tensile force at serviceability limit state. (SFS-EN 1993-1-8 p. 31).

3.5.2 Tightening torque

Preload force for each bolt size is determined by using equation 49. After the preload force is known the tightening torque may be determined by equation (Björk et al. 2014 p. 143):

$$M_A = \frac{1}{2} \cdot F_{p,C} \cdot (1.155 \cdot \mu_G \cdot d_2 \cdot \mu_K \cdot D_{km} + \frac{P}{\pi}) \quad (51)$$

where $F_{p,C}$ is preload force, μ_G is the friction coefficient of threads, d_2 is the pitch diameter of bolt, μ_K is the friction coefficient of bolt's head, D_{km} is the diameter of contact area between head and plate and P is the pitch of thread. Friction coefficients are chosen based on the material and surface finish used in the joint. In this case friction coefficient are taken as 0.15 (Björk et al. 2014 p. 144).

3.5.3 Fatigue of bolts

Fatigue assessment of bolts is determined according to SFS-EN 1993-1-9. Possible fatigue failure in bolts may occur by the effect of tensile or shear force. When determining fatigue effects of tensile force, the preload force may be taken account in the assessment (SFS-EN 1993-1-9 p. 21). In this case tensile forces at serviceability state are lower than the preload force. Therefore, the tensile fatigue is not threat for stability of the sculpture. However, the shear fatigue should be examined.

The shear fatigue is examined in the situation where the sculpture is rotating at maximum operating wind velocity (10 m/s). The shear fatigue strength for constant amplitude stresses may be determined by the following equation (SFS-EN 1993-1-9 p. 14):

$$\Delta\tau_R^m \cdot N_R = \Delta\tau_C^m \cdot 2 \cdot 10^6 \quad \text{when } N \leq 10^8 \text{ and } m = 5 \quad (52)$$

where $\Delta\tau_R$ is shear stress range, N_R is total amount of cycles and $\Delta\tau_C$ is a shear fatigue class.

Equation 52 may be adjusted to the form where the maximum stress range is solved:

$$\Delta\tau_R = \sqrt[m]{\frac{\Delta\tau_C^m \cdot 2 \cdot 10^6}{N_R}} \quad (53)$$

The fatigue class τ_C and factor m may be determined from the Figure 63.

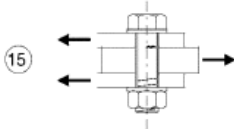
100 m = 5		<p><u>Yksi- tai kaksileikkeiset leikkausrasitettut ruuvit:</u> Kierteet eivät ole leikkaustasossa 15) — Soviteruuvit — tavalliset ruuvit, kun kuorman suunta ei muutu (ruuvien lujuusluokat 5.6, 8.8 tai 10.9).</p>	15) $\Delta\tau$ lasketaan ruuvin kierteettömän varren pinta-alan mukaan.
--------------	---	---	--

Figure 63. Shear fatigue class for bolted joint (SFS-EN 1993-1-9 p. 20)

The cut off limit $\Delta\tau_L$ which is the lowest stress range that may lead to fatigue failure may be calculated by using the equation (SFS-EN 1993-1-9 p. 15):

$$\Delta\tau_L = 0.457 \cdot \Delta\tau_C \quad (54)$$

3.6 Welds

The design resistance of fillet welds is determined by simplified method according to SFS-EN 1993-1-8. The simplified method assumes that all the applied forces are affecting on

shear direction. Therefore, the welds should satisfy the following criterion (SFS-EN 1993-1-8 p. 44):

$$F_{w,Ed} \leq F_{w,Rd} \quad (55)$$

where $F_{w,Ed}$ is the design value for the force per unit length and $F_{w,Rd}$ is the design weld resistance per unit length.

The design force per unit length may be determined by equation:

$$F_{w,Ed} = \frac{F_R}{l_w} \quad (56)$$

where F_R is the resultant force applied to the weld and l_w is the length of the weld. In this case, the sum of the tensile and shear forces in bolted joints next to the specific weld is used for the resultant force.

The design weld resistance per unit length $F_{w,Rd}$ may be determined by using equation (SFS-EN 1993-1-8 p. 44):

$$F_{w,Rd} = \frac{\frac{f_u}{\sqrt{3}}}{\beta_w \cdot \gamma_{M2}} \cdot a \quad (57)$$

where f_u is the ultimate tensile strength of the weakest part joined, β_w is the correlation factor taken from Figure 64, γ_{M2} is the partial safety factor (= 1.25) and a is the throat thickness of the weld.

Standard and steel grade			Correlation factor β_w
EN 10025	EN 10210	EN 10219	
S 235 S 235 W	S 235 H	S 235 H	0,8
S 275 S 275 N/NL S 275 M/ML	S 275 H S 275 NH/NLH	S 275 H S 275 NH/NLH S 275 MH/MLH	0,85
S 355 S 355 N/NL S 355 M/ML S 355 W	S 355 H S 355 NH/NLH	S 355 H S 355 NH/NLH S 355 MH/MLH	0,9
S 420 N/NL S 420 M/ML		S 420 MH/MLH	1,0
S 460 N/NL S 460 M/ML S 460 Q/QL/QL1	S 460 NH/NLH	S 460 NH/NLH S 460 MH/MLH	1,0

Figure 64. Correlation factor β_w for fillet welds (SFS-EN 1993-1-8 p. 44).

After the design force and resistance are determined, the usage of the weld resistance may be calculated by equation:

$$\text{Usage of the weld resistance} = \frac{F_{w,Ed}}{F_{w,Rd}} \cdot 100 \% \quad (58)$$

4 Results

The results obtained by methods presented in chapter 3 are presented in this chapter. Stress and displacement plots are presented by using eDrawings Pro -viewer therefore plots appear visually different than in Solidworks.

4.1 Static analysis

Maximum Von Mises -stresses and displacement obtained by FE-analysis are presented in Table 11 and stress and displacement plots in Figure 65 - Figure 95. The maximum Von Mises -stresses are global maximum values estimated from the stress plots therefore local stress concentrations caused by changes in element type (shell → solid → shell) or bonded corners that are carrying the load too much due to the lack of welds in FE-model are ignored.

Table 11. The maximum Von Mises -stress and displacements obtained by FE-analysis

Load case number	Configuration and load case	Max Von Mises -stress [MPa] ($f_{y,5355} = 345$ MPa)	Max Von Mises -stress in shafts [MPa] ($f_{y,1,4401} = 200$ MPa)	Max displacement [mm]
1	Gravity only	35	36	0.2
2	Mean wind velocity 5 m/s without concrete core	69	60	21.7
3	Max operating wind velocity 10 m/s without concrete core	103	60	43.3
4	Max operating wind velocity 10 m/s with concrete core	103	60	32.6

5	Storm wind velocity 23 m/s without concrete core	207	80	99.1
6	Storm wind velocity 23 m/s with concrete core	207	80	73.5
7	Snow load, the ring perpendicular compared to ground	42	44	0.2
8	Snow load, the ring parallel compared to ground	241	160	39.3
9	Electric motor bracket, storm wind velocity 23 m/s	241	-	1.2

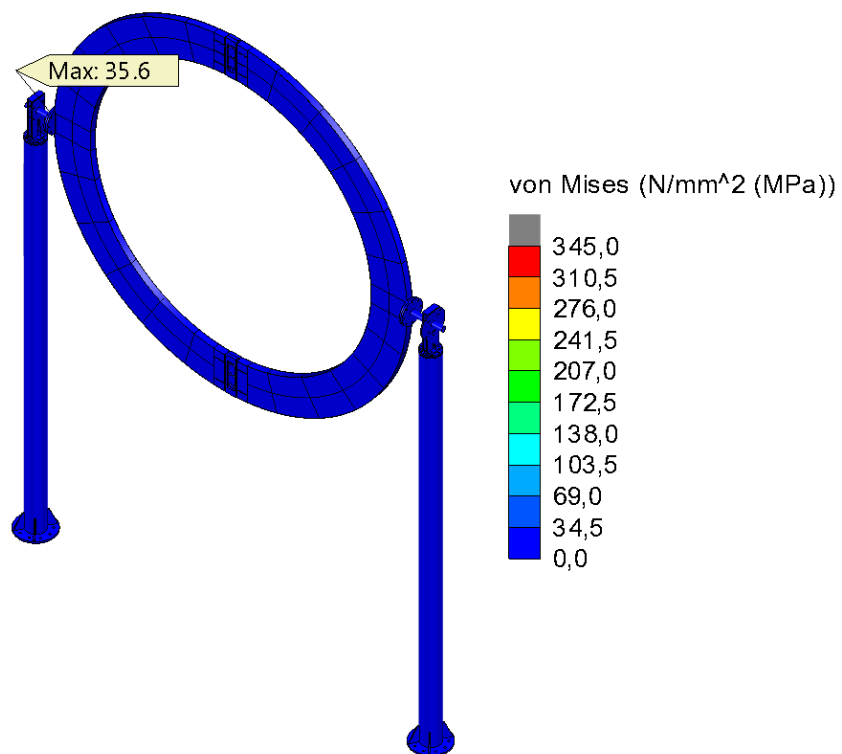


Figure 65. Von Mises -stresses at top surface of the shell elements with gravity force and **without** concrete core. Stress range 0-345 MPa, deformation scale 10.

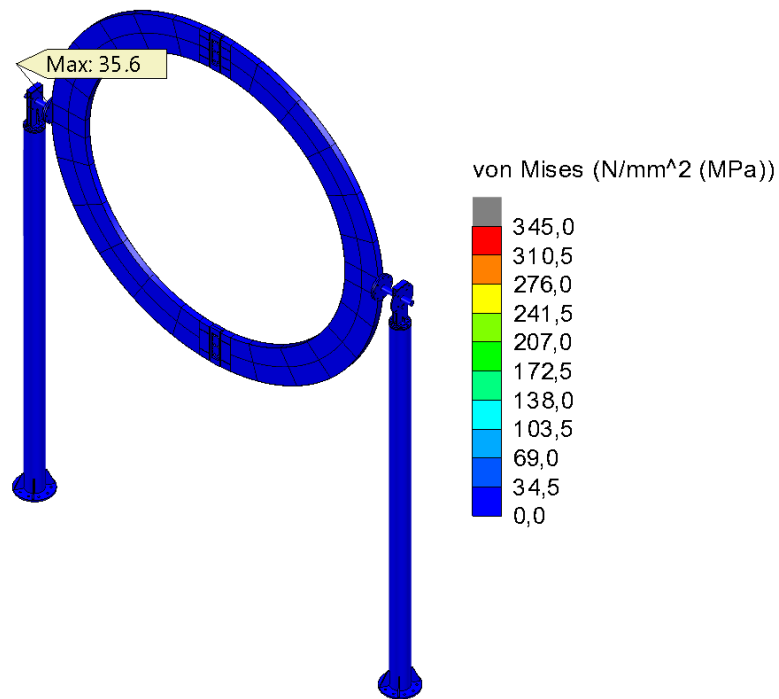


Figure 66. Von Mises -stresses at bottom surface of the shell elements with gravity force and **without** concrete core. Stress range 0-345 MPa, deformation scale 10.

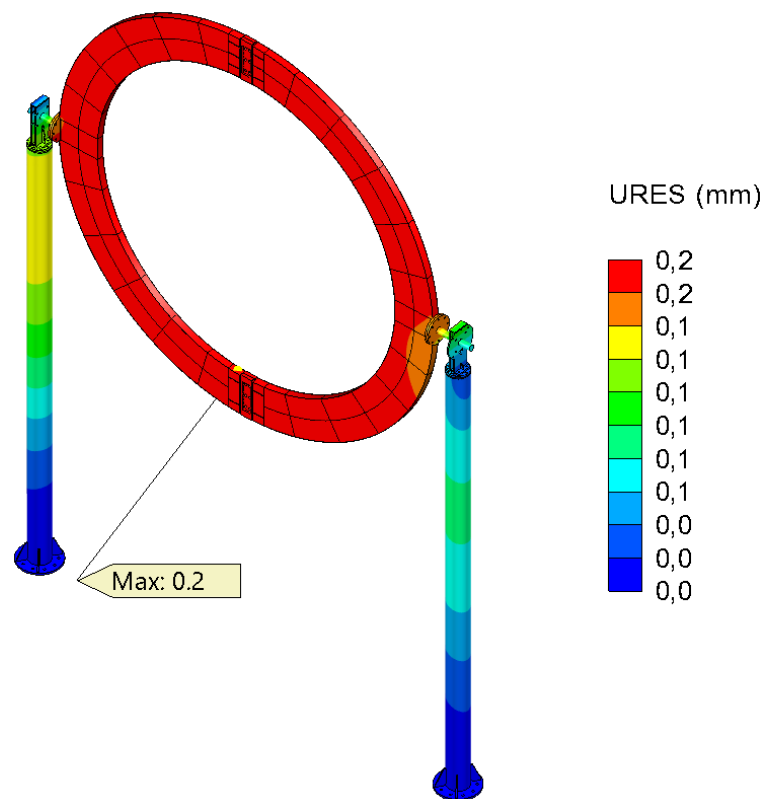


Figure 67. Resultant displacements of the structure with gravity force and **without** concrete core. Deformation scale 10.

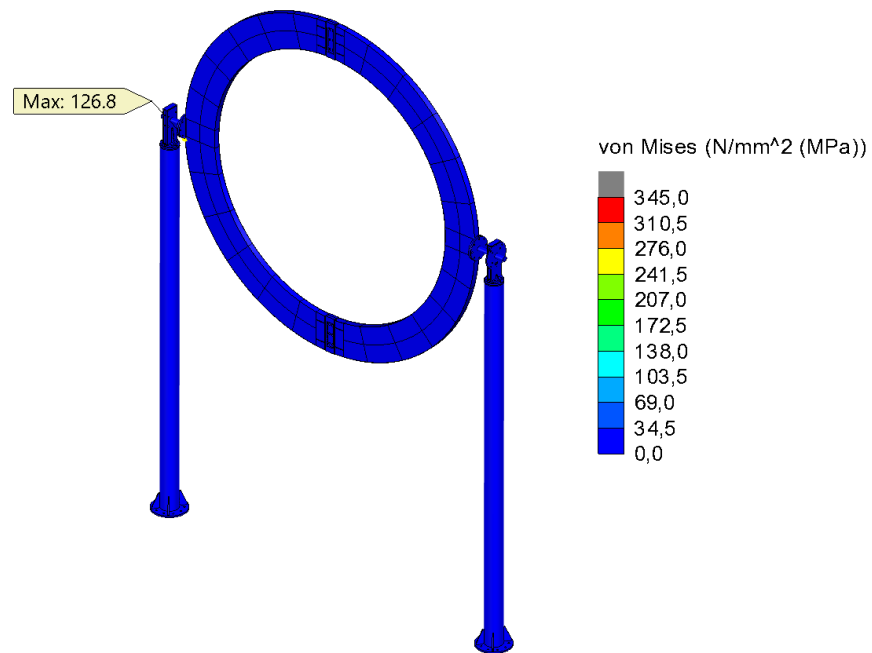


Figure 68. Von Mises -stresses at top surface of the shell elements with 5 m/s wind force and **without** concrete core. Stress range 0-345 MPa, deformation scale 10.

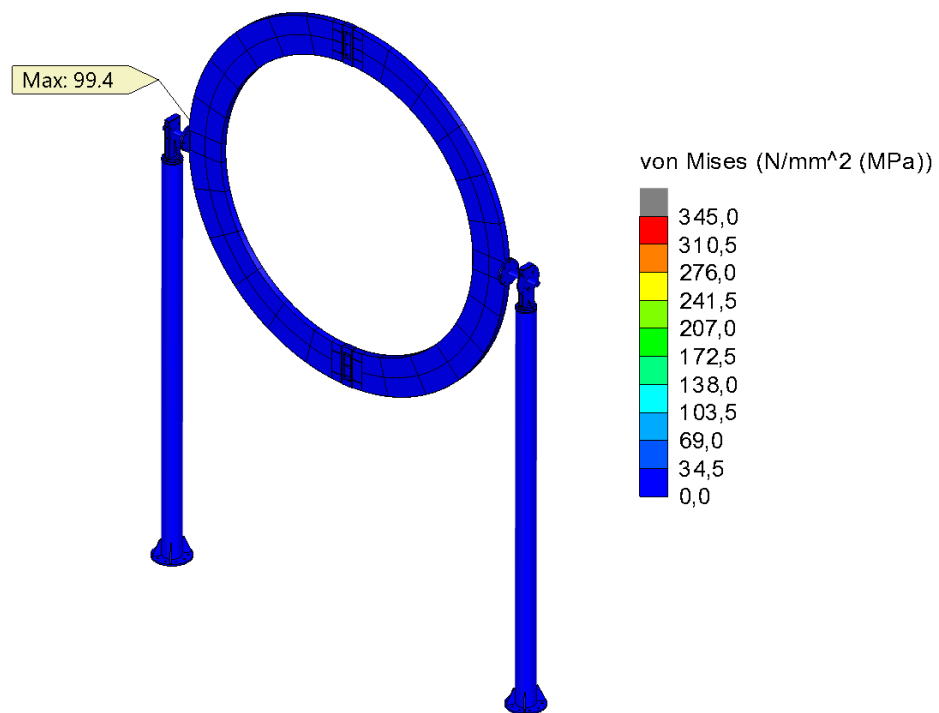


Figure 69. Von Mises -stresses at bottom surface of the shell elements with 5 m/s wind force and **without** concrete core. Stress range 0-345 MPa, deformation scale 10.

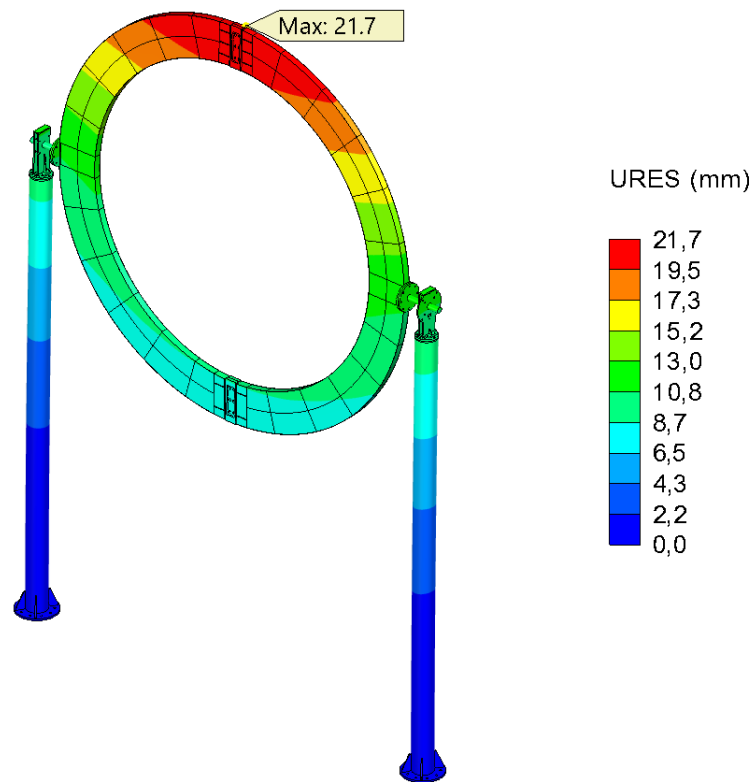


Figure 70. Resultant displacements of the structure with 5 m/s wind force and **without** concrete core. Deformation scale 10.

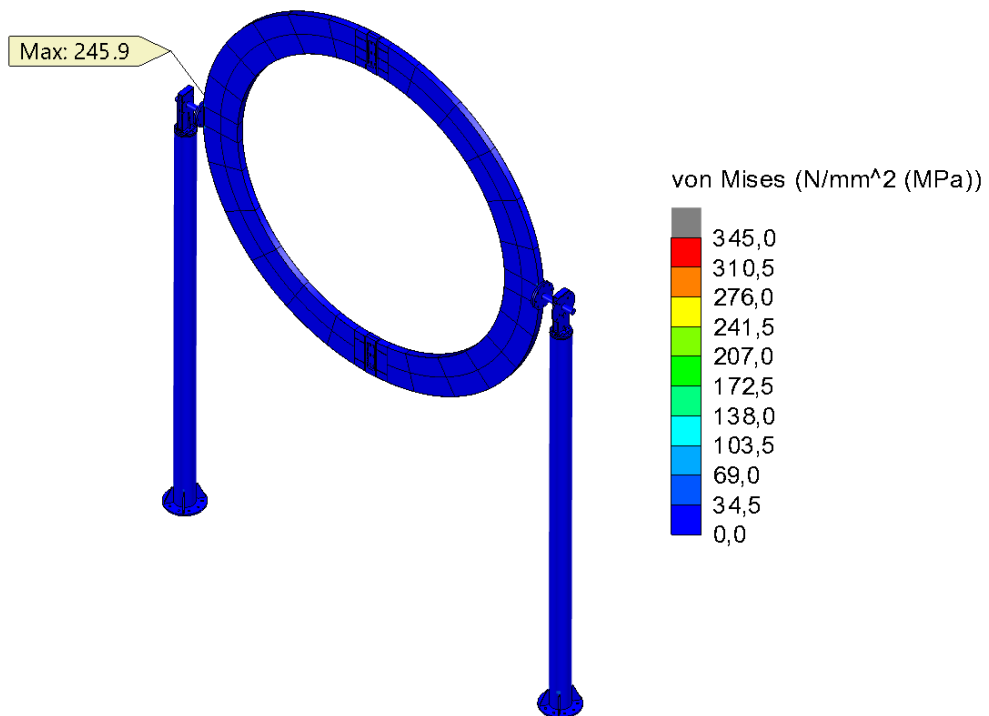


Figure 71. Von Mises -stresses at the top surface of the shell elements with 10 m/s wind force and **without** concrete core. Stress range 0-345 MPa, deformation scale 10.

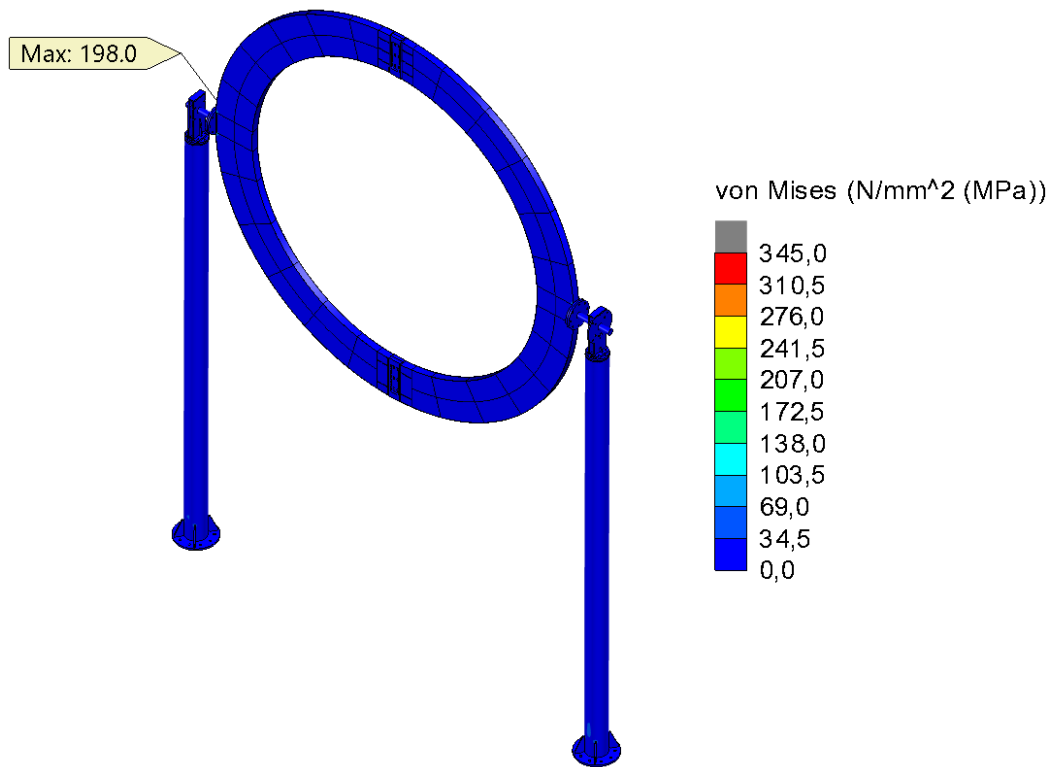


Figure 72. Von Mises -stresses at the bottom surface of the shell elements with 10 m/s wind force and **without** concrete core. Stress range 0-345 MPa, deformation scale 10

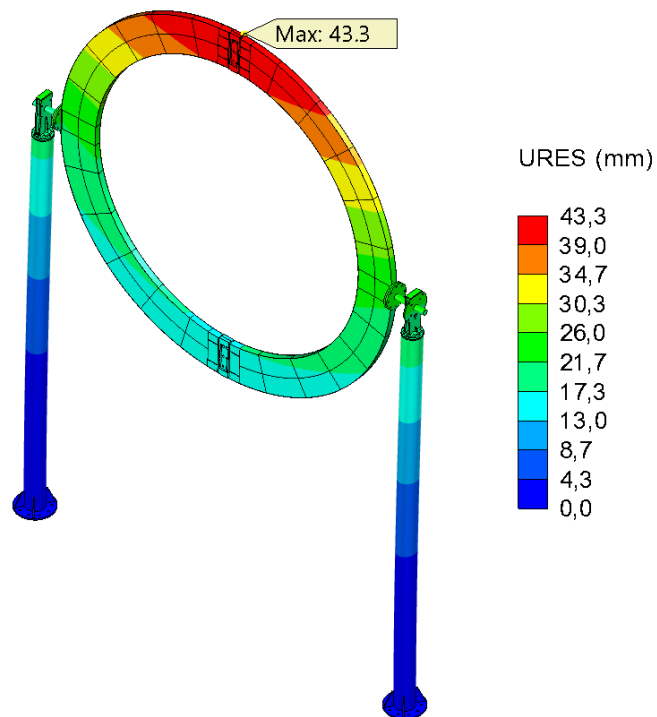


Figure 73. Resultant displacements of the structure with 10 m/s wind force and **without** concrete core. Deformation scale 10.

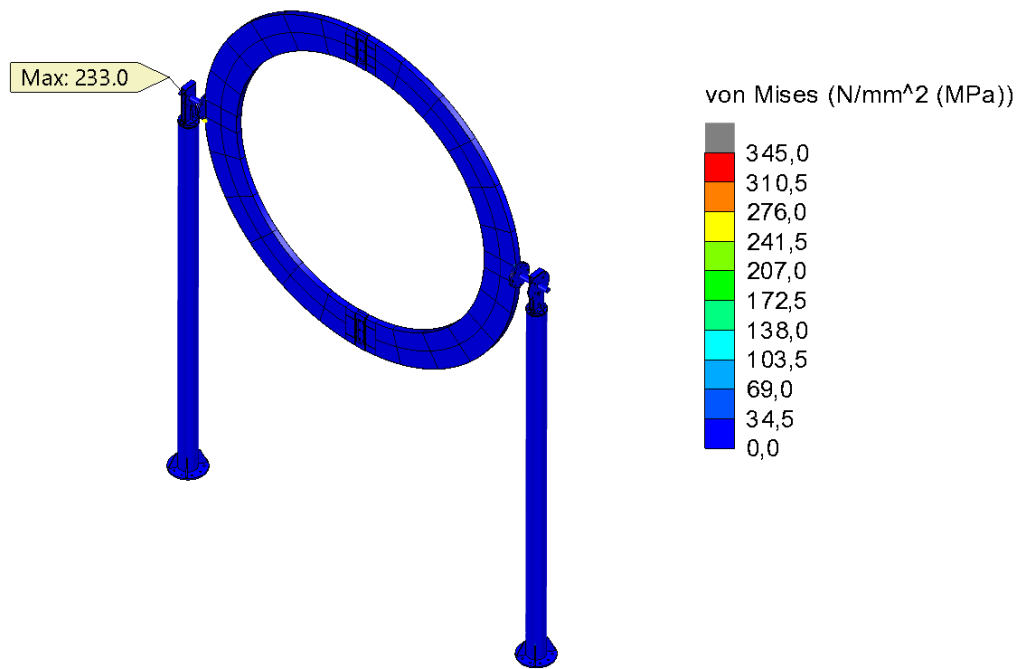


Figure 74. Von Mises -stresses at the top surface of the shell elements with 10 m/s wind force and **with** concrete core. Stress range 0-345 MPa, deformation scale 10

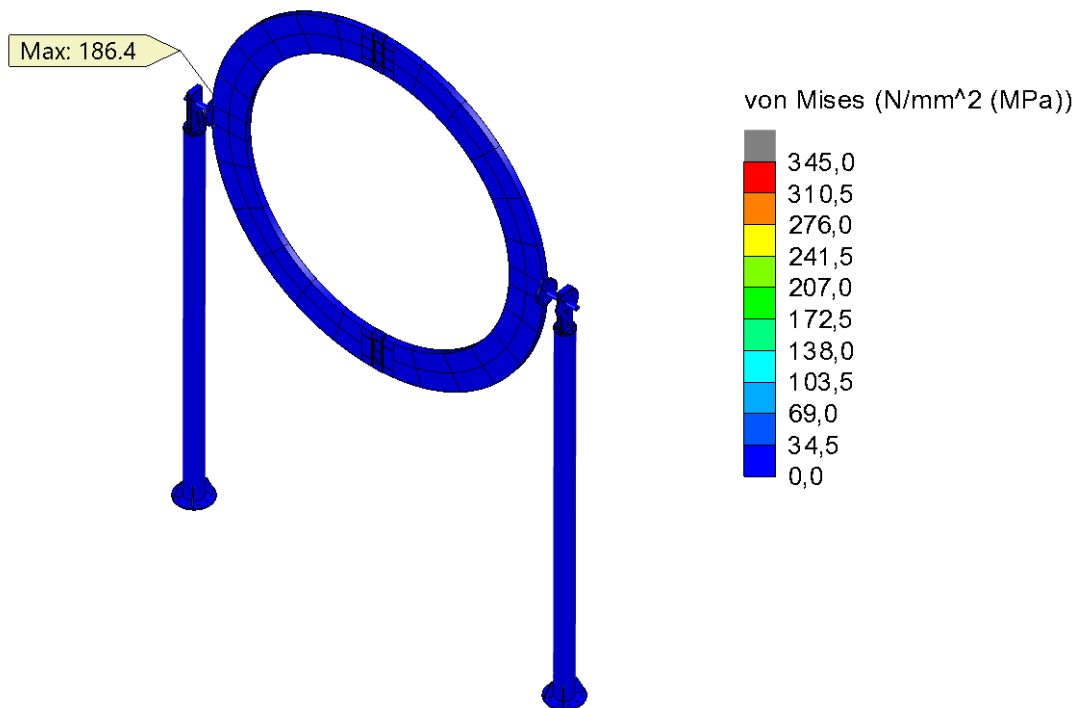


Figure 75. Von Mises -stresses at the bottom surface of the shell elements with 10 m/s wind force and **with** concrete core. Stress range 0-345 MPa, deformation scale 10

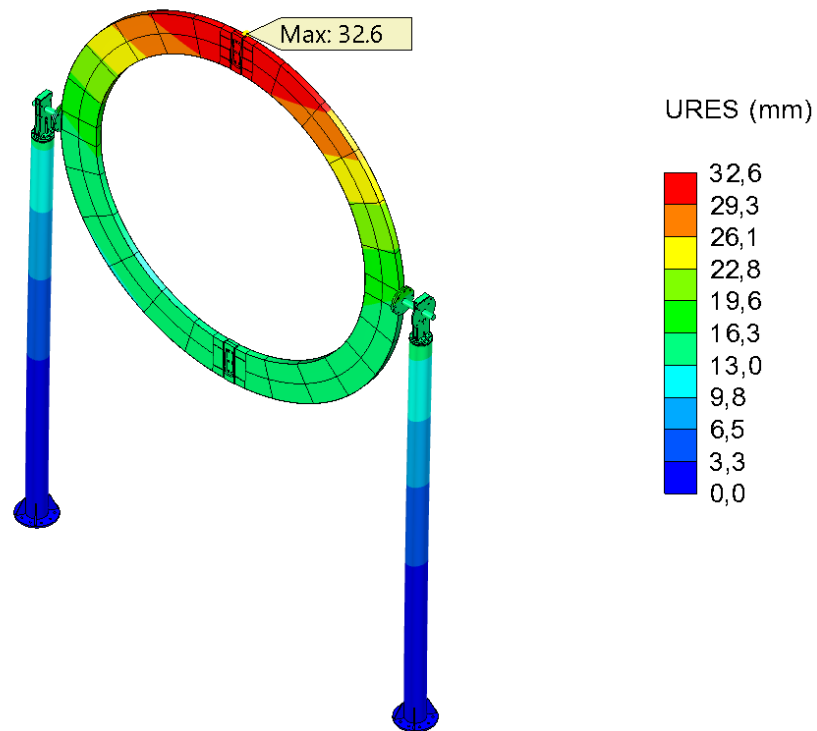


Figure 76. Resultant displacements of the structure with 10 m/s wind force and **with** concrete core. Deformation scale 10.

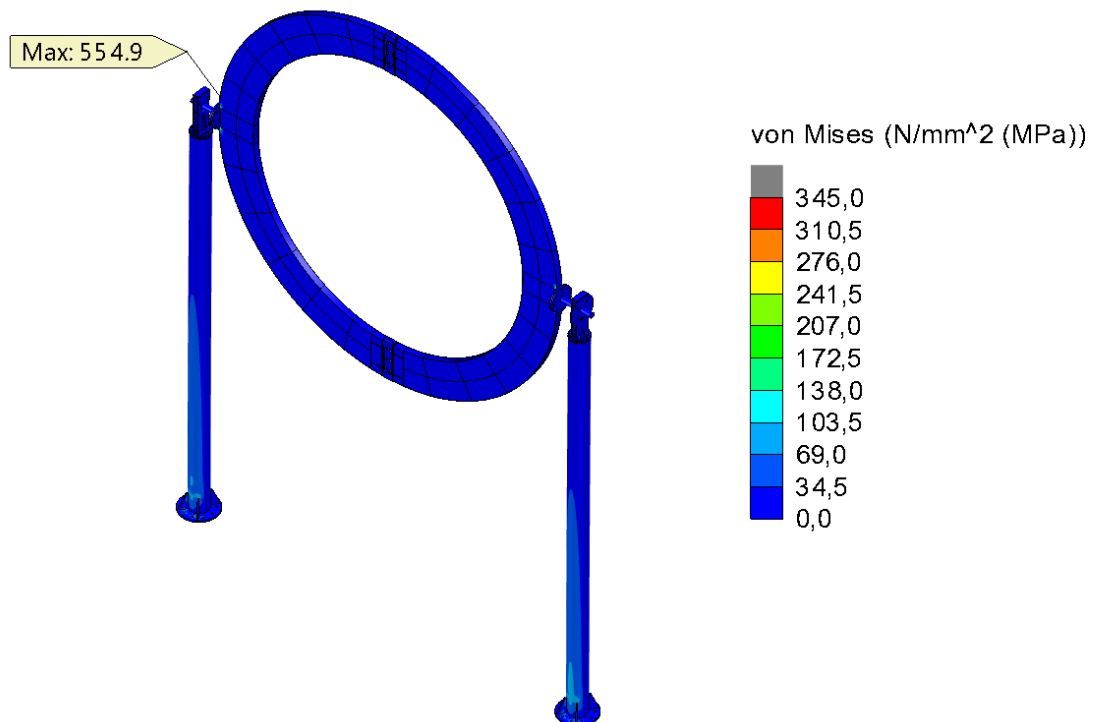


Figure 77. Von Mises -stresses at the top surface of the shell elements with 23 m/s wind force and **without** concrete core. Stress range 0-345 MPa, deformation scale 10

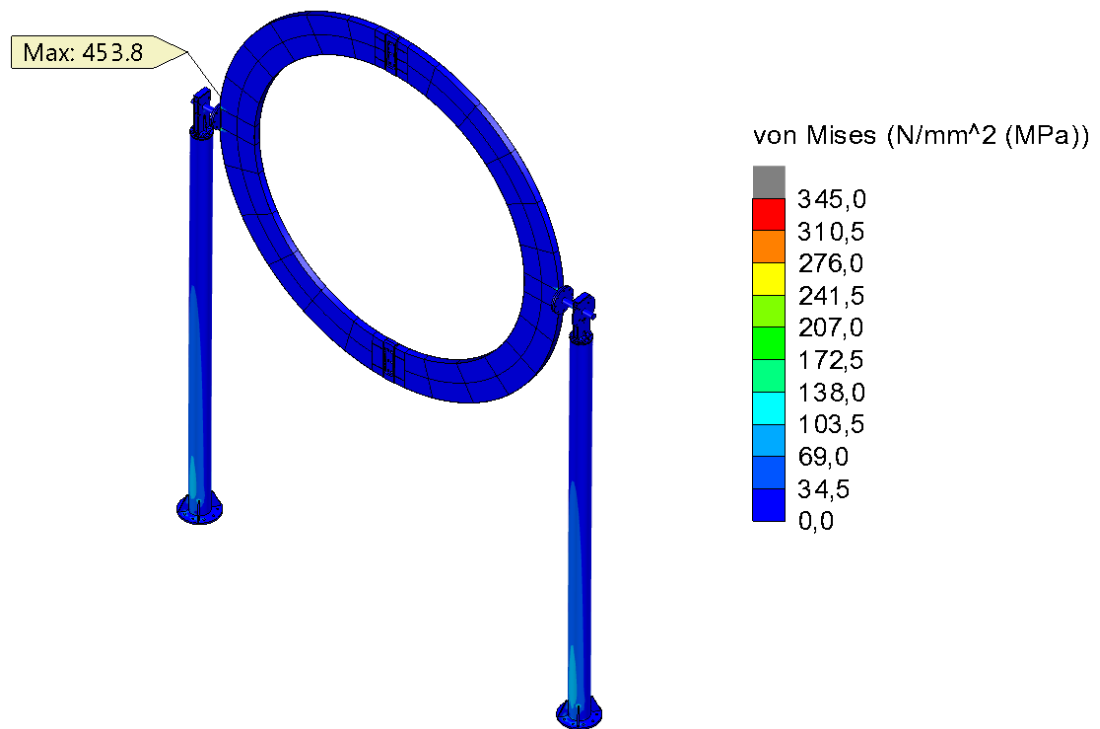


Figure 78. Von Mises -stresses at the bottom surface of the shell elements with 23 m/s wind force and **without** concrete core. Stress range 0-345 MPa, deformation scale 10

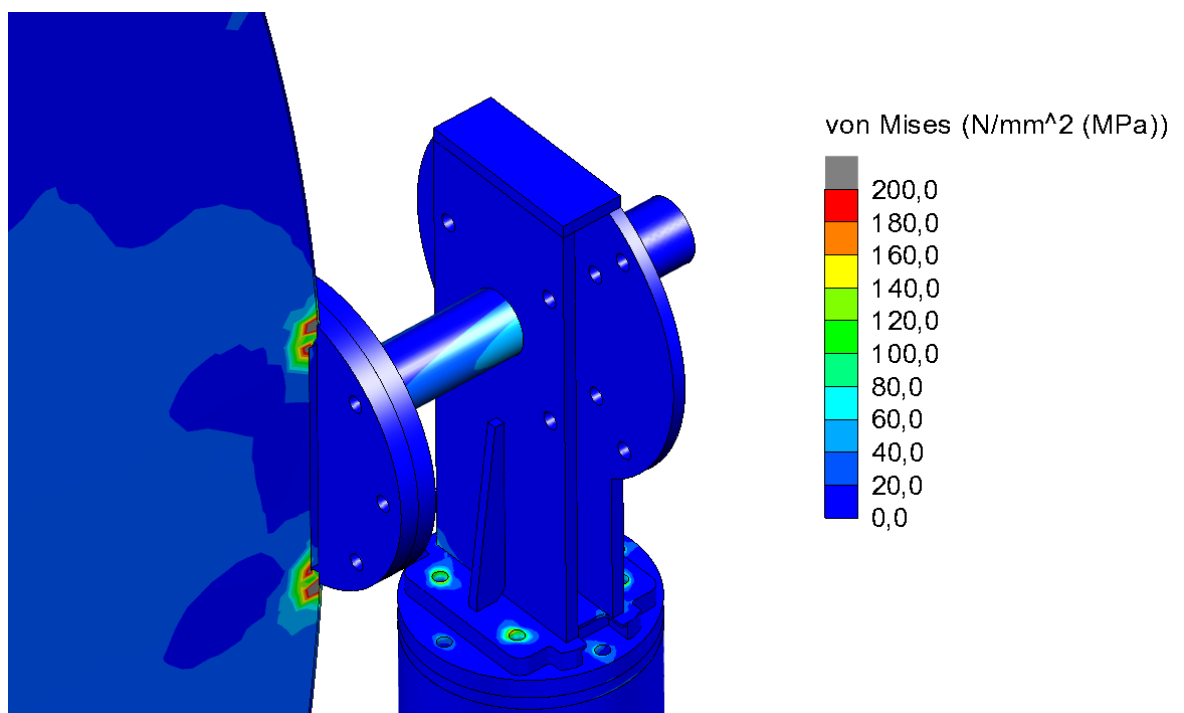


Figure 79. Von Mises -stress in the shafts with 23 m/s wind force and **without** concrete core. Stress range 0-200 MPa, deformation scale 10

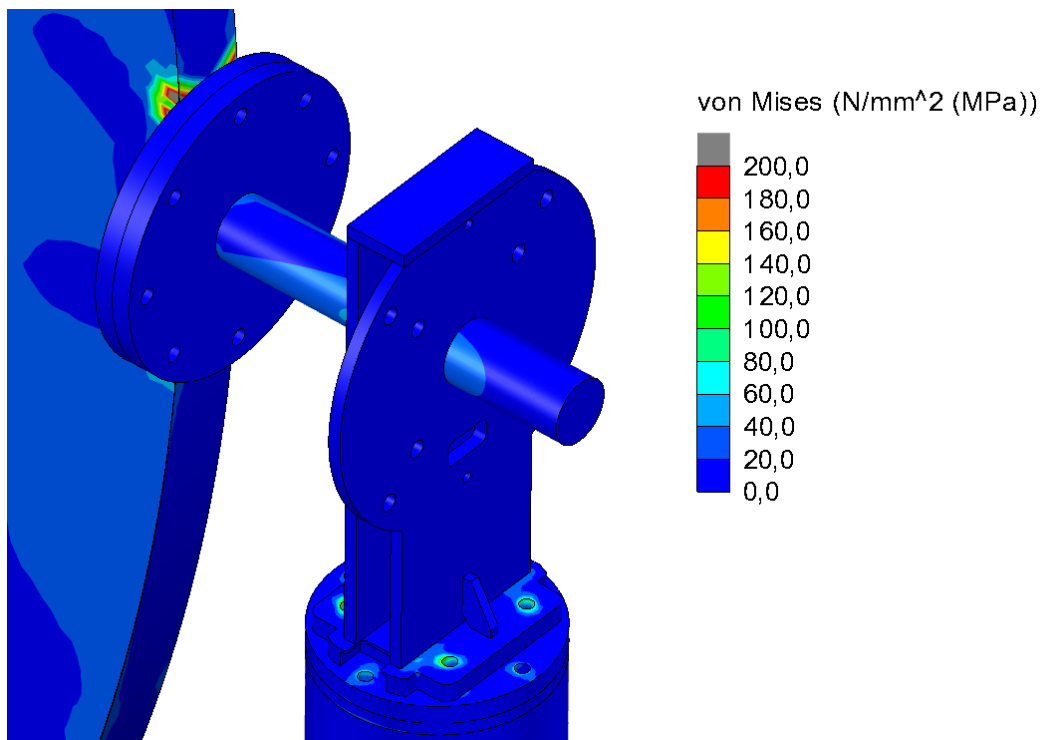


Figure 80. Von Mises -stress in the shafts with 23 m/s wind force and **without** concrete core. Stress range 0-200 MPa, deformation scale 10

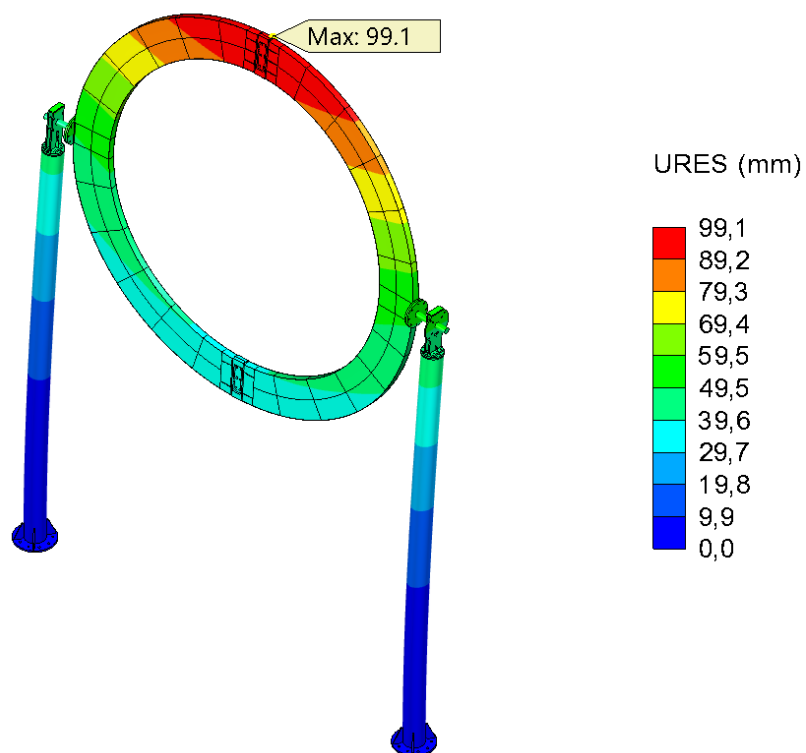


Figure 81. Resultant displacements of the structure with 23 m/s wind force and **without** concrete core. Deformation scale 10.

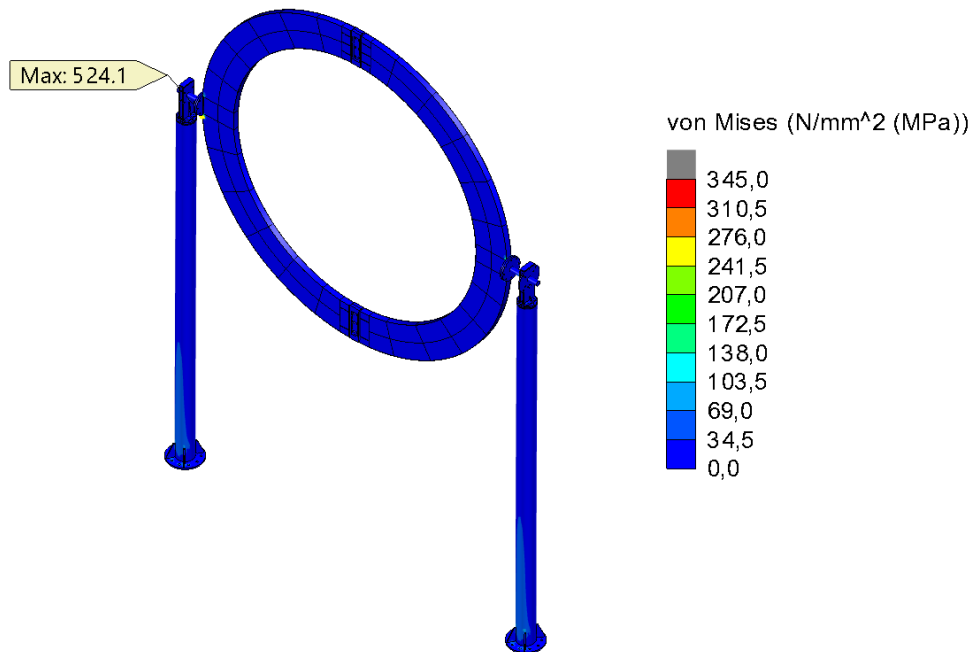


Figure 82. Von Mises -stresses at the top surface of the shell elements with 23 m/s wind force and **with** concrete core. Stress range 0-345 MPa, deformation scale 10

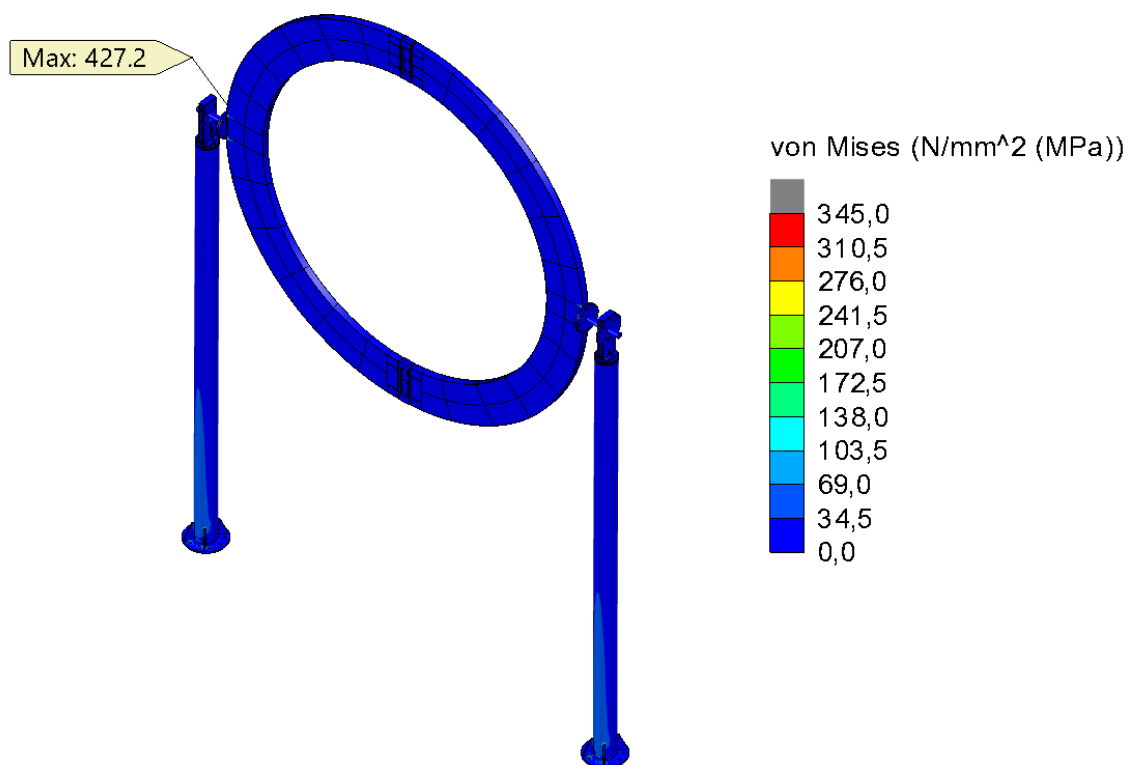


Figure 83. Von Mises -stresses at the bottom surface of the shell elements with 23 m/s wind force and **with** concrete core. Stress range 0-345 MPa, deformation scale 10

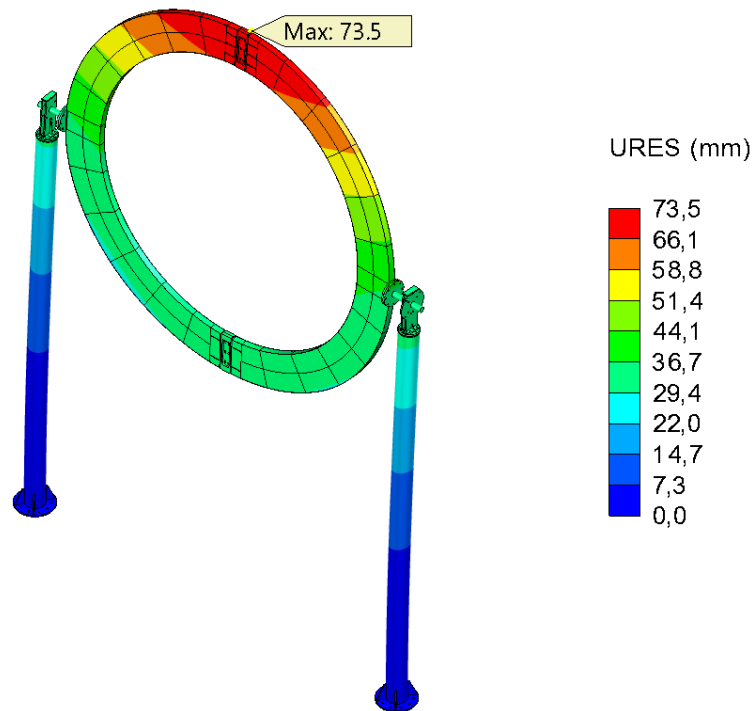


Figure 84. Resultant displacements of the structure with 23 m/s wind force and **with** concrete core. Deformation scale 10.

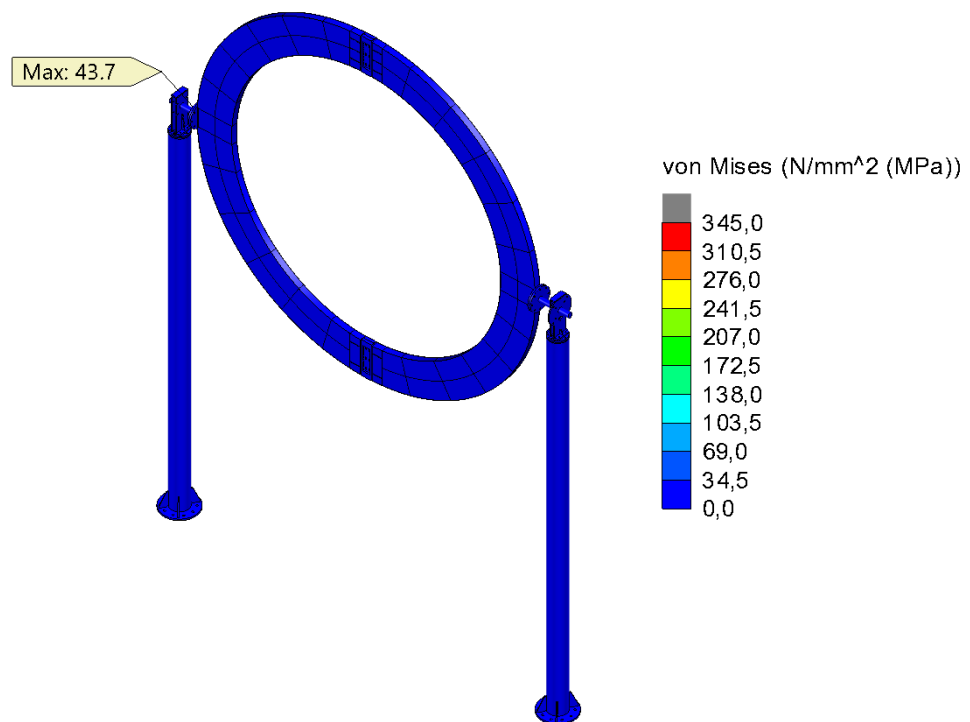


Figure 85. Von Mises -stresses at the top surface of the shell elements with snow load and **without** concrete core. Stress range 0-345 MPa, deformation scale 10

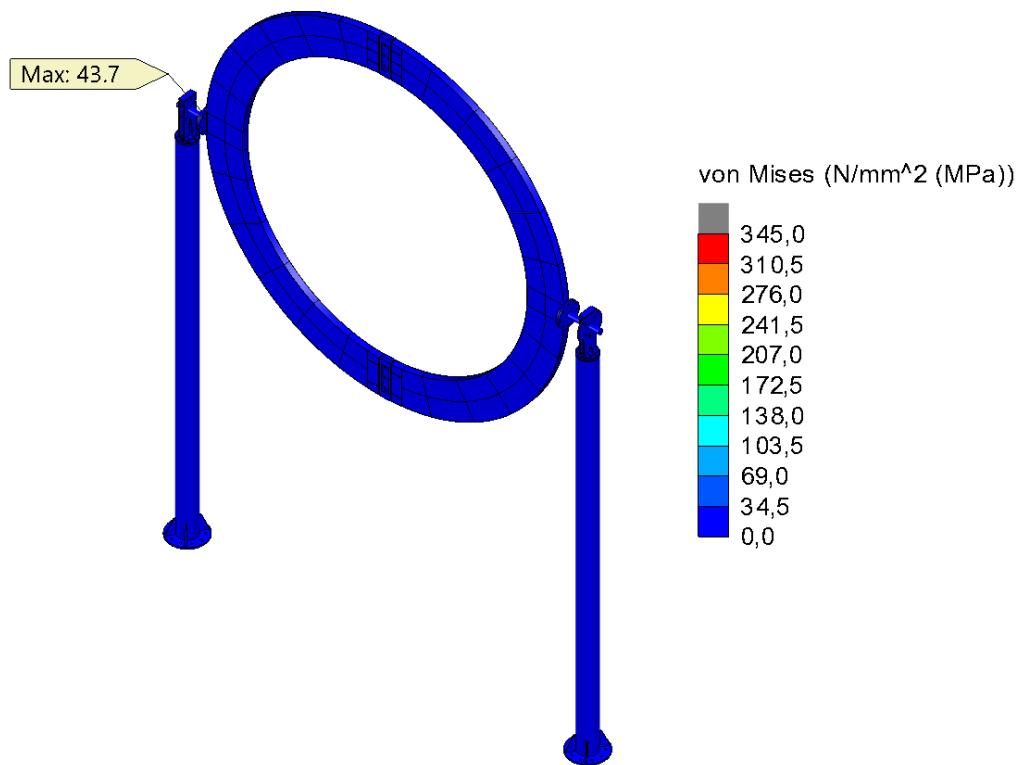


Figure 86. Von Mises -stresses at the bottom surface of the shell elements with snow load and **without** concrete core. Stress range 0-345 MPa, deformation scale 10

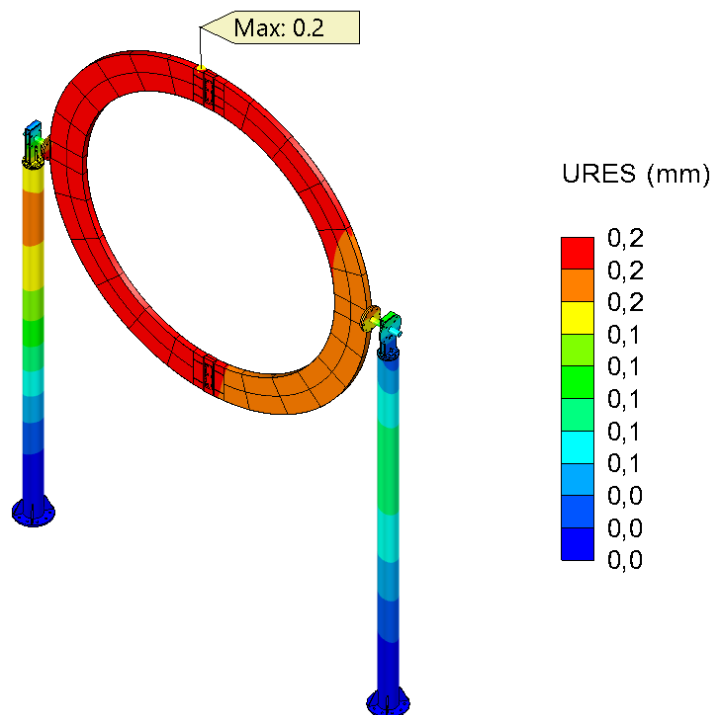


Figure 87. Resultant displacements of the structure with snow load and **without** concrete core. Deformation scale 10.

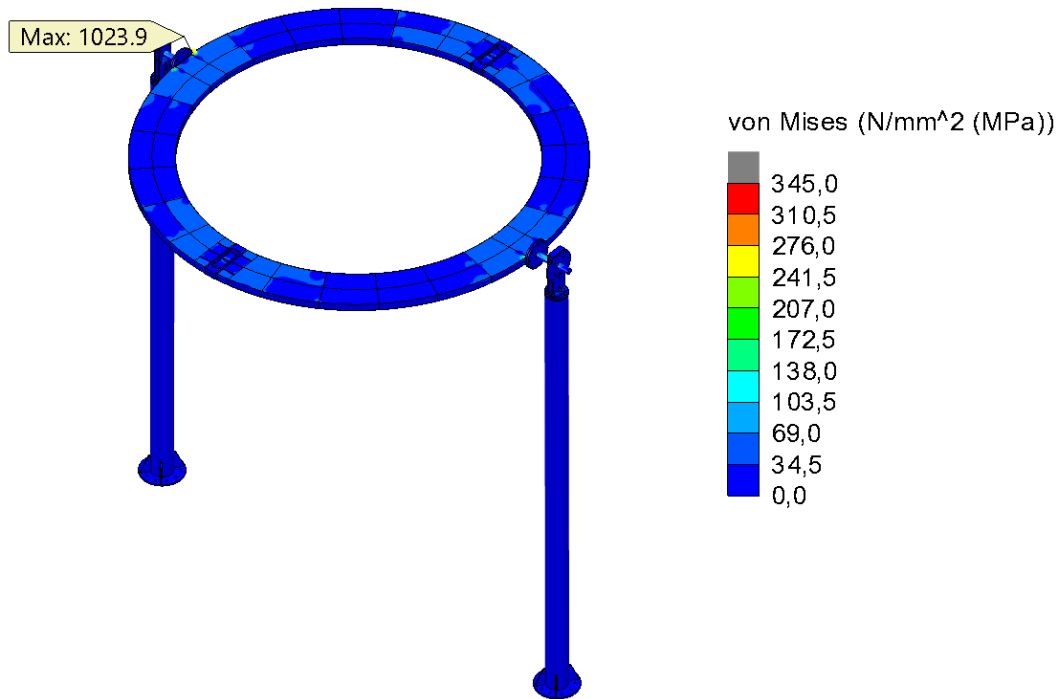


Figure 88. Von Mises -stresses at the top surface of the shell elements with snow load in failure mode and **without** concrete core. Stress range 0-345 MPa, deformation scale 10

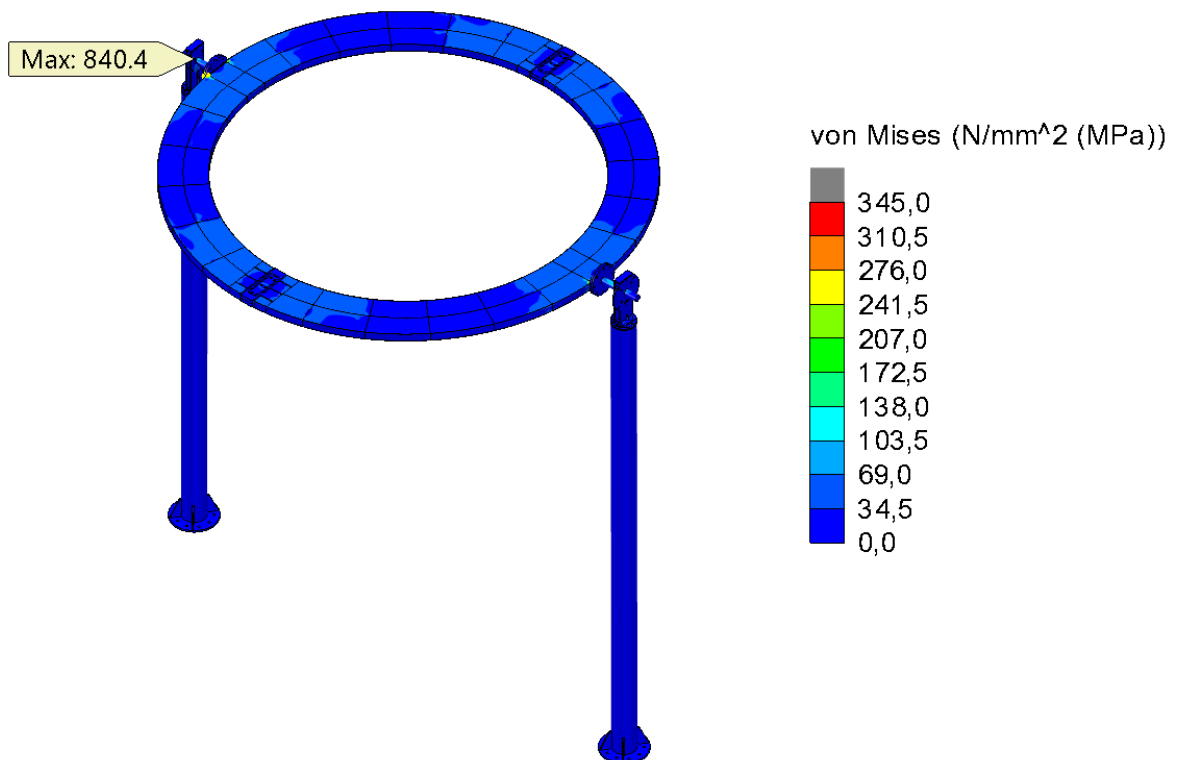


Figure 89. Von Mises -stresses at the bottom surface of the shell elements with snow load in failure mode and **without** concrete core. Stress range 0-345 MPa, deformation scale 10

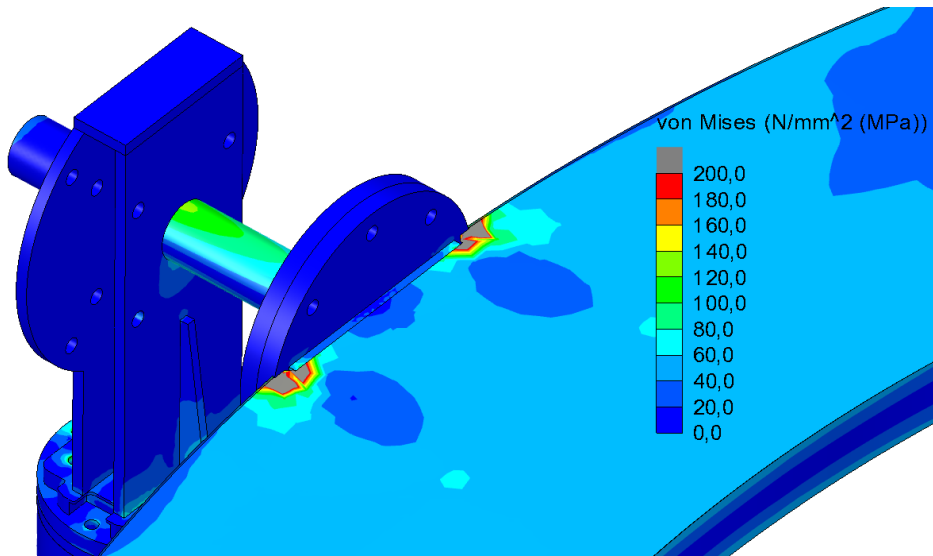


Figure 90. Von Mises -stress in the shafts with snow load in failure mode and **without** concrete core. Stress range 0-200 MPa, deformation scale 10

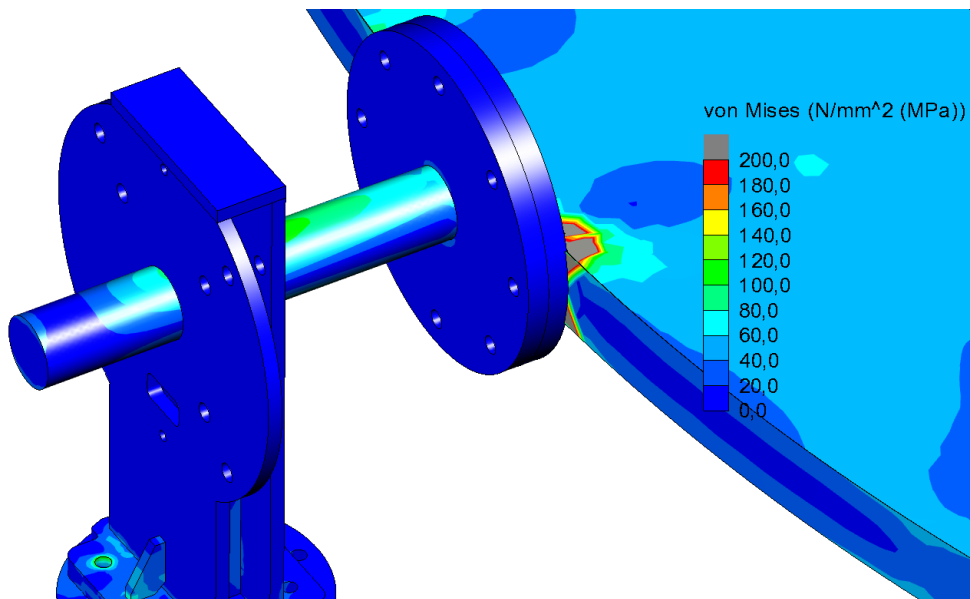


Figure 91. Von Mises -stress in the shafts with snow load in failure mode and **without** concrete core. Stress range 0-200 MPa, deformation scale 10

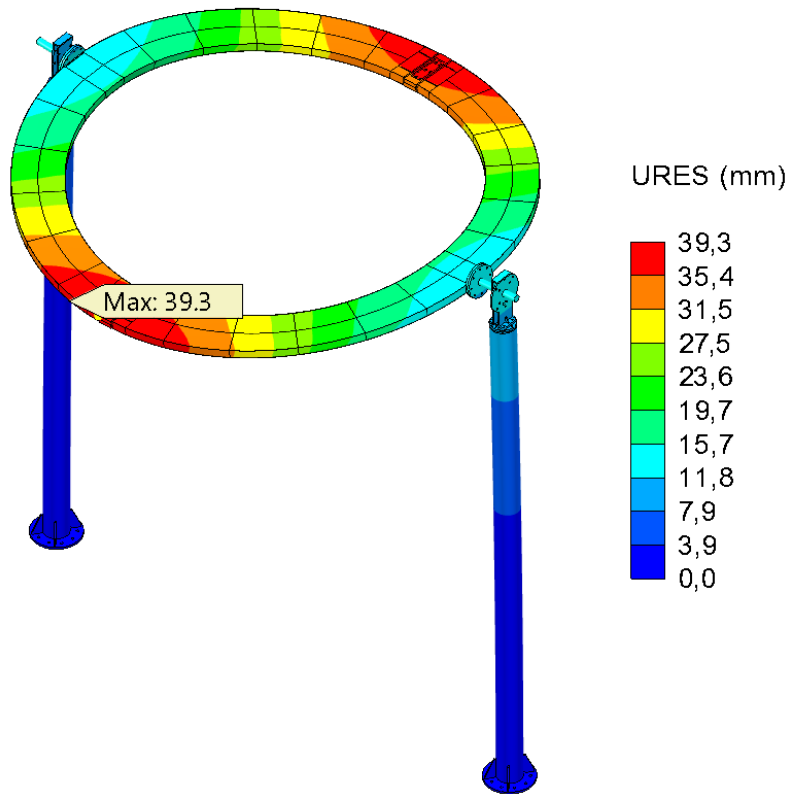


Figure 92. Resultant displacements of the structure with snow load in failure mode and **without** concrete core. Deformation scale 10.

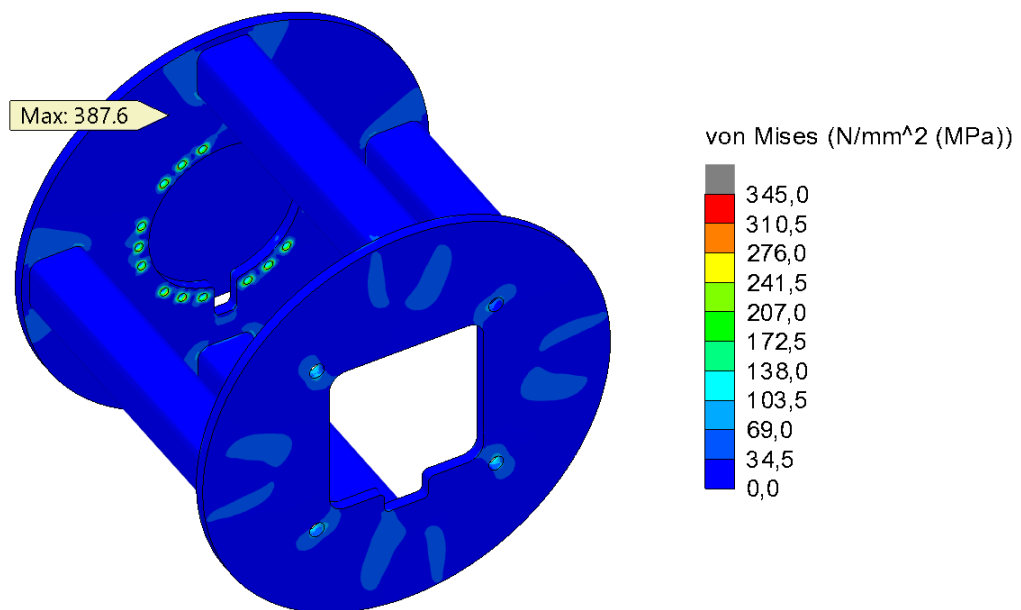


Figure 93. Von Mises -stresses in the motor mounting bracket at the top surface of the shell elements with torque caused by 23 m/s wind load. Stress range 0-345 MPa, deformation scale 10

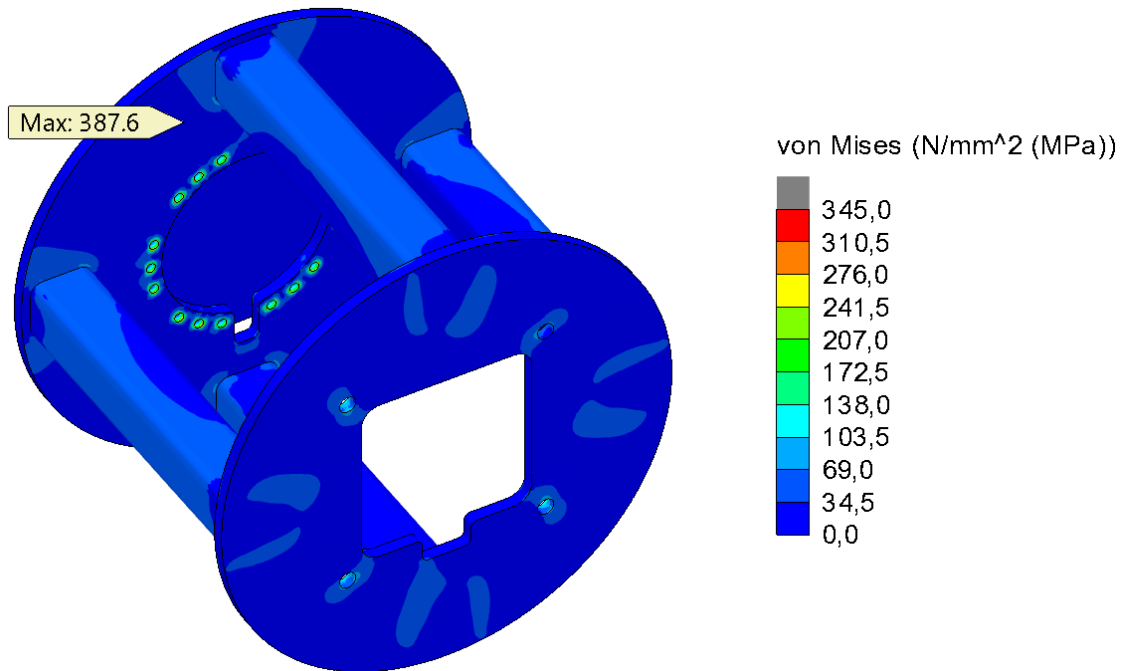


Figure 94. Von Mises -stresses in the motor mounting bracket at the bottom surface of the shell elements with torque caused by 23 m/s wind load. Stress range 0-345 MPa, deformation scale 10

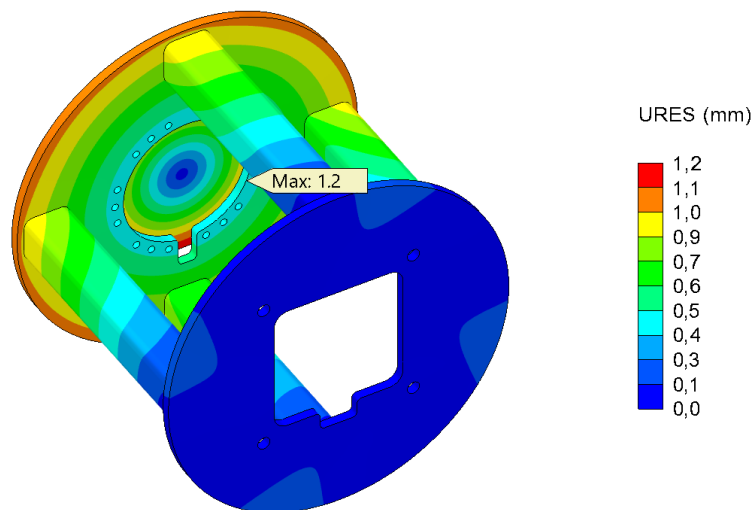


Figure 95. Displacements in the mounting bracket with torque caused by 23 m/s wind load. Deformation scale 10.

4.2 Natural frequency and vibration

Natural frequencies determined by FE-analysis are presented in Table 12 and mode shapes in Figure 96 - Figure 100. Only frequencies that are critical for vortex shedding vibration with normal wind velocity are examined.

Table 12. First 12 natural frequencies of the sculpture.

Mode no.	Frequency [rad/s]	Frequency [Hz]	Period [s]
1	12.5	2.0	0.50
2	15.3	2.4	0.41
3	18.9	3.0	0.33
4	20.6	3.2	0.30
5	41.2	6.6	0.15
6	87.7	14.0	0.07
7	90.4	14.4	0.07
8	99.5	15.8	0.06
9	101.5	16.2	0.06
10	105.9	16.9	0.06
11	133.4	21.2	0.05
12	162.1	25.8	0.04

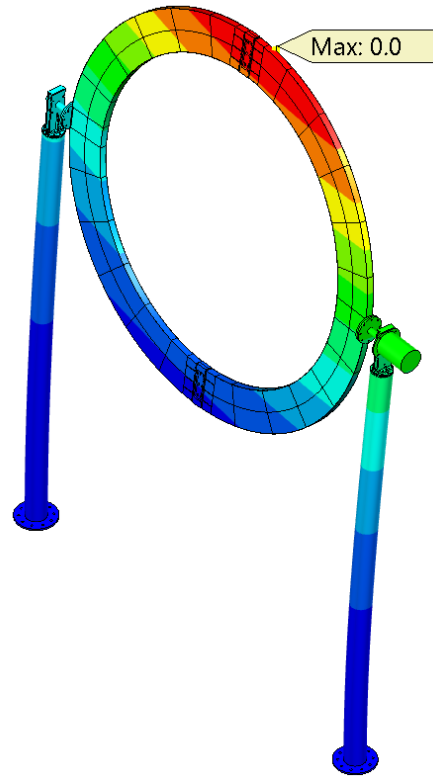


Figure 96. Mode shape 1 / 2.0 Hz

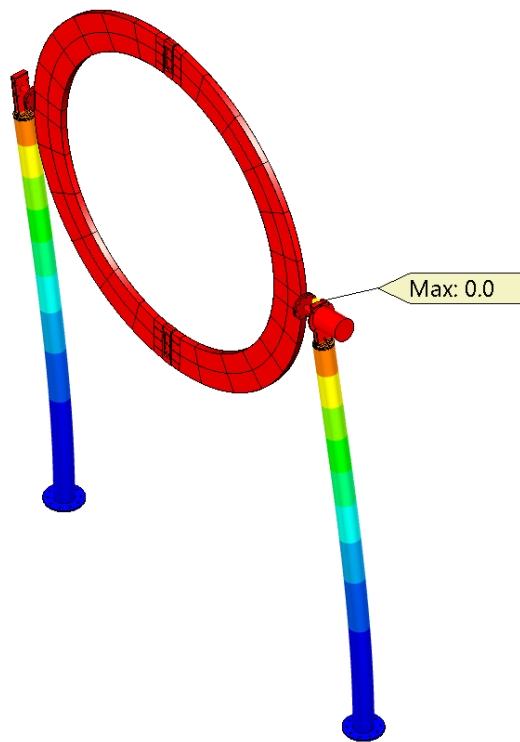


Figure 97. Mode shape 2 / 2.4 Hz

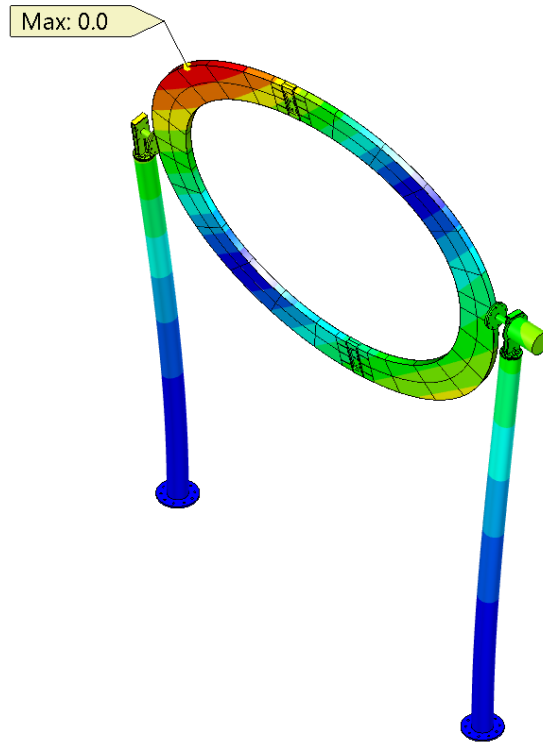


Figure 98. Mode shape 3 / 3.0 Hz

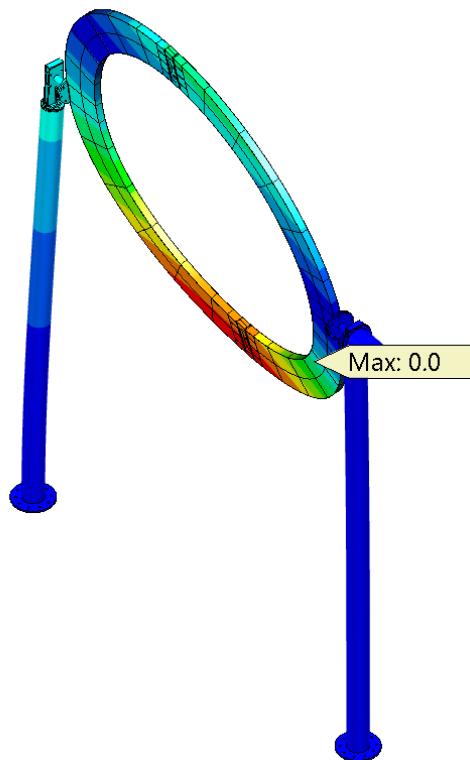


Figure 99. Mode shape 4 / 3.3 Hz

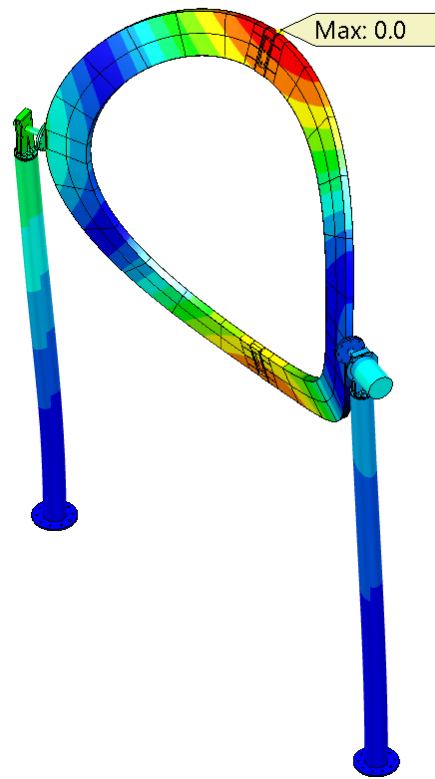


Figure 100. Mode shape 5 / 6.6 Hz

4.3 Fatigue

Hot Spot -stresses and fatigue lives of the welded details are presented in Table 13 - Table 20 and Figure 101 - Figure 113. More detailed table is presented in Appendix 5.

Table 13. Hot Spot -stress at the weld between posts and foundation plates (Figure 101)

Mode no.	Lateral force caused by vortex shedding [N]	Stress at 0.4t distance from the lower weld toe [MPa]	Stress at 1.0t distance from the lower weld toe [MPa]	Stress at 0.4t distance from the upper weld toe [MPa]	Stress at 1.0t distance from the upper weld toe [MPa]	Hot Spot -stress at the lower weld toe [MPa]	Hot Spot -stress at the upper weld toe [MPa]
RF	1000.0	1.8	1.7	3.3	2.6	1.9	3.8
1	204.7	0.4	0.3	0.7	0.5	0.4	0.8
2	297.7	0.5	0.5	1.0	0.8	0.6	1.1
3	465.1	0.8	0.8	1.5	1.2	0.9	1.8
4	562.8	1.0	1.0	1.9	1.5	1.1	2.1
5	2250.9	4.1	3.8	7.4	5.9	4.2	8.5
6	10128.1	18.2	17.2	33.4	26.3	18.9	38.2
7	10715.1	19.3	18.2	35.4	27.9	20.0	40.4
8	12899.9	23.2	21.9	42.6	33.5	24.1	48.6
9	13561.3	24.4	23.1	44.8	35.3	25.3	51.1
10	14758.6	26.6	25.1	48.7	38.4	27.6	55.6
11	23224.3	41.8	39.5	76.6	60.4	43.4	87.5
12	34396.2	61.9	58.5	113.5	89.4	64.2	129.6

Table 14. Fatigue lives for the weld between posts and foundation plates (Figure 101). In the table FOS stands for the factor of safety.

Mode no.	FAT-class	Obtained fatigue life for lower weld toe	Obtained fatigue life for upper weld toe	Number of cycles caused by vortex shedding	FOS (lower weld toe)	FOS (upper weld toe)
RF		REFERENCE FORCE				
1	90	26 119 871 867 196	3 174 867 342 799	210 029 559	124 363	15 116
2	90	8 491 571 410 642	1 032 149 502 791	243 094 796	34 931	4 246
3	90	2 226 822 247 706	270 669 981 400	224 618 221	9 914	1 205
4	90	1 256 788 805 951	152 762 531 038	193 198 739	6 505	791
5	90	19 644 916 100	2 387 837 233	815 453	24 091	2 928
6	90	215 645 613	26 211 699	1	215 645 613	26 211 699
7	90	182 110 876	22 135 556	0	-	-
8	90	104 367 562	12 685 865	0	-	-
9	90	89 829 835	10 918 806	0	-	-
10	90	69 692 988	8 471 174	0	-	-
11	90	17 885 318	2 173 958	0	-	-
12	90	5 505 454	669 187	0	-	-

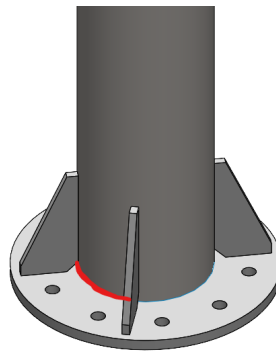


Figure 101. Welded detail examined in Table 14 and Table 14.

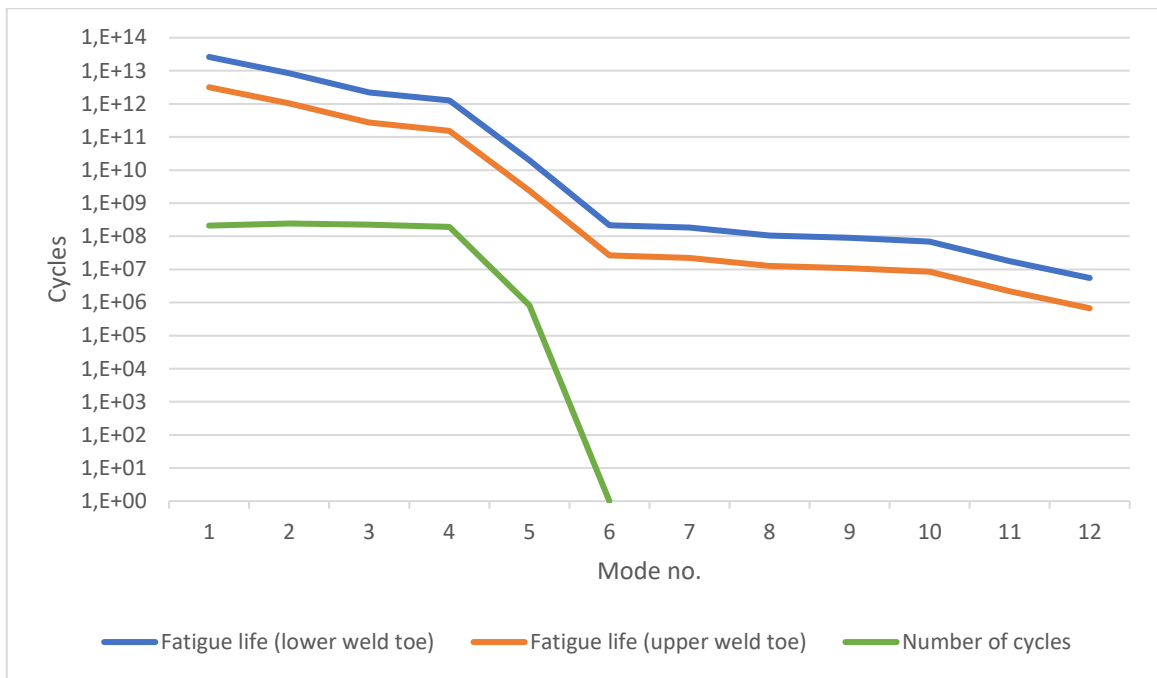


Figure 102. Obtained fatigue life in welded detail presented in Figure 101 compared to number of cycles caused by vortex shedding (logarithmic scale).

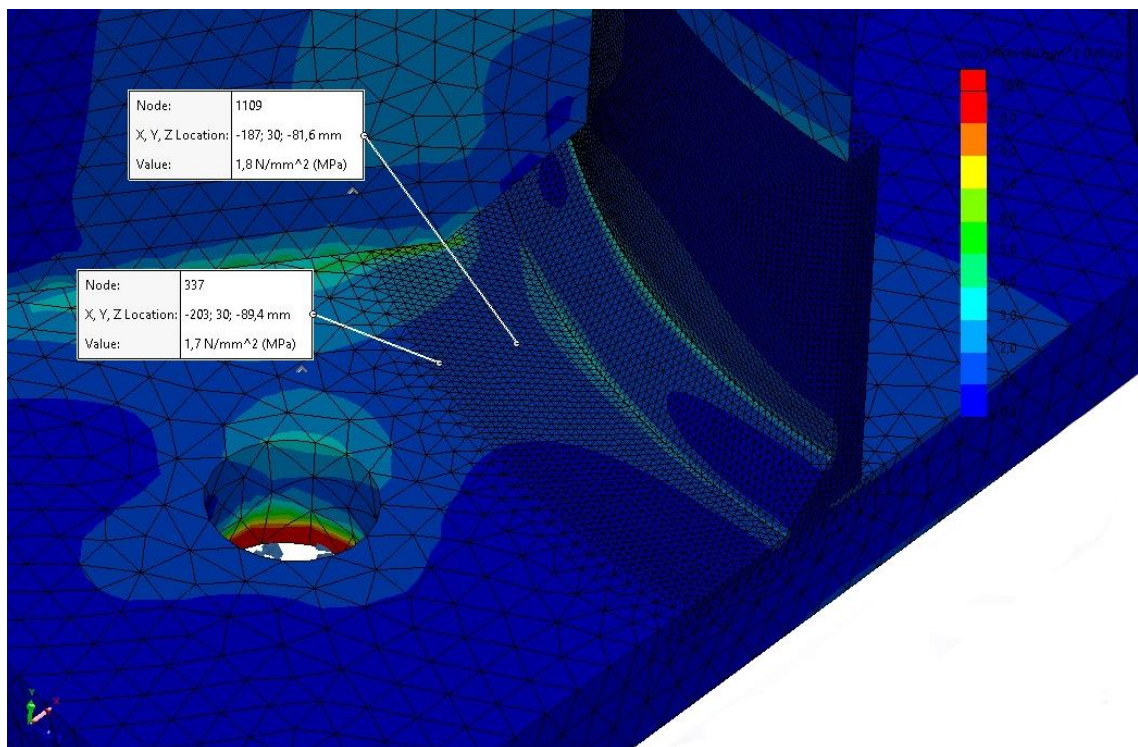


Figure 103. Stresses $\sigma_{0,4t}$ and $\sigma_{1,0t}$ next to the lower weld toe (posts).

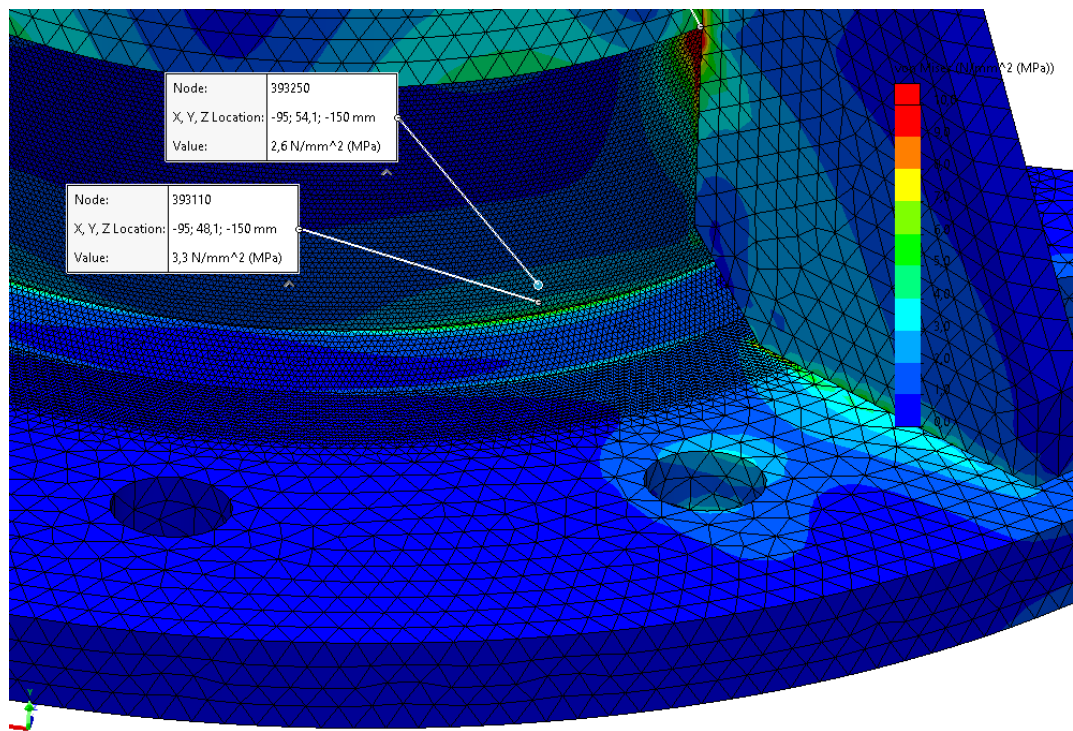


Figure 104. Stresses $\sigma_{0,4t}$ and $\sigma_{1,0t}$ next to the upper weld toe (posts)

Table 15. Hot Spot -stress at the bottom weld of shaft carrier (Figure 105).

Mode no.	Lateral force caused by vortex shedding [N]	Stress at 0,4t distance from the lower weld toe [MPa]	Stress at 1,0t distance from the lower weld toe [MPa]	Stress at 0,4t distance from the upper weld toe [MPa]	Stress at 1,0t distance from the upper weld toe [MPa]	Hot Spot -stress at the lower weld toe [MPa]	Hot Spot -stress at the upper weld toe [MPa]
RF	1000.0	-	-	5.2000	2.3000	-	7.1
1	204.7	-	-	1.06	0.47	-	1.5
2	297.7	-	-	1.55	0.68	-	2.1
3	465.1	-	-	2.42	1.07	-	3.3
4	562.8	-	-	2.93	1.29	-	4.0
5	2250.9	-	-	11.70	5.18	-	16.1
6	10128.1	-	-	52.67	23.29	-	72.3
7	10715.1	-	-	55.72	24.64	-	76.5

8	12899.9	-	-	67.08	29.67	-	92.1
9	13561.3	-	-	70.52	31.19	-	96.9
10	14758.6	-	-	76.74	33.94	-	105.4
11	23224.3	-	-	120.77	53.42	-	165.9
12	34396.2	-	-	178.86	79.11	-	245.7

Table 16. Fatigue lives for the bottom weld of shaft carrier (Figure 105). In the table FOS stands for the factor of safety.

Mode no.	FAT-class	Obtained fatigue life for lower weld toe	Obtained fatigue life for upper weld toe	Number of cycles caused by vortex shedding	FOS (lower weld toe)	FOS (upper weld toe)
RF		REFERENCE FORCE				
1	90	-	466 403 762 911	210 029 559	-	2 221
2	90	-	151 627 882 368	243 094 796	-	624
3	90	-	39 762 763 039	224 618 221	-	177
4	90	-	22 441 573 652	193 198 739	-	116
5	90	-	350 785 135	815 453	-	430
6	90	-	3 850 629	1	-	3 850 629
7	90	-	3 251 823	0	-	-
8	90	-	1 863 616	0	-	-
9	90	-	1 604 027	0	-	-
10	90	-	1 244 458	0	-	-
11	90	-	319 365	0	-	-
12	90	-	98 307	0	-	-

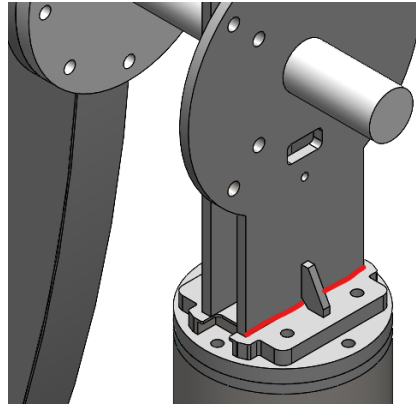


Figure 105. Welded detail examined in Table 15 and Table 16.

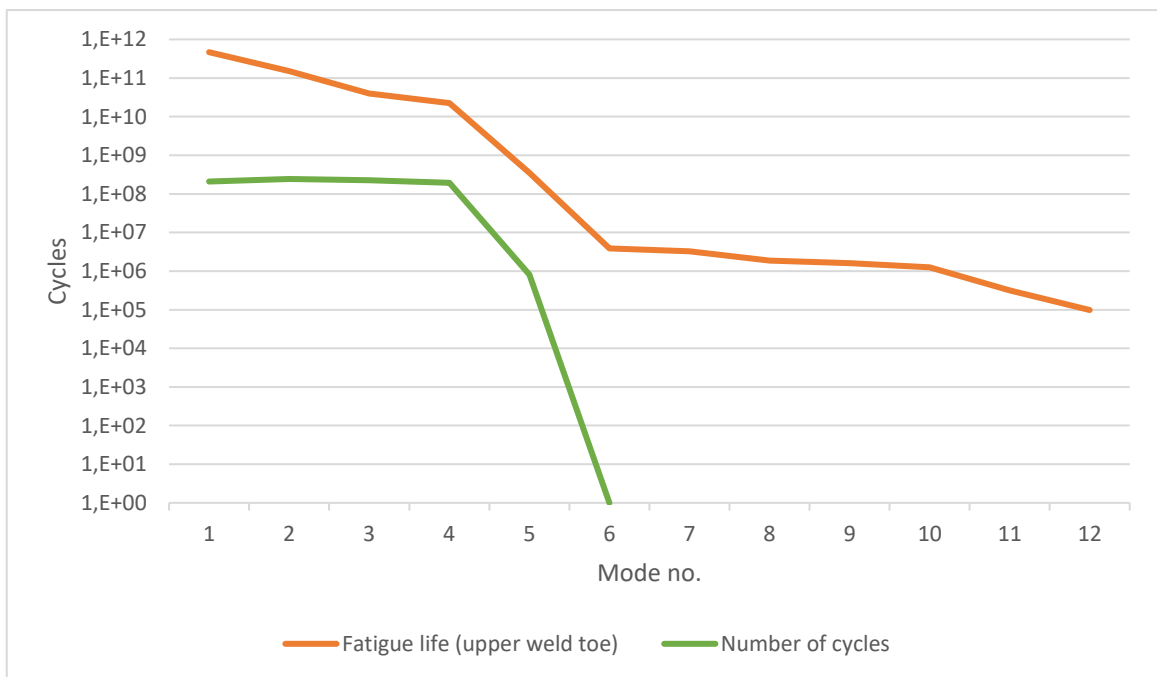


Figure 106. Obtained fatigue life in welded detail presented in Figure 105 compared to number of cycles caused by vortex shedding (logarithmic scale).

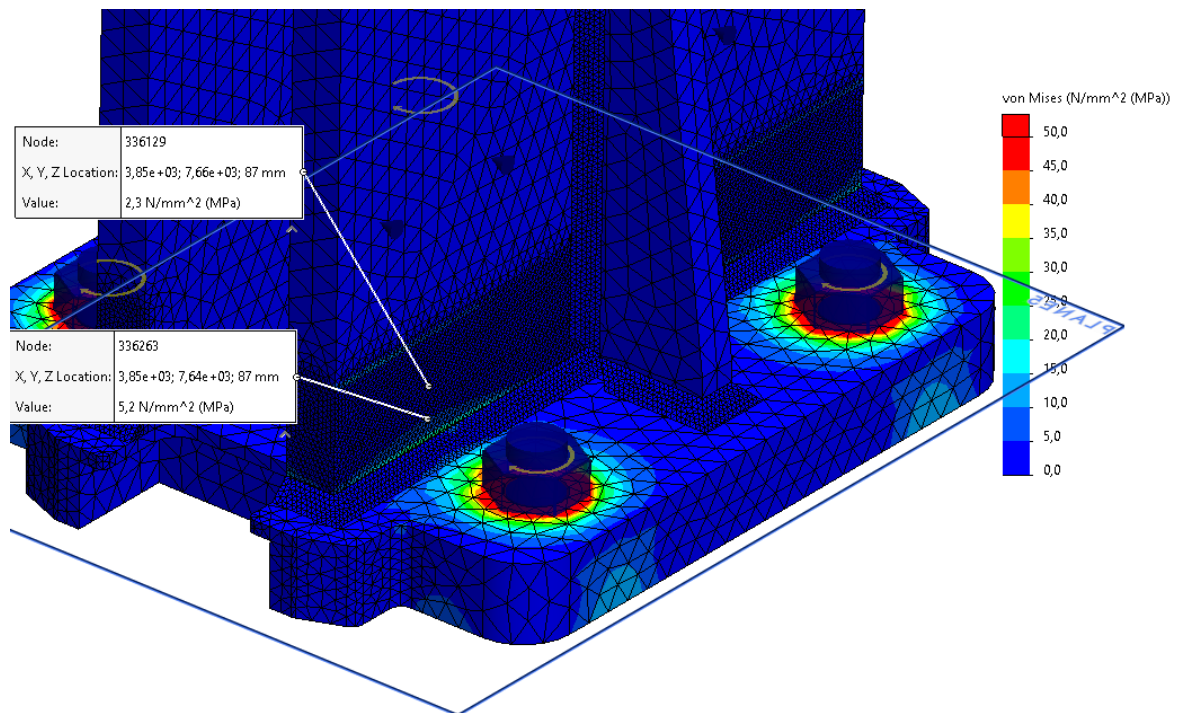


Figure 107. Stresses $\sigma_{0,4t}$ and $\sigma_{1,0t}$ next to the upper weld toe (shaft carriers).

Table 17. Hot Spot -stress in the ring shafts (Figure 108).

Mode no.	Lateral force caused by vortex shedding [N]	Stress at 0,4t distance from the lower weld toe [MPa]	Stress at 1,0t distance from the lower weld toe [MPa]	Stress at 0,4t distance from the upper weld toe [MPa]	Stress at 1,0t distance from the upper weld toe [MPa]	Hot Spot -stress at the lower weld toe [MPa]	Hot Spot -stress at the upper weld toe [MPa]
RF	1000.0	0.700	0.400	2.400	2.800	0.901	2.132
1	3.8	0.003	0.002	0.009	0.011	0.003	0.008
2	5.5	0.004	0.002	0.013	0.015	0.005	0.012
3	8.6	0.006	0.003	0.021	0.024	0.008	0.018
4	10.4	0.007	0.004	0.025	0.029	0.009	0.022
5	41.4	0.029	0.017	0.099	0.116	0.037	0.088
6	186.2	0.130	0.074	0.447	0.521	0.168	0.397
7	197	0.138	0.079	0.473	0.552	0.177	0.420
8	237.2	0.166	0.095	0.569	0.664	0.214	0.506

9	249.4	0.175	0.100	0.599	0.698	0.225	0.532
10	271.4	0.190	0.109	0.651	0.760	0.245	0.579
11	427	0.299	0.171	1.025	1.196	0.385	0.910
12	632.4	0.443	0.253	1.518	1.771	0.570	1.348

Table 18. Fatigue lives for the ring shafts (Figure 108). In the table FOS stands for the factor of safety.

Mode no.	FAT -class	Obtained fatigue life for lower weld toe	Obtained fatigue life for upper weld toe	Number of cycles caused by vortex shedding	FOS (lower weld toe)	FOS (upper weld toe)
RF		REFERENCE FORCE				
1	90	3.63E+19	2.74E+18	122 852 469	2.96E+11	2.23E+10
2	90	1.20E+19	9.04E+17	189 317 101	6.33E+10	4.78E+09
3	90	3.13E+18	2.37E+17	292 840 327	1.07E+10	8.08E+08
4	90	1.77E+18	1.34E+17	340 191 680	5.21E+09	3.93E+08
5	90	2.81E+16	2.12E+15	259 109 246	1.08E+08	8.18E+06
6	90	3.09E+14	2.33E+13	42 427	7.28E+09	5.49E+08
7	90	2.61E+14	1.97E+13	20 380	1.28E+10	9.66E+08
8	90	1.49E+14	1.13E+13	1 284	1.16E+11	8.78E+09
9	90	1.28E+14	9.70E+12	551	2.33E+11	1.76E+10
10	90	9.97E+13	7.53E+12	118	8.45E+11	6.38E+10
11	90	2.56E+13	1.93E+12	1	2.56E+13	1.93E+12
12	90	7.88E+12	5.95E+11	0	-	-

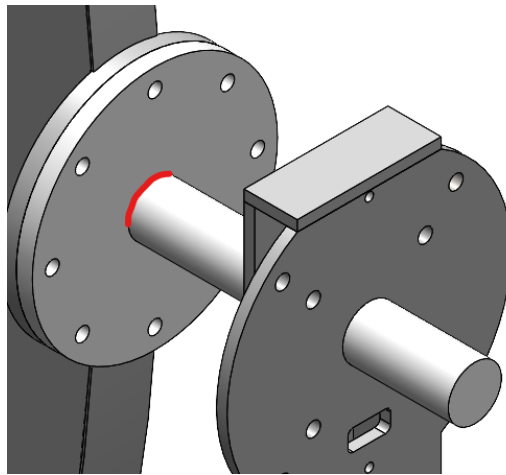


Figure 108. Welded detail examined in Table 17 and Table 18.

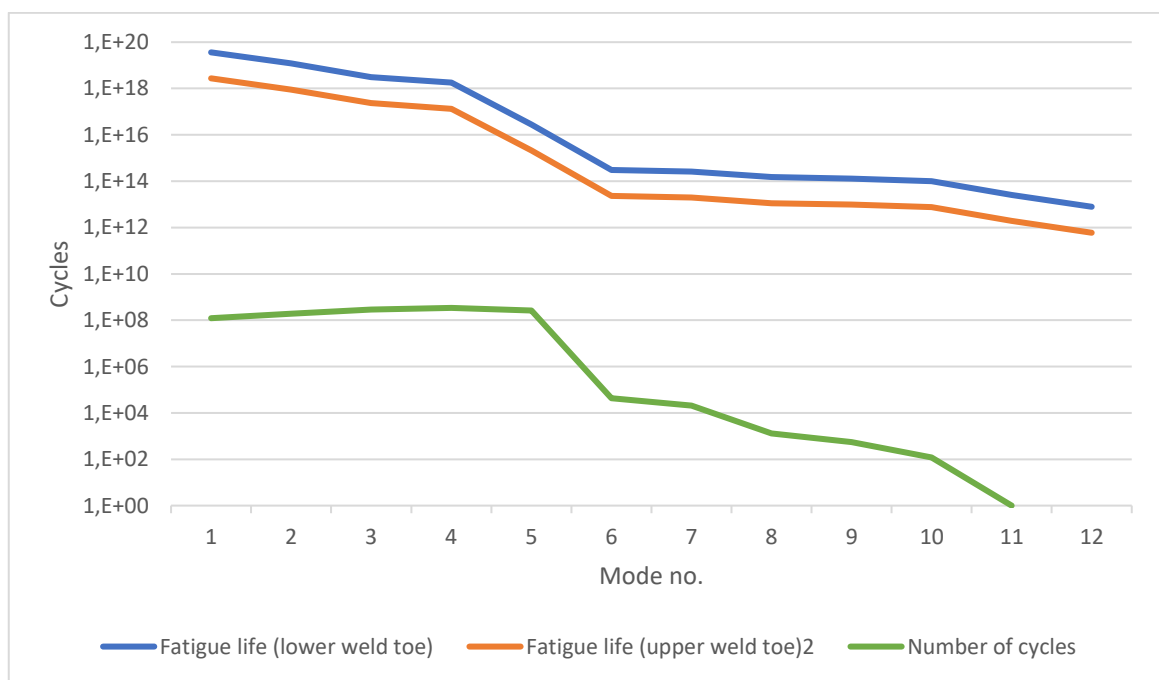


Figure 109. Obtained fatigue life in welded detail presented in Figure 108 compared to number of cycles caused by vortex shedding (logarithmic scale).

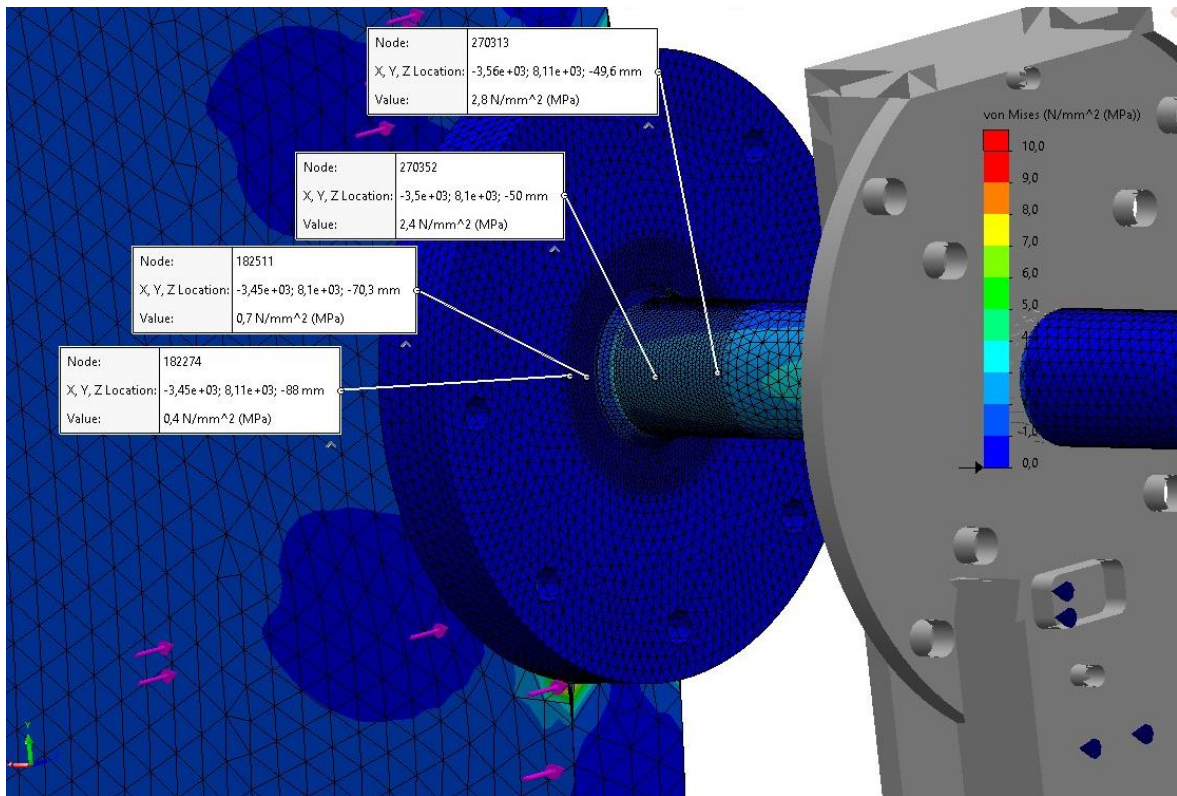


Figure 110. Stresses $\sigma_{0,4t}$ and $\sigma_{1,0t}$ next to the upper and lower weld toe (ring shafts).

Table 19. Hot Spot -stress in the ring flanges (Figure 111).

Mode no.	Lateral force caused by vortex shedding [N]	Stress at 0,4t distance from the lower weld toe [MPa]	Stress at 1,0t distance from the lower weld toe [MPa]	Stress at 0,4t distance from the upper weld toe [MPa]	Stress at 1,0t distance from the upper weld toe [MPa]	Hot Spot -stress at the lower weld toe [MPa]	Hot Spot -stress at the upper weld toe [MPa]
RF	1000.0	0.6000	0.4000	-	-	0.7340	-
1	3.8	0.0023	0.0015	-	-	0.0028	-
2	5.5	0.0039	0.0022	-	-	0.0050	-
3	8.6	0.0060	0.0034	-	-	0.0077	-
4	10.4	0.0073	0.0042	-	-	0.0094	-
5	41.4	0.0290	0.0166	-	-	0.0373	-
6	186.2	0.1303	0.0745	-	-	0.1678	-

7	197	0.1379	0.0788	-	-	0.1775	-
8	237.2	0.1660	0.0949	-	-	0.2137	-
9	249.4	0.1746	0.0998	-	-	0.2247	-
10	271.4	0.1900	0.1086	-	-	0.2445	-
11	427	0.2989	0.1708	-	-	0.3847	-
12	632.4	0.4427	0.2530	-	-	0.5698	-

Table 20. Fatigue lives for the ring flanges (Figure 111). In the table FOS stands for the factor of safety.

Mode no.	FAT-class	Obtained fatigue life for lower weld toe	Obtained fatigue life for upper weld toe	Number of cycles caused by vortex shedding	FOS (lower weld toe)	FOS (upper weld toe)
RF		REFERENCE FORCE				
1	90	6.72E+19	-	122 852 469	5.47E+11	-
2	90	1.20E+19	-	189 317 101	6.33E+10	-
3	90	3.13E+18	-	292 840 327	1.07E+10	-
4	90	1.77E+18	-	340 191 680	5.21E+09	-
5	90	2.81E+16	-	259 109 246	1.08E+08	-
6	90	3.09E+14	-	42 427	7.28E+09	-
7	90	2.61E+14	-	20 380	1.28E+10	-
8	90	1.49E+14	-	1 284	1.16E+11	-
9	90	1.28E+14	-	551	2.33E+11	-
10	90	9.97E+13	-	118	8.45E+11	-
11	90	2.56E+13	-	1	2.56E+13	-
12	90	7.88E+12	-	0	-	-

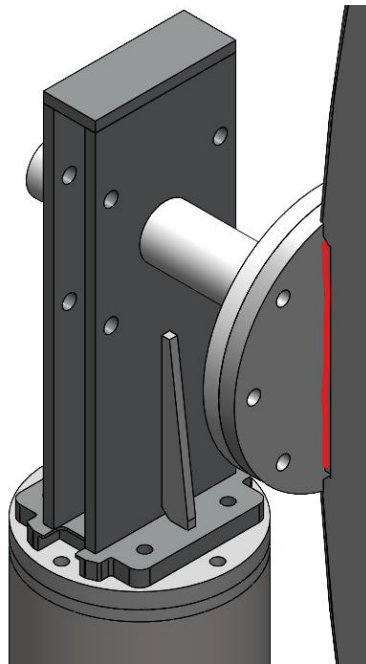


Figure 111. Welded detail examined in Table 17 and Table 18.

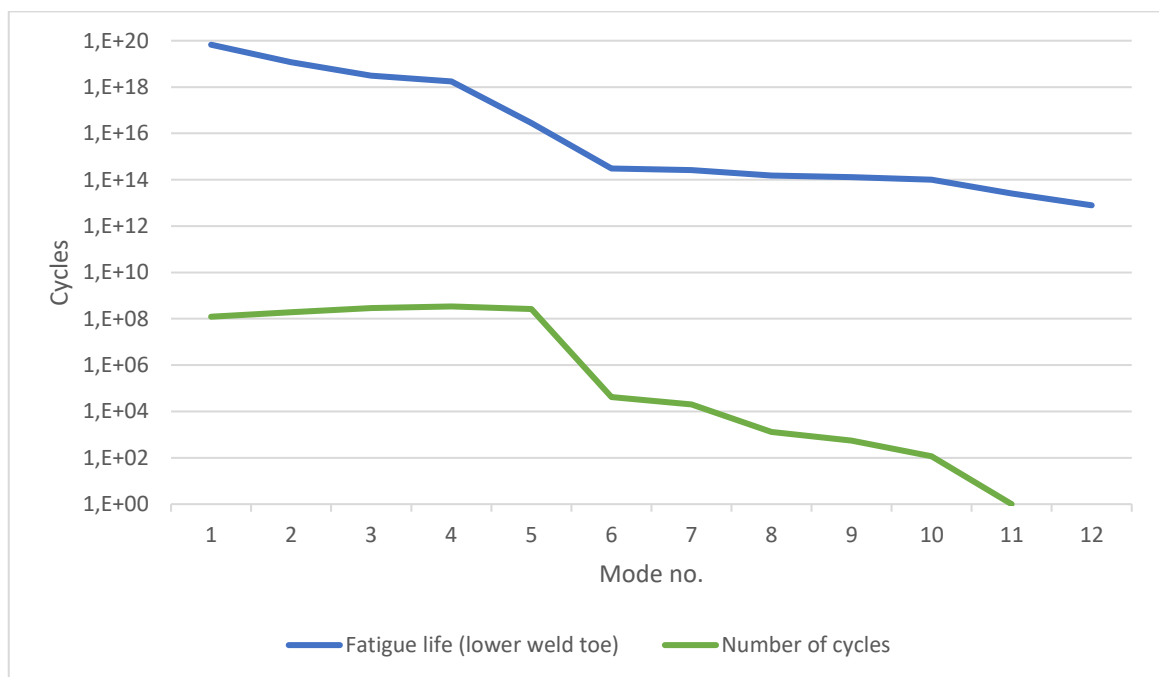


Figure 112. Obtained fatigue life in welded detail presented in Figure 111 compared to number of cycles caused by vortex shedding (logarithmic scale).

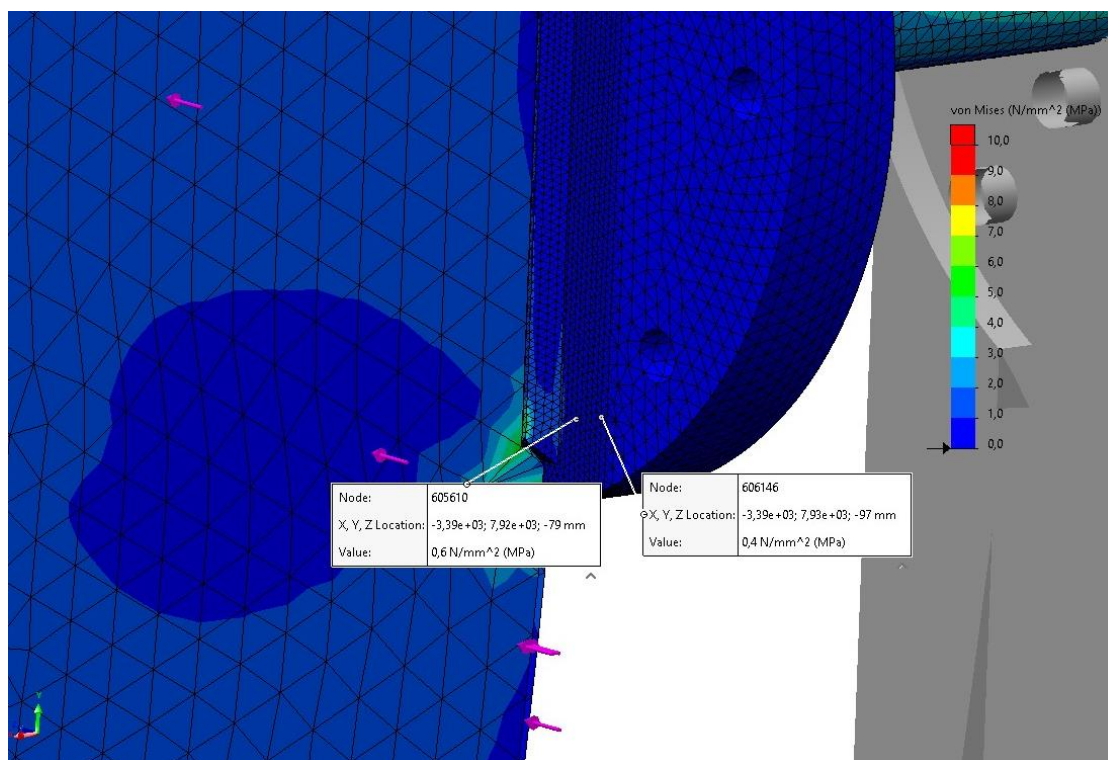


Figure 113. Stresses $\sigma_{0,4t}$ and $\sigma_{1,0t}$ next to the lower weld toe (ring flanges).

4.4 Bolted joints

The results for the analyses of bolted joints are presented in this chapter.

4.4.1 Static capacity

Bolt forces determined by analytical calculations and FE-analysis are presented in Table 21. Analytical calculations for bolt forces are presented in Appendix 4. Serviceability limit state is determined at 23 m/s storm wind and ultimate limit state at failure snow load or 2.0 times serviceability state depending on which one has higher value. For bearing resistance $F_{b,Rd}$ the lowest value between edge and inner bolt criteria is chosen. Requirements for bolted joints are presented on pages 61-62 with equations 34-38.

Table 21. Bolt forces at 23 m/s storm wind.

		Joints between ring halves	Joints between shafts and ring	Joints between shaft carriers and endcaps	Joints between endcaps and posts	Foundation bolts	
		<i>Size / class</i>	<i>M24 8.8</i>	<i>M24 8.8</i>	<i>M20 8.8</i>	<i>M20 8.8</i>	<i>M36 8.8</i>
<i>Design forces (analytical)</i>	$F_{t,Ed,ser}$	82 950 N	49 050 N	16 350 N	22 100 N	35 680 N	
	$F_{v,Ed,ser}$	23 260 N	4 900 N	14 300 N	8 778 N	36 600 N	
	$F_{t,Ed}$	116 450 N	68 860 N	32 700 N	44 200 N	71 400 N	
	$F_{v,Ed}$	46 520 N	9 800 N	28 600 N	17 556 N	73 200 N	
<i>Design forces (FE-analysis)</i>	$F_{t,Ed,ser}$	786 N	690 N	630 N	770 N	9 740 N	
	$F_{v,Ed,ser}$	585 N	500 N	9 480 N	3 920 N	3 950 N	
	$F_{t,Ed}$	1 572 N	1 380 N	1 260 N	1 540 N	19 480 N	
	$F_{v,Ed}$	1 170 N	1 000 N	18 960 N	7 840 N	7 900 N	
<i>Design resistance</i>	$F_{t,Rd}$	203 330 N	203 330 N	141 120 N	141 120 N	470 590 N	
	$F_{s,Rd,ser}$	40 580 N	57 610 N	38 364 N	36 942 N	132 590 N	
	$F_{v,Rd}$	135 550 N	135 550 N	94 080 N	94 080 N	313 730 N	
	$F_{b,Rd}$	832 000 N	499 380 N	509 090 N	335 920 N	661 283 N	
	$B_{b,Rd}$	644 960 N	744 180 N	637 870 N	637 870 N	1 169 400 N	

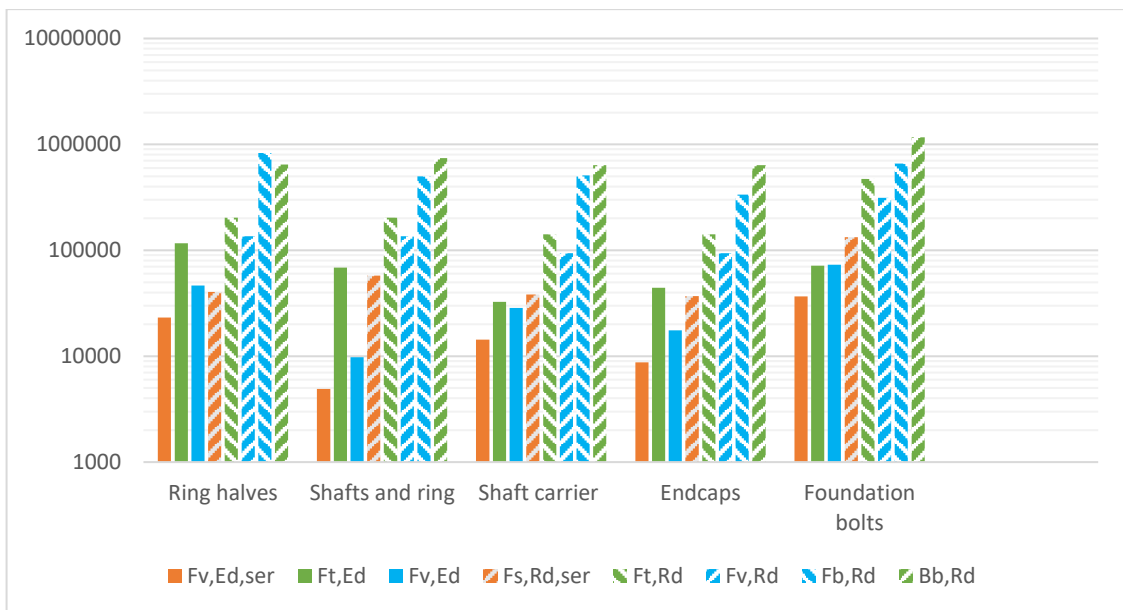


Figure 114. Analytically determined bolt forces compared to design resistances. Solid bars present design forces and hatched bars design resistances. The hatched bars are limits for the solid bars with the same colour.

4.4.2 Preload force and tightening torque

Tightening torque for each bolt sizes is presented in Table 22.

Table 22. Tightening torques for bolted joints.

Size	$F_M [N]$	μ_G	$d_2 [mm]$	μ_K	$D_{km} [mm]$	$P [mm]$	$M_A [Nm]$
M20	137 200	0.15	18.376	0.15	30	2.5	580
M24	197 680	0.15	22.051	0.15	36	3.0	1005
M36	457 520	0.15	33.402	0.15	55	4.0	3500

4.4.3 Shear fatigue of bolts

Shear fatigue assessment of bolts is presented in Table 23. SMATH calculations are presented in Appendix 7.

Table 23. Shear fatigue assessment of bolts.

	M24 8.8	M20 8.8	M36 8.8
Maximum shear force [N]	23 260	14 300	36 600
Nominal stress area A_s [mm ²]	353	245	817
Maximum shear stress [MPa]	65.9	58.4	44.8
FAT-class [MPa]	100	100	100
Maximum stress range for 11580000 cycles [MPa]	70.3	70.3	70.3
Cut off limit [MPa]	45.7	45.7	45.7

4.5 Welds

Design forces and resistances obtained for welds by using equations presented in chapter 3.6 are presented in Table 24. SMath calculations are presented in Appendix 8.

Table 24. Design forces and resistances in different welded joints of the structure

	Ring halves	Ring flanges	Shafts	Shaft carrier	Posts
Resultant force F_w	162 970 N	78 660 N	78 660 N	61 300 N	147 600 N
Length of weld l_w	1380 mm	492 mm	157 mm	400 mm	550 mm
Resultant force per unit length $F_{w,Ed}$	119 N/mm	160 N/mm	502 N/mm	154 N/mm	269 N/mm
Ultimate strength f_u	470 MPa	470 MPa	470 MPa	470 MPa	470 MPa
Correlation factor β_w	0.9	0.9	0.9	0.9	0.9
Partial safety factor γ_{M2}	1.25	1.25	1.25	1.25	1.25
Throat thickness a	4 mm	6 mm	6 mm	6 mm	10 mm
Design resistance per unit length $F_{w,Rd}$	964 N/mm	1447 N/mm	1447 N/mm	1447 N/mm	2412 N/mm
Usage of capacity	13 %	12 %	35 %	11 %	12 %

5 Conclusions

In this thesis the structural analysis of the steel sculpture was performed. In the analysis the static strength of structural components, joints and welds were examined. In addition to that the fatigue assessment and vibration analysis was performed. Load conditions were determined according to SFS-EN 1991 and structural analysis according to SFS-EN 1993.

The main goal of the thesis was to ensure that the sculpture will resist all the predictable load cases that may occur during its operating time without static or fatigue failure. The sculpture should also maintain its stability without major vibration in the structure that may cause the failure. Since the ring is rotating around the axles that are supported by bearings, the major displacements are not allowed to maintain the parallelism and concentricity of the shafts.

Structural analysis was performed by using FE-analysis, Hot Spot -method and analytical calculations. Couple major changes were made during the analysis process to improve the strength properties of the structure. Firstly, the ring was strengthened with additional 4 mm thick stiffeners that were applied inside the ring. With those, the stability of the ring was improved, and the ring acted stiffer and was not so vulnerable for vibration. Stiffeners are presented in Figure 115.

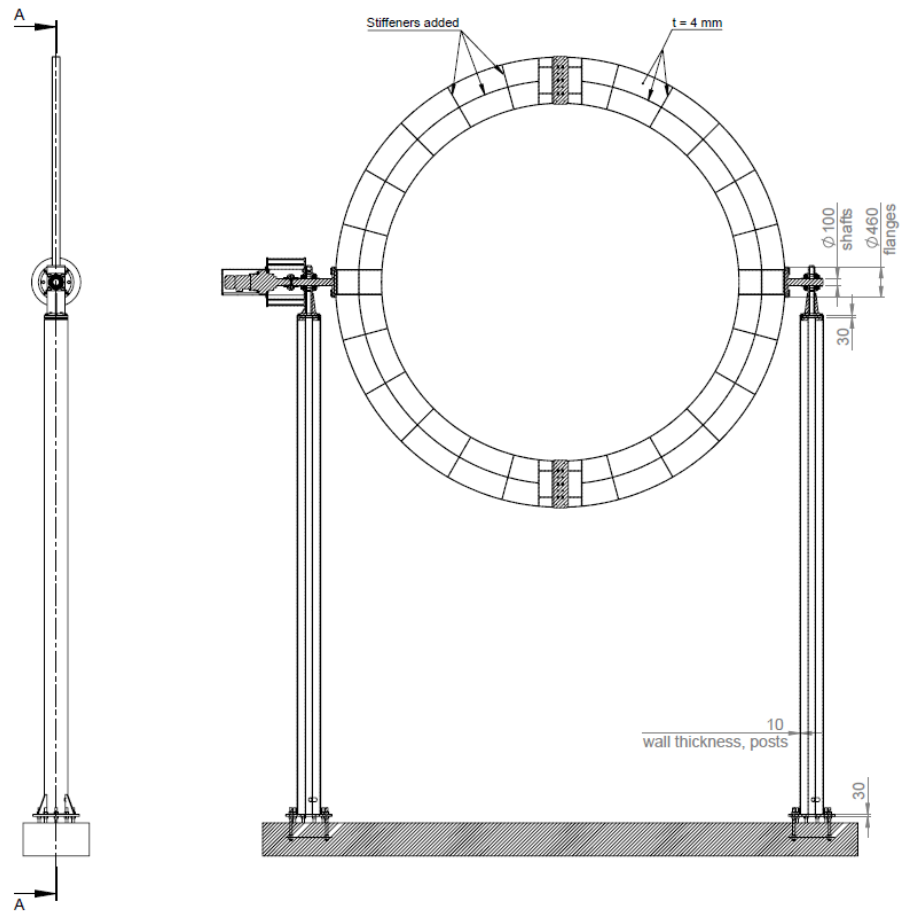


Figure 115. Stiffeners added to the ring

Secondly, gussets were added to the bottom joints of the posts to improve the fatigue strength of the posts. With those the structural stresses next to the weld toe were decreased and fatigue life increased to match with the requirements given for the sculpture. It was not allowed to make major changes to the shape and look of the sculpture so the gussets were dimensioned so that they will not be on sight after the foundation is buried to the ground (depth about 400 mm). The gussets are presented in Figure 116.

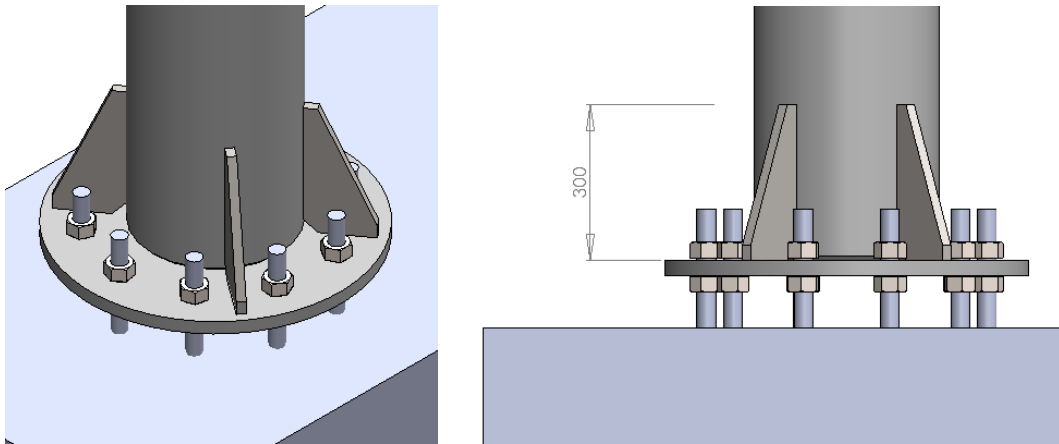


Figure 116. Gussets added to the bottom joint of posts.

Thirdly, the diameter of ring flanges that connects the ring to the shafts was increased to improve fatigue strength of the flanges. In revised version there is more room between the weld toe and the edge of the flange. With that the local stress concentration could be decreased and fatigue life increased. The flange in both versions is presented in Figure 117.

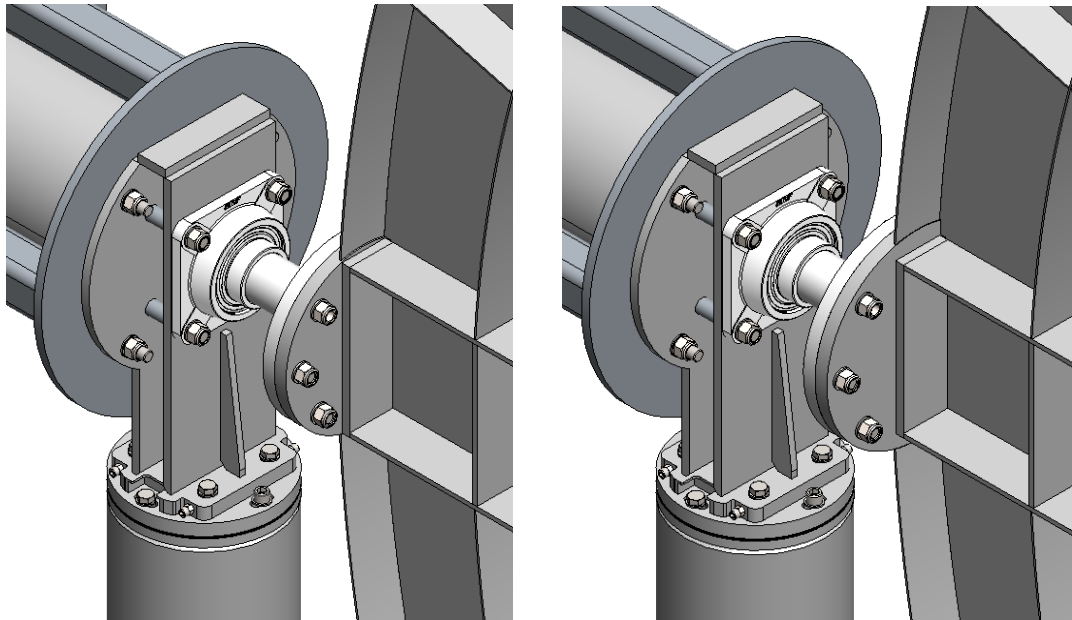


Figure 117. Revised ring flange. The diameter of the flange was increased from 400 mm to 460 mm.

In addition to these, minor changes were made in the bolted joints to maximize the design resistance of the joints. Mainly, the distance from the bolt to the axis of rotation were maximized. Example for that is presented in Figure 118.

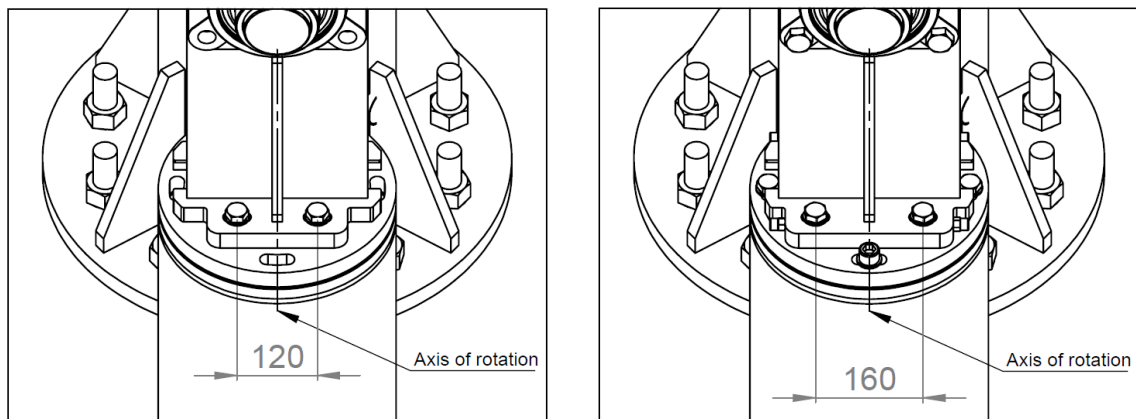


Figure 118. The example for the minor change in a bolted joint. The effective distance of the bolt could be increased from 60 mm to 80 mm.

The bolt forces determined by FE-analysis differs quite much compared to the analytically determined values. That is mainly caused by conservative approach on the analytical calculations (appendix 4). In analytical approach, it is assumed that the load is not equally distributed between bolts and the structural element could rotate freely around its rotational axis. In fact, most of the bolts are under compression or loaded only by shear force. In addition, the bolted connection -interaction in Solidworks Simulation models the bolt with tension only beam elements and fixes the elements to the edges of the holes with rigid bars (Figure 119). Because of that, the bolted connections give inaccurate results for compressed bolts and the bolt forces are not reliable. However, the durability of the bolts in the sculpture may be ensured by the analytical calculations performed.

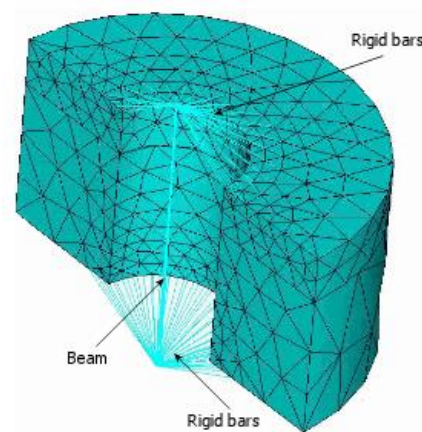


Figure 119. Structure of the bolted connections in Solidworks Simulation (Hudson 2019)

In addition to the wind and snow actions, the thermal actions were also examined. With the equations presented in chapter 2.3 the thermal expansion of the structure was determined. The most critical component for thermal expansion is the ring since it is attached to two fixed structural members. After the calculations could be stated that the theoretical amount of linear expansion in the ring has minor effects on the structure and that can be handled by using a floating joint that allows axial movement in the free ring shaft (Figure 120). Calculations for thermal expansion are presented in appendix 3. The ring shaft on the other side of the sculpture is attached to the electric motor with flexible coupling and key.

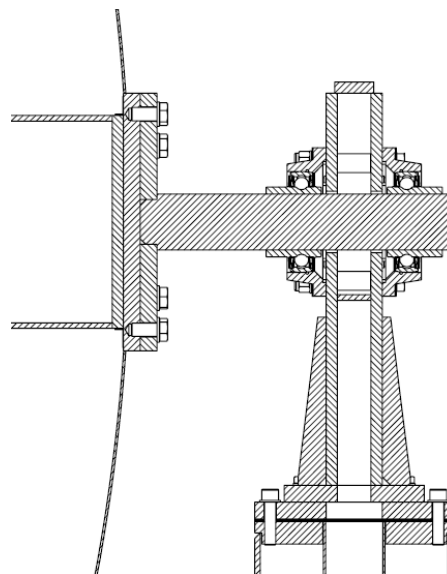


Figure 120. Joint between the free ring shaft and shaft carrier that allows axial movement

Overall, it can be stated that the structure can resist all predictable load cases that may occur during its operating time and with regular maintenance, the operating of the sculpture can be ensured. The sculpture can be seen in Hämeenlinna in the summer or fall of 2023 and then the results of this master's thesis can be verified. The final sculpture will hopefully be as close as possible to the original design presented in Figure 121.



Figure 121. The original design of the sculpture created by artist Johanna Rope (Rope 2018).

5.1 Further research

The research performed in this thesis may be developed to cover buckling analysis of the structure and the fatigue analysis of other welded joints that are not examined in this thesis. Also, the analyses presented in this thesis could be performed with analytical methods and the results could be compared to the results presented in chapter 4. In that way, the validity of the results could be verified.

References

- Bergman, J. 2019. Rakenteiden lujuus ja vakaus. Ministry of the Environment. Accessed 16 May 2022. Available at <https://www.ym.fi/download/noname/%7B5070311E-F267-47BC-A593-AEAA20EA31FE%7D/153592>.
- Björk, T., Hautala, P., Huhtala, K., Kivioja, S., Kleimola, M., Lavi, M., Martikka, H., Miettinen, J., Ranta, A., Rinkinen, J. & Salonen, P. 2014. Koneenosien suunnittelu. 6. painos. Helsinki, Sanoma Pro Oy. Pp. 134-144.
- Finnish Transport Infrastructure Agency. 2000. Betonirakenneohjeet. Accessed 26.5.2022. Available at: <https://julkaisut.vayla.fi/sillat/julkaisut/brako00.pdf>
- Hudson, A. 2019. Distributed Coupling for Bolts and Pins in SOLIDWORKS Simulation 2020. Javelin Tech. Accessed 30.5.2022. Available at: <https://www.javelin-tech.com/blog/2019/09/solidworks-simulation-distributed-coupling-bolts-pins/>
- Ilmatieteenlaitos. 2022. Suomen tuuliatlas. Accessed 26.5.2022. Available at: <http://tuuliatlas.fmi.fi/fi/#>
- Niemi, E, Wolfgang, F & Maddox S.J. 2018. Structural Hot-Spot Stress Approach to Fatigue Analysis of Welded Components. International Institute of Welding. Second edition. Springer. Pp. 1-72.
- Rope, J. 2018. Daily Mirror (Päivän peili) sculpture. Accessed 30.5.2022. Available at: <https://www.johannarope.com/dailymirror2018>
- SFS-EN 10025-2. 2019. Hot rolled products of structural steel. Part 2: Technical delivery conditions for non-alloy structural steel. Helsinki, Finnish Standards Association SFS. 33 p.
- SFS-EN 10088-3. 2014. Stainless steels. Part 3: Technical delivery conditions for semi-finished products, bars, rods, wire, sections, and bright products of corrosion resisting steels for general purposes. Helsinki, Finnish Standards Association SFS. 33 p.
- SFS-EN 1991-1-1. 2002. Actions of structures. Part 1-1: General actions. Densities, self-weight, imposed loads for building. Helsinki, Finnish Standards Association SFS. 71 p.

SFS-EN 1991-1-3. 2002. Actions of structures. Part 1-3: General actions. Snow loads. Helsinki, Finnish Standards Association SFS. 81 p.

SFS-EN 1991-1-4. 2002. Actions of structures. Part 1-4: General actions. Wind actions. Helsinki, Finnish Standards Association SFS. 254 p.

SFS-EN 1991-1-5. 2002. Actions of structures. Part 1-5: General actions. Thermal actions. Helsinki, Finnish Standards Association SFS. 68 p.

SFS-EN 1991-1-5. 2002. Annex 6. Actions of structures. Part 1-5: General actions. Thermal actions. National Annex. Helsinki, Finnish Standards Association SFS. 4 p.

SFS-EN 1993-1-8. 2005. Design of steel structures. Part 1-8: Design of joints. Helsinki, Finnish Standards Association SFS. 133 p.

SFS-EN 1993-1-9. 2005. Design of steel structures. Part 1-9: Fatigue. Helsinki, Finnish Standards Association SFS. 41 p.

Singh, S.P & Mittal, S. 2005. Vortex-induced oscillations at low Reynolds numbers: Hysteresis and vortex-shedding modes. *Journal of fluid and structures*. Vol. 20. Pp. 1085-1094.

Appendix 1. Wind load calculations

Load case 2 Wind load SFS-EN 1991 - 1 - 4

Structural factor:

$$c_{sfd} := 1$$

Force coefficient can be determined based on the rules of signboards

Force coefficient:

$$c_f := 1,80$$

Reference height:

$$z_e := 8,05 \text{ m}$$

Turbulence factor:

$$k_1 := 1,0$$

Terrain orography factor:

$$c_0(z) := 1$$

Roughness length:

$$z_0 := 0,3 \text{ m}$$

Roughness factor for terrain category II:

$$z_{0,II} := 0,05 \text{ m}$$

Reference height:

$$z := 8,05 \text{ m}$$

Wind turbulence intensity:

$$I_v(z) := \frac{k_1}{c_0(z) \cdot \ln\left(\frac{z}{z_0}\right)}$$

Wind turbulence intensity at reference height:

$$I_v(z_e) = 0,304$$

Air density:

$$\rho_{ilms} := 1,25 \frac{\text{kg}}{\text{m}^3}$$

Terrain factor depending on roughness length:

$$k_z := 0,19 \cdot \left(\frac{z}{z_{0,II}}\right)^{0,07} = 0,2712$$

Roughness factor:

$$c_r := k_z \cdot \ln\left(\frac{z}{z_0}\right) = 0,892$$

Directional factor:

$$c_{dir} := 1,0$$

Season factor:

$$c_{\text{season}} := 1,0$$

Fundamental value for the basic wind:

$$v_{b,0} := 23 \frac{\text{m}}{\text{s}}$$

Basic wind velocity:

$$v_b := c_{\text{dir}} \cdot c_{\text{season}} \cdot v_{b,0} = 23 \frac{\text{m}}{\text{s}}$$

Mean wind velocity:

$$v_m := c_r \cdot c_{\theta}(z_e) \cdot v_b = 20,5167 \frac{\text{m}}{\text{s}}$$

Peak velocity pressure:

$$q_p := \left(1 + 7 \cdot I_v(z_e)\right) \cdot \frac{1}{2} \cdot \rho_{\text{air}} \cdot v_m^2 = 822,9016 \frac{\text{N}}{\text{m}^2}$$

Reference area:

$$A_{\text{ref}} := \left(\pi \cdot (3,4 \text{ m})^2\right) - \pi \cdot (2,704 \text{ m})^2 = 13,3467 \text{ m}^2$$

Resultant wind force:

$$F_w := c_{\text{scd}} \cdot c_f \cdot q_p \cdot A_{\text{ref}} = 19769,4262 \text{ N}$$

Vortex shedding (posts):

Outer diameter of the posts:

$$b_{\text{tolppa}} := 0,355 \text{ m}$$

Number i mode of natural frequency:

$$n_{i,y} := 1,99 \text{ Hz}$$

Strouhal number:

$$St_{\text{tolppa}} := 0,18$$

Critical wind speed:

$$v_{cr,\text{tolppa}} := \frac{b_{\text{tolppa}} \cdot n_{i,y}}{St_{\text{tolppa}}} = 3,9247 \frac{\text{m}}{\text{s}}$$

Mass (post):

$$m_{\text{total}} := 4080 \text{ kg}$$

Structural damping:

$$\delta_{s,\text{tolppa}} := 0,08$$

Height of the post:

$$h_{\text{tolppa}} := 8,3 \text{ m}$$

Structure type based factor:

$$\zeta_{\text{tolppa}} := 1,0$$

Normalised mode shape of the structure:

$$\phi_{1,\text{tolppa}}(z) := \left(\frac{z}{h_{\text{tolppa}}} \right)^{\zeta_{\text{tolppa}}}$$

Mass per unit (post):

$$m_{\text{tolppa}}(z) := \frac{m_{\text{total}}}{h_{\text{tolppa}}} \cdot z$$

Equivalent mass of fundamental mode:

$$m_{1,e,\text{tolppa}} := \frac{\int_0^{h_{\text{tolppa}}} m_{\text{tolppa}}(s) \cdot \phi_{1,\text{tolppa}}(s)^2 \, ds}{\int_0^{h_{\text{tolppa}}} \phi_{1,\text{tolppa}}(s)^2 \, ds} = 3060 \frac{\text{kg}}{\text{m}}$$

Scruton number:

$$Sc_{tolppa} := \frac{2 \cdot \delta_{s,tolppa} \cdot m_{1,e,tolppa}}{\rho_{ilmz} \cdot b_{tolppa}^2} = 3107,9548$$

Kinematic viscosity of air:

$$\nu := 15 \cdot 10^{-6} \frac{\text{m}^2}{\text{s}}$$

Reynolds number:

$$Re_{tolppa} := \frac{b_{tolppa} \cdot v_{cr,tolppa}}{\nu} = 92885,0926$$

Factor m:

$$m_{tolppa} := 1$$

Factor n:

$$n_{tolppa} := 1$$

Distance between two node points:

$$L_{j,tolppa} := h_{tolppa} = 8,3 \text{ m}$$

l/b:

$$\lambda_{tolppa} := \frac{L_{j,tolppa}}{b_{tolppa}} = 23,3803$$

Correlation length factor:

$$K_{w,tolppa} := 3 \cdot \frac{L_{j,tolppa}}{b_{tolppa}} \cdot \left(1 - \frac{L_{j,tolppa}}{b_{tolppa}} + \frac{1}{3} \cdot \left(\frac{L_{j,tolppa}}{b_{tolppa}} \right)^2 \right) = 1$$

Mode shape factor:

$$K_{tolppa} := 0,13$$

Distance between posts:

$$a_{tolppien,väli} := 7600 \text{ mm}$$

Ratio of a and b:

$$\frac{a_{tolppien,väli}}{b_{tolppa}} = 21,4085$$

Lateral force coefficient:

$$c_{lat,tolppa} := c_{lat,single,tolppa}$$

Basic lateral force coefficient:

$$c_{lat,0,tolppa} := 0,7$$

Critical wind velocity ratio:

$$\frac{v_{cr,tolppa}}{v_m} = 0,1913$$

Modified lateral force coefficient:

$$c_{lat,tolppa} := c_{lat,0,tolppa} = 0,7$$

Maximum displacement:

$$y_{F,max,tolppa} := \left(\frac{1}{St_{tolppa}} \cdot \frac{1}{2} \cdot \frac{1}{SC_{tolppa}} \cdot K_{tolppa} \cdot K_{w,tolppa} \cdot c_{lat,tolppa} \right) \cdot b_{tolppa} = 0,3208 \text{ mm}$$

Load caused by vortex shedding:

$$F_{w,tolppa}(s) := m_{tolppa}(s) \cdot (2 \cdot n \cdot n_{i,y})^2 \cdot \phi_{i,tolppa}(s) \cdot y_{F,max,tolppa}$$

$$F_{w,tolppa}(L_j, tolppa) = 204,6332 \text{ N}$$

Number of load cycles:

Lifetime in seconds:

$$T := 3,2 \text{ s} \cdot 10^7 \cdot 15 = 4,8 \cdot 10^8 \text{ s}$$

Bandwidth factor:

$$\varepsilon_0 := 0,3$$

Weibull distributed wind velocity:

$$v_0 := 0,2 \cdot v_m = 4,1033 \frac{\text{m}}{\text{s}}$$

+

Total cycles:

$$N_{tolppa} := 2 \cdot T \cdot n_{i,y} \cdot \varepsilon_0 \cdot \left(\frac{v_{cr,tolppa}}{v_0} \right)^2 \cdot \exp \left(- \left(\frac{v_{cr,tolppa}}{v_0} \right)^2 \right) = 2,10029559 \cdot 10^8$$

Galloping (posts):

Factor of galloping instability:

$$a_G := 10$$

First cross-wind frequency of structure:

$$n_{1,y} := 1,99 \text{ Hz}$$

Critical wind velocity for galloping:

$$v_{CG, \text{tolppa}} := \frac{2 \cdot S_{C, \text{tolppa}}}{a_G} \cdot n_{1,y} \cdot b_{\text{tolppa}} = 439,1229 \frac{\text{m}}{\text{s}}$$

Mean wind velocity:

$$v_m = 20,5167 \frac{\text{m}}{\text{s}} \quad \text{---> OK!}$$

Vortex shedding (ring):

Thickness of the ring:

$$b_{\text{kehä}} := 0,120 \text{ m}$$

Strouhal number:

$$St_{\text{kehä}} := 0,109$$

Critical wind velocity:

$$v_{cr, \text{kehä}} := \frac{b_{\text{kehä}} \cdot n_{1,y}}{St_{\text{kehä}}} = 2,1908 \frac{\text{m}}{\text{s}}$$

Mass (ring):

$$m_{\text{kehä}} := 1500 \text{ kg}$$

Structural damping:

$$\delta_{s, \text{kehä}} := 0,5$$

Height of the ring:

$$h_{\text{kehä}} := 6,8 \text{ m}$$

Structure type base factor:

$$\zeta_{\text{kehä}} := 0,6$$

Normalised mode shape of the structure:

$$\phi_{1, \text{kehä}}(z) := \left(\frac{z}{h_{\text{kehä}}} \right)^{\zeta_{\text{kehä}}}$$

Mass per unit (ring):

$$m_{\text{kehä}}(z) := \frac{m_{\text{kehä}}}{h_{\text{kehä}}} \cdot z$$

Equivalent mass of fundamental mode:

$$m_{1,e,\text{kehä}} := \frac{\int_0^{h_{\text{kehä}}} m_{\text{kehä}}(s) \cdot \phi_{1,\text{kehä}}(s)^2 ds}{\int_0^{h_{\text{kehä}}} \phi_{1,\text{kehä}}(s)^2 ds} = 1031,2498 \frac{\text{kg}}{\text{m}}$$

Scruton number:

$$SC_{\text{kehä}} := \frac{2 \cdot \delta_{s,\text{kehä}} \cdot m_{1,e,\text{kehä}}}{\rho_{\text{ilmä}} \cdot b_{\text{kehä}}^2} = 57291,6547$$

Kinematic viscosity of air:

$$\nu := 15 \cdot 10^{-6} \frac{\text{m}^2}{\text{s}}$$

Reynolds number:

$$Re_{\text{kehä}} := \frac{b_{\text{kehä}} \cdot v_{cr,\text{kehä}}}{\nu} = 17526,6055$$

Factor m:

$$m_{\text{kehä}} := 1$$

Factor n:

$$n_{\text{kehä}} := 1$$

Distance between two node points:

$$L_{j,\text{kehä}} := h_{\text{kehä}} = 6,8 \text{ m}$$

1/b:

$$\lambda_{\text{kehä}} := \frac{L_{j,\text{kehä}}}{b_{\text{kehä}}} = 56,6667$$

Correlation length factor:

$$K_{w,\text{kehä}} := 3 \cdot \frac{L_{j,\text{kehä}}}{b_{\text{kehä}}} \cdot \left(1 - \frac{L_{j,\text{kehä}}}{\lambda_{\text{kehä}}} + \frac{1}{3} \cdot \left(\frac{L_{j,\text{kehä}}}{\lambda_{\text{kehä}}} \right)^2 \right) = 1$$

Mode shape factor:

$$K_{\text{kehä}} := 0,13$$

Basic lateral force coefficient:

$$c_{lat,0,kehä} := 0,7$$

Critical wind velocity ratio:

$$\frac{v_{cr,kehä}}{v_m} = 0,1068$$

Lateral force coefficient:

$$c_{lat,kehä} := c_{lat,0,kehä} = 0,7$$

Displacement caused by vortex shedding:

$$y_{F,max,kehä} := \left(\frac{1}{St_{kehä}} \cdot \frac{1}{2} \cdot \frac{1}{Sc_{kehä}} \cdot K_{kehä} \cdot K_{w,kehä} \cdot c_{lat,kehä} \right) \cdot b_{kehä} = 0,016 \text{ mm}$$

Load caused by vortex shedding:

$$F_{w,kehä} (s) := m_{kehä} (s) \cdot (2 \cdot n \cdot n_{i,y})^2 \cdot \phi_{1,kehä} (s) \cdot y_{F,max,kehä}$$

$$F_{w,kehä} (L_{j,kehä}) = 3,7621 \text{ N}$$

Number of load cycles:

Lifetime in seconds:

$$T := 3,2 \text{ s} \cdot 10^7 \cdot 15 = 4,8 \cdot 10^8 \text{ s}$$

Bandwidth factor:

$$\varepsilon_0 := 0,3$$

Total cycles:

$$N_{kehä} := 2 \cdot T \cdot n_{i,y} \cdot \varepsilon_0 \cdot \left(\frac{v_{cr,kehä}}{v_0} \right)^2 \cdot \exp \left(- \left(\frac{v_{cr,kehä}}{v_0} \right)^2 \right) = 1,22852469 \cdot 10^8$$

Galloping (ring):

Critical wind velocity for galloping:

$$v_{CG,kehä} := \frac{2 \cdot S_{c,kehä}}{a_G} \cdot n_{1,y} \cdot b_{kehä} = 2736,2494 \frac{m}{s}$$

Mean wind velocity:

$$v_m = 20,5167 \frac{m}{s} \quad \rightarrow \text{OK!}$$

$$F_{w,tolppa}(h_{tolppa}) = 204,6332 \text{ N}$$

$$F_{w,kehä}(h_{kehä}) = 3,7621 \text{ N}$$

$$Y_{F,max,tolppa} = 0,3208 \text{ mm}$$

$$Y_{F,max,kehä} = 0,016 \text{ mm}$$

$$N_{tolppa} = 2,1003 \cdot 10^8$$

$$N_{kehä} = 1,22852469 \cdot 10^8$$

$$v_{cr,tolppa} = 3,9247 \frac{m}{s}$$

$$v_{cr,kehä} = 2,1908 \frac{m}{s}$$

$$v_{CG,tolppa} = 439,1229 \frac{m}{s}$$

$$v_{CG,kehä} = 2736,2494 \frac{m}{s}$$

Appendix 2. Snow load calculations

+ Load case 1 Snow load SFS-EN 1991 - 1 - 3

Undrifted snowload

Snow load shape coefficient:

$$\mu_i := 0,8$$

Exposure coefficient:

$$C_e := 1,0$$

Thermal coefficient:

$$C_t := 1,0$$

Snow load, zone number:

$$Z := 2,5$$

Diameter of the ring:

$$d_{\text{kehän,ulko}} := 6800 \text{ mm}$$

Altitude above Sea Level:

$$A_{\text{korkeus,merenpinnasta}} := 80 \text{ m}$$

Thickness of the ring:

$$t_{\text{kehä}} := 120 \text{ mm}$$

Radius of the ring:

$$r_{\text{kehän,ulko}} := \frac{d_{\text{kehän,ulko}}}{2} = 3,4 \text{ m}$$

Characteristic value for snow load:

$$s_k := \left(0,790 \frac{\text{kN}}{\text{m}} \cdot Z + 0,375 \frac{\text{kN}}{\text{m}} \right) + \frac{A_{\text{korkeus,merenpinnasta}}}{336 \frac{\text{m}}{\text{kN}}} = 2,5881 \frac{\text{kN}}{\text{m}}$$

Persistent or transient snow load:

$$s := \mu_i \cdot C_e \cdot C_t \cdot s_k = 2,0705 \frac{\text{kN}}{\text{m}}$$

Face area of the ring:

$$A_{\text{kehän,otsapinta}} := \left(\pi \cdot (3,4 \text{ m})^2 \right) - \pi \cdot (2,7 \text{ m})^2 = 13,4146 \text{ m}^2$$

Upper area of the ring:

$$A_{\text{kehän,yläpinta}} := \frac{2 \cdot \pi \cdot r_{\text{kehän,ulko}}}{2} \cdot t_{\text{kehä}} = 1,2818 \text{ m}^2$$

Snow load, upper area (normal circumstances):

$$F_{\text{normaali,lumikuorma}} := s \cdot A_{\text{kehän,yläpinta}} = 2653,8739 \text{ N}$$

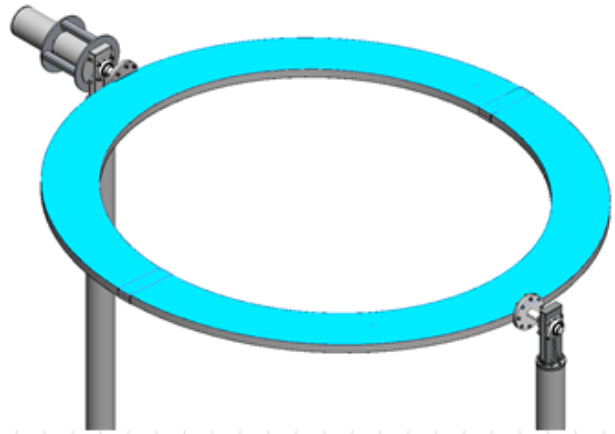
Snow load in malfunction situation when ring has stopped on perpendicular position:

$$F_{\text{onnettomuus,kuorma}} := s \cdot A_{\text{kehän,otsapinta}} = 27774,6112 \text{ N}$$

Upper area of the ring:



Face area of the ring:



Appendix 3. Thermal action calculations

Thermal actions SFS-EN 1991 - 1 - 5

Minimum temperature (probability 2%):

$$T_{\min} := -38 \text{ K} + 273,15 \text{ K} = 235,15 \text{ K}$$

Maximum temperature (probability 2%):

$$T_{\max} := 34 \text{ K} + 273,15 \text{ K} = 307,15 \text{ K}$$

Factor for solar radiation:

$$T_s := 42 \text{ K}$$

Nominal length:

$$l_o := 6800 \text{ mm}$$

Dark surface:

$$T_{\max,i} := T_{\max} + T_s = 349,15 \text{ K}$$

Temperature difference:

$$\Delta T := T_{\max,i} - T_{\min} = 114 \text{ K}$$

Coefficient of linear expansion:

$$\alpha_{\text{teräs}} := 12 \cdot 10^{-6} \cdot \frac{1}{\text{K}}$$

Linear expansion (axial movement to bearing):

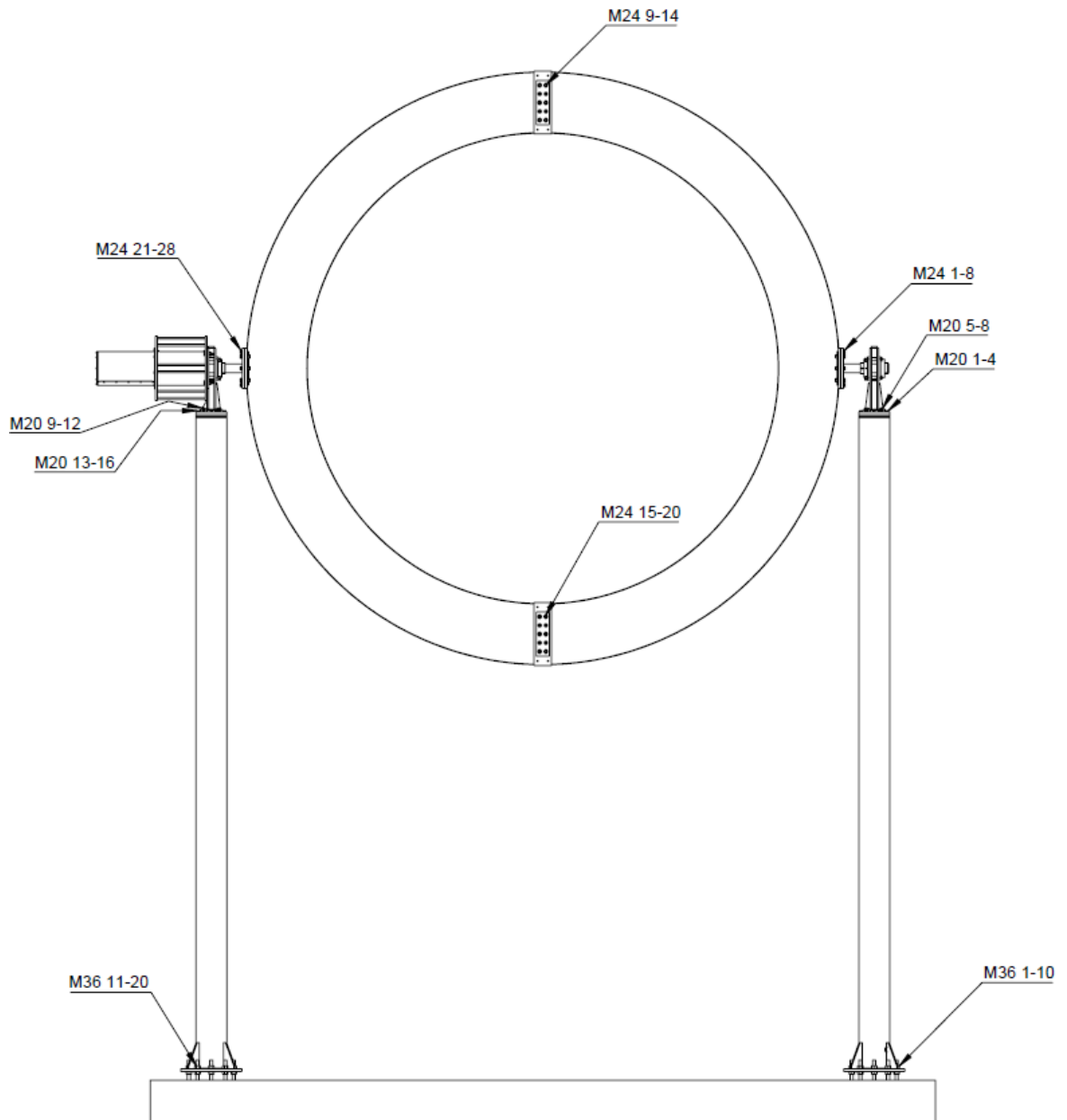
Total transition:

$$\Delta l := \alpha_{\text{teräs}} \cdot l_o \cdot \Delta T = 9,3024 \text{ mm}$$

+

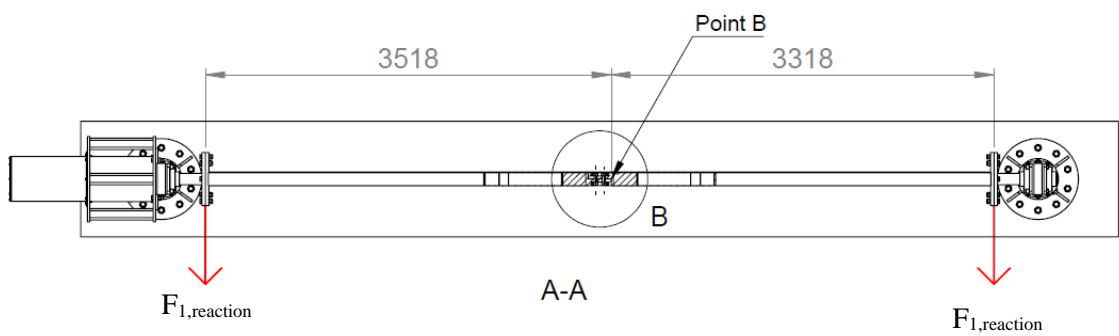
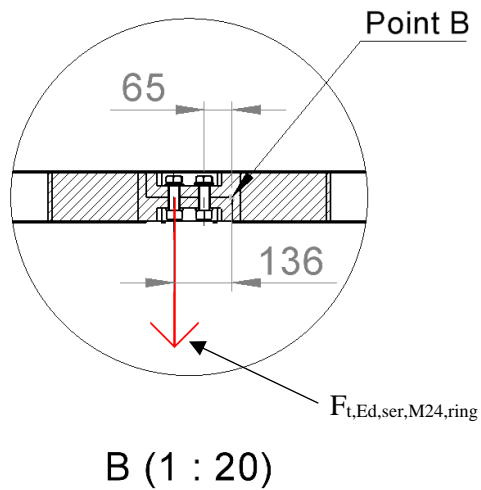
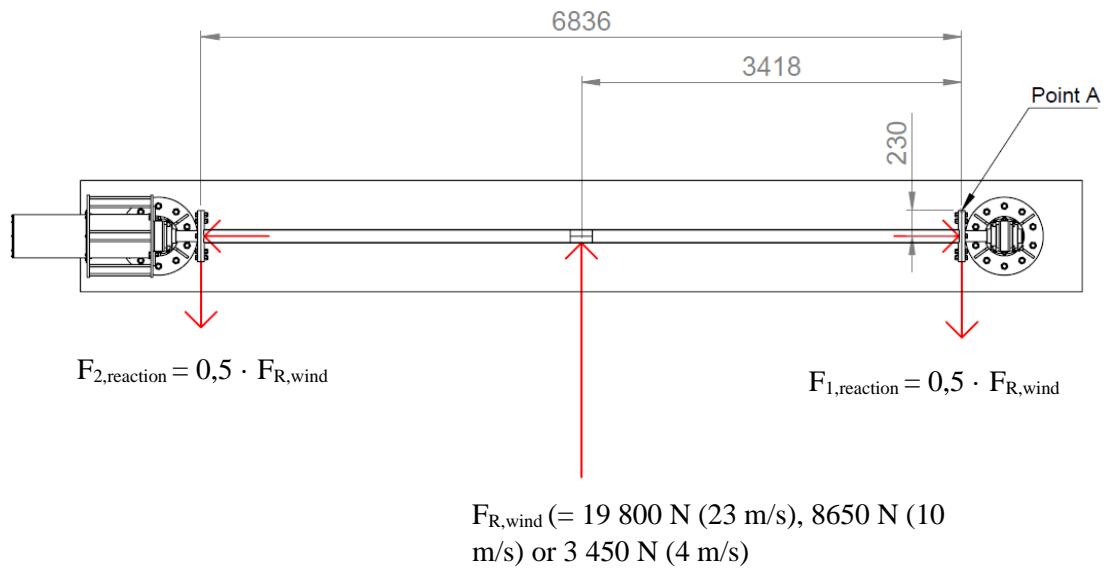
Appendix 4. Analytical calculations for bolt forces

Bolted joints in the structure:



Wind and snow load:

Tensile force on the ring's bolts (M24 9-14 & M24 15-20):



Based on the equilibrium of bending moments in respect of point B:

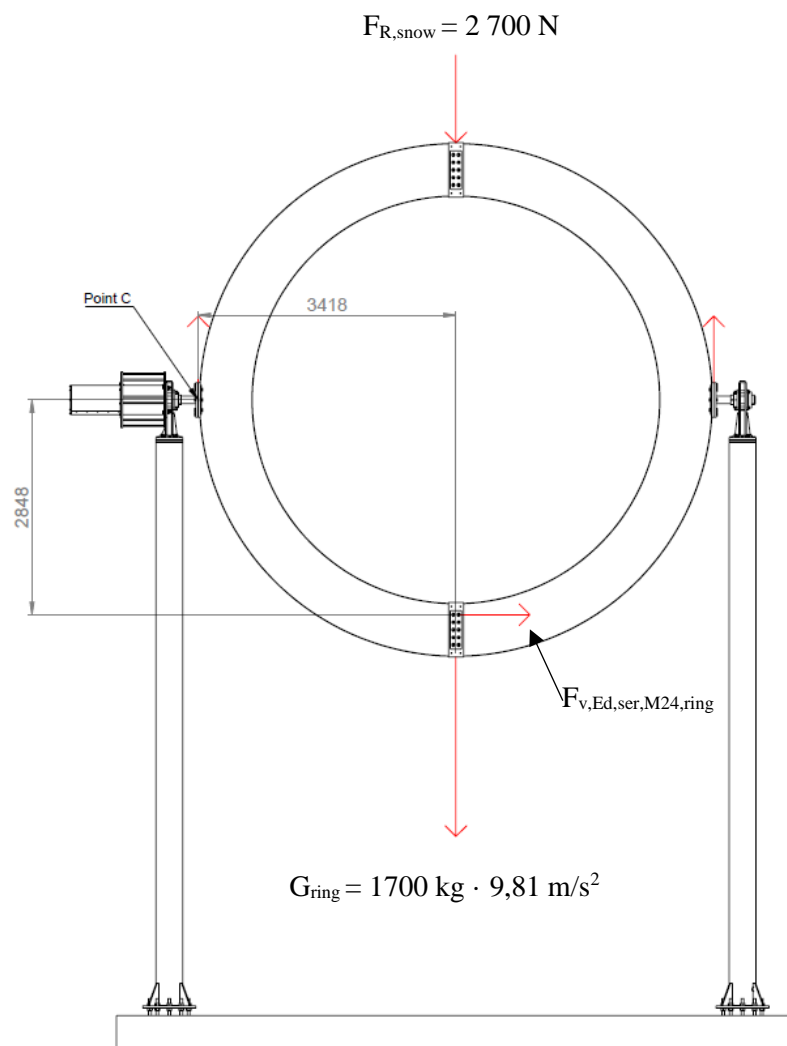
$$F_{t,Ed,ser,ring} = \frac{F_{1,reaction} \cdot 3318 \text{ mm} + F_{2,reaction} \cdot 3518 \text{ mm}}{136 \text{ mm}} \quad (1)$$

It is assumed that only six bolts carry the load (on the safe side):

$$F_{t,Ed,ser,ring,per \text{ bolt}} = \frac{F_{t,Ed,ser,ring}}{6} \quad (2)$$

The failure situation where the ring stops to parallel position compared to the ground can be calculated with the equations 1 and 2 by calculation reaction forces $F_{1,reaction}$ and $F_{2,reaction}$ in respect of the failure snow load $F_{R,snow, failure} = 27\,800 \text{ N}$.

Shear force on the ring's bolts (M24 9-14 & M24 15-20):



Based on the equilibrium of bending moments in respect of point C:

$$F_{v,Ed,ser,ring} = \frac{F_{R,snow} \cdot 3418 \text{ mm} + G_{ring} \cdot 3418 \text{ mm}}{2848 \text{ mm}} \quad (3)$$

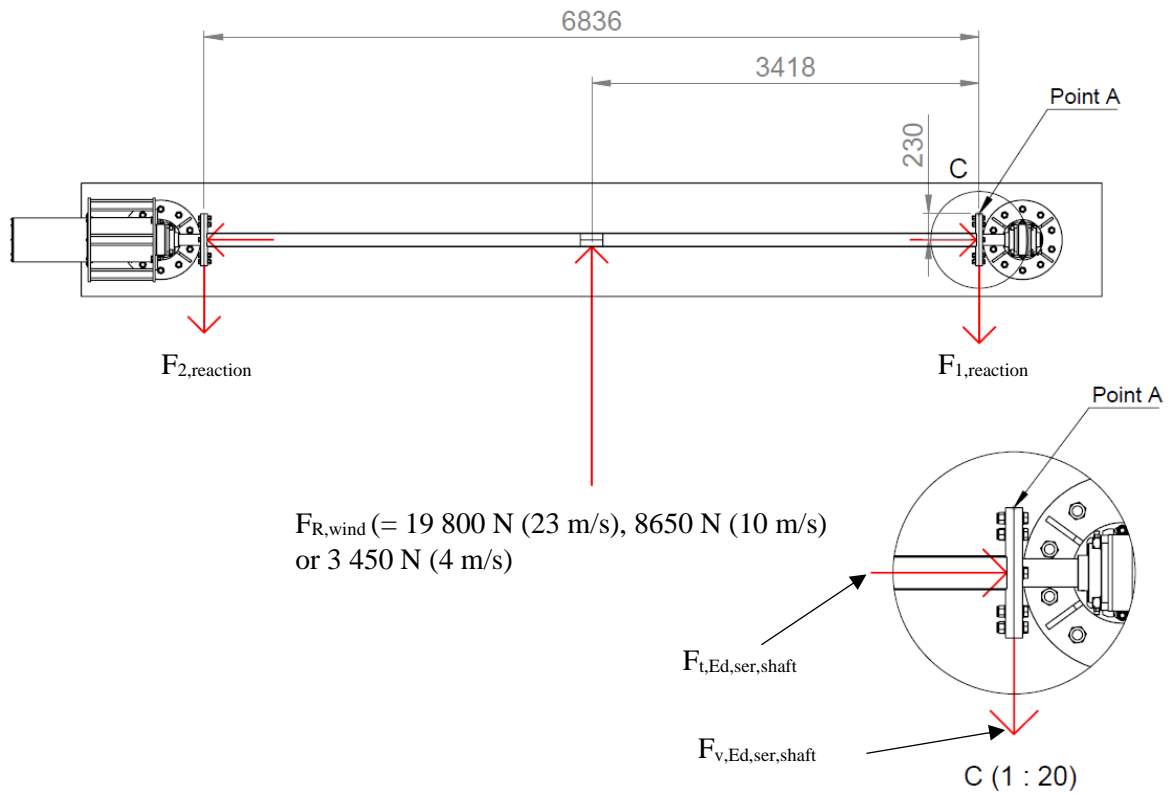
It is assumed that only one bolt carries the shear load (manufacturing tolerances → on the safe side):

$$F_{v,Ed,ser,ring,per \text{ bolt}} = F_{v,Ed,ser,ring} \quad (4)$$

Design tensile and shear forces for M24 9-14 and M24 15-20 are:

	Tensile force	Shear force
Storm wind 23 m/s	82 940 N	23 260 N
Maximum operating wind 10 m/s	36 235 N	23 260 N
Mean wind velocity in Hämeenlinna 4 m/s, used in fatigue assessment	14 455 N	23 260 N
Snow load in failure mode	116 450 N	-

Tensile force on the shaft's bolts (M24 1-8 & M24 21-28):

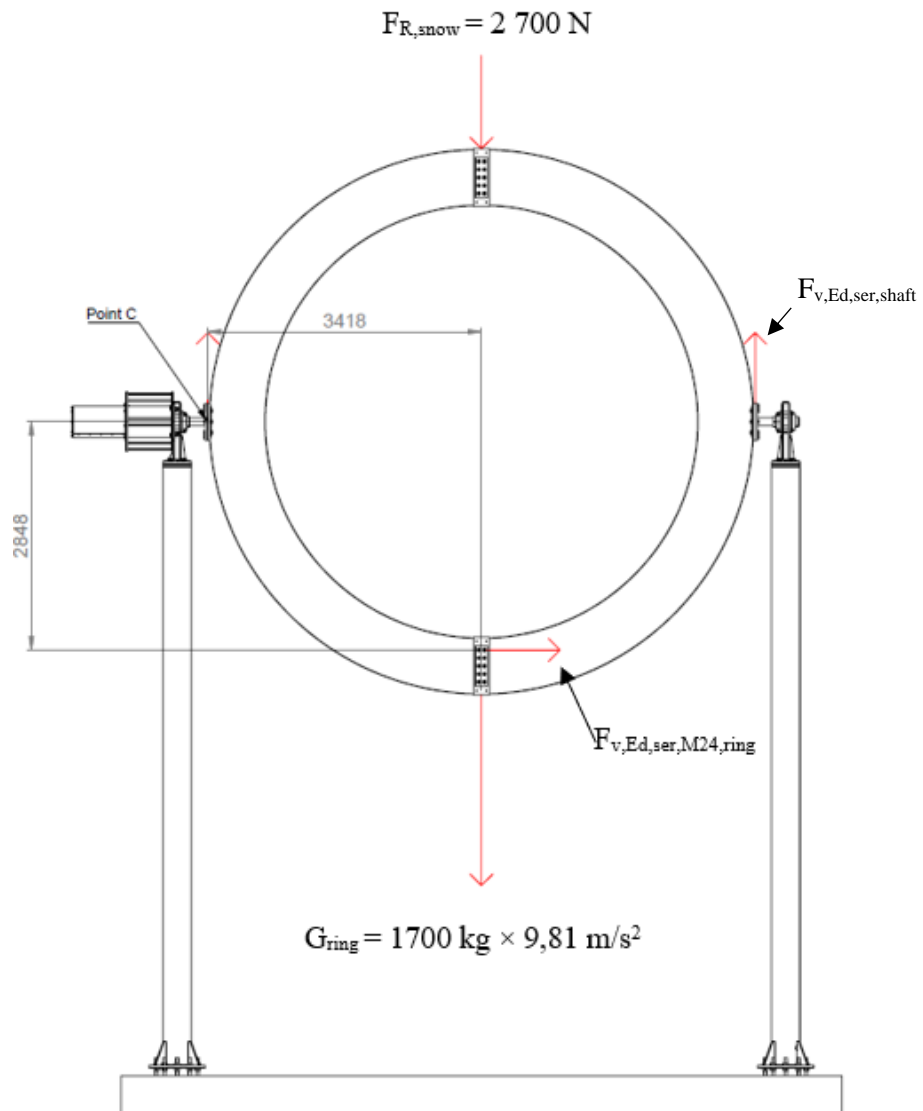


Based on the equilibrium of bending moments in respect of point A:

$$F_{t,Ed,ser,shaft} = \frac{\frac{1}{2} \cdot F_{R,wind} \cdot 3418\text{ mm}}{230\text{ mm}} \quad (5)$$

It is assumed that only three bolts (3/8) carry the tensile load (manufacturing tolerances → on the safe side):

$$F_{t,Ed,ser,shaft,per\ bolt} = \frac{F_{t,Ed,ser,shaft}}{3} \quad (6)$$



The shear force (per side) may be calculated based on the equilibrium of forces:

$$F_{v,Ed,ser,shaft} = \frac{1}{2} \cdot (G_{ring} + F_{R,snow} + F_{R,wind}) \quad (7)$$

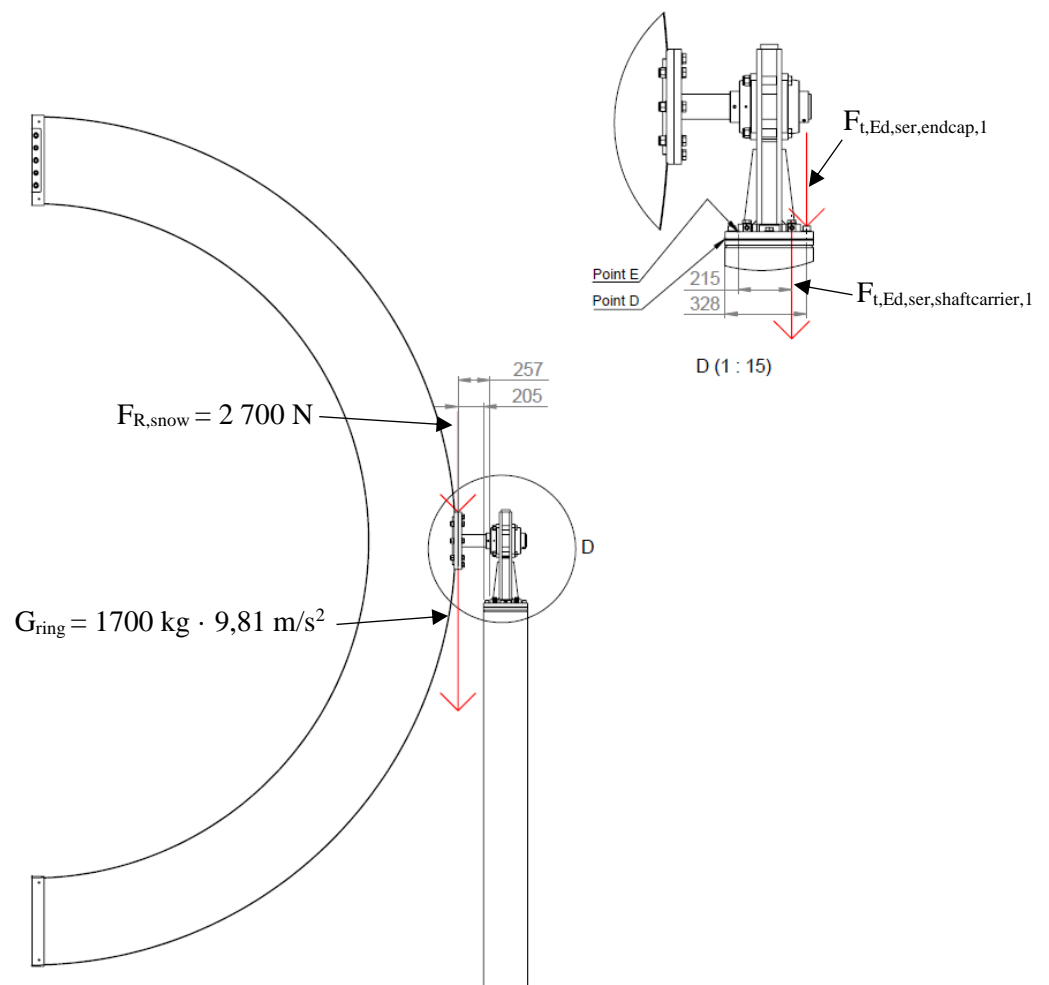
It is assumed that only four bolts (4/8) carry the shear load (manufacturing tolerances \rightarrow on the safe side):

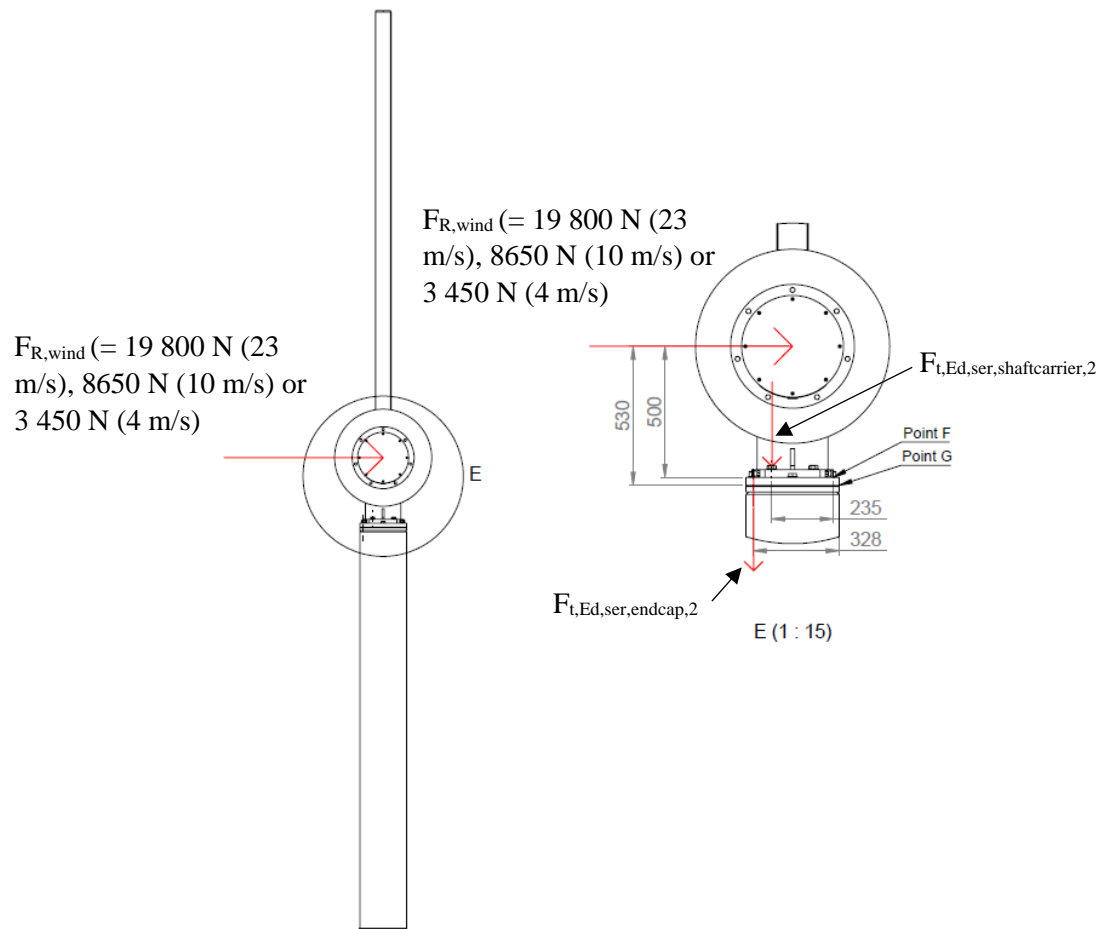
$$F_{v,Ed,ser,shaft,per\ bolt} = \frac{F_{v,Ed,ser,shaft}}{4} \quad (8)$$

Design tensile and shear forces for shaft's bolts M24 1-8 and M24 21-28 are:

	Tensile force	Shear force
Storm wind 23 m/s	49 050 N	4 900 N
Maximum operating wind 10 m/s	21 450 N	3 550 N
Mean wind velocity in Hämeenlinna 4 m/s, used in fatigue assessment	8 545 N	2 855 N
Snow load in failure mode	68 900 N	5 600 N

Tensile force on the shaft carrier's and end cap's bolts (M20 5-8 & M20 9-12):





Based on the equilibrium of bending moments in respect of points D and E:

$$F_{t,Ed,ser,shaftcarrier,1} = \frac{\frac{1}{2} \cdot (G_{ring} + F_{R,snow}) \cdot 257 \text{ mm}}{215 \text{ mm}} \quad (9)$$

$$F_{t,Ed,ser,endcap,1} = \frac{\frac{1}{2} \cdot (G_{ring} + F_{R,snow}) \cdot 205 \text{ mm}}{328 \text{ mm}} \quad (10)$$

Based on the equilibrium of bending moments in respect of points F and G:

$$F_{t,Ed,ser,shaftcarrier,2} = \frac{\frac{1}{2} \cdot F_{R,wind} \cdot 500 \text{ mm}}{235 \text{ mm}} \quad (11)$$

$$F_{t,Ed,ser,endcap,2} = \frac{\frac{1}{2} \cdot F_{R,wind} \cdot 530 \text{ mm}}{328 \text{ mm}} \quad (12)$$

Total tensile forces are:

$$F_{t,Ed,ser,shaftcarrier} = F_{t,Ed,ser,shaftcarrier,1} + F_{t,Ed,ser,shaftcarrier,2} \quad (13)$$

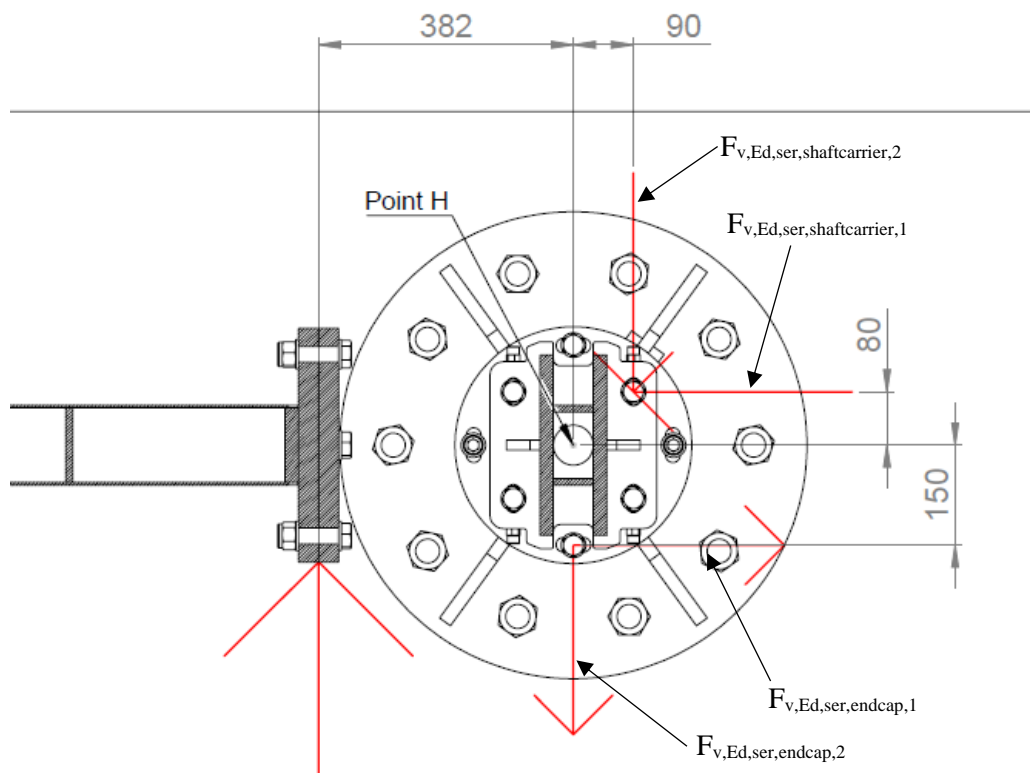
$$F_{t,Ed,ser,endcap} = F_{t,Ed,ser,endcap,1} + F_{t,Ed,ser,endcap,2} \quad (14)$$

It is assumed that in the shaft carrier two bolts (2/4) are carrying the tensile load (on the safe side). However, in the endcap assumption is that only one bolt is carrying the tensile load. Therefore, the loads per bolt are:

$$F_{t,Ed,ser,shaftcarrier,per\ bolt} = \frac{F_{t,Ed,ser,shaftcarrier}}{2} \quad (15)$$

$$F_{t,Ed,ser,endcap,per\ bolt} = F_{t,Ed,ser,endcap} \quad (16)$$

Shear force on the shaft carrier's and end cap's bolts (M20 5-8 & M20 9-12):



$F_{R,wind}$ (= 19 800 N (23 m/s), 8650 N (10 m/s) or 3 450 N (4 m/s))

Based on the equilibrium of bending moments in respect of point H:

$$F_{v,Ed,ser,shaftcarrier,1} = \frac{\frac{1}{2} \cdot F_{R,wind} \cdot 382 \text{ mm}}{80 \text{ mm}} \quad (17)$$

$$F_{v,Ed,ser,endcap,1} = \frac{\frac{1}{2} \cdot F_{R,wind} \cdot 382 \text{ mm}}{150 \text{ mm}} \quad (18)$$

Based on the equilibrium of forces:

$$F_{v,Ed,ser,shaftcarrier,2} = \frac{F_{R,wind}}{2} \quad (19)$$

$$F_{v,Ed,ser,endcap,2} = \frac{F_{R,wind}}{2} \quad (20)$$

Total shear forces are:

$$F_{v,Ed,ser,shaftcarrier} = F_{v,Ed,ser,shaftcarrier,1} + F_{v,Ed,ser,shaftcarrier,2} \quad (21)$$

$$F_{v,Ed,ser,endcap} = F_{v,Ed,ser,endcap,1} + F_{v,Ed,ser,endcap,2} \quad (22)$$

It is assumed that all four bolts (4/4) carry the shear load, the loads per bolt are:

$$F_{v,Ed,ser,shaftcarrier,per \text{ bolt}} = \frac{F_{v,Ed,ser,shaftcarrier}}{4} \quad (23)$$

$$F_{v,Ed,ser,endcap,per \text{ bolt}} = \frac{F_{v,Ed,ser,endcap}}{4} \quad (24)$$

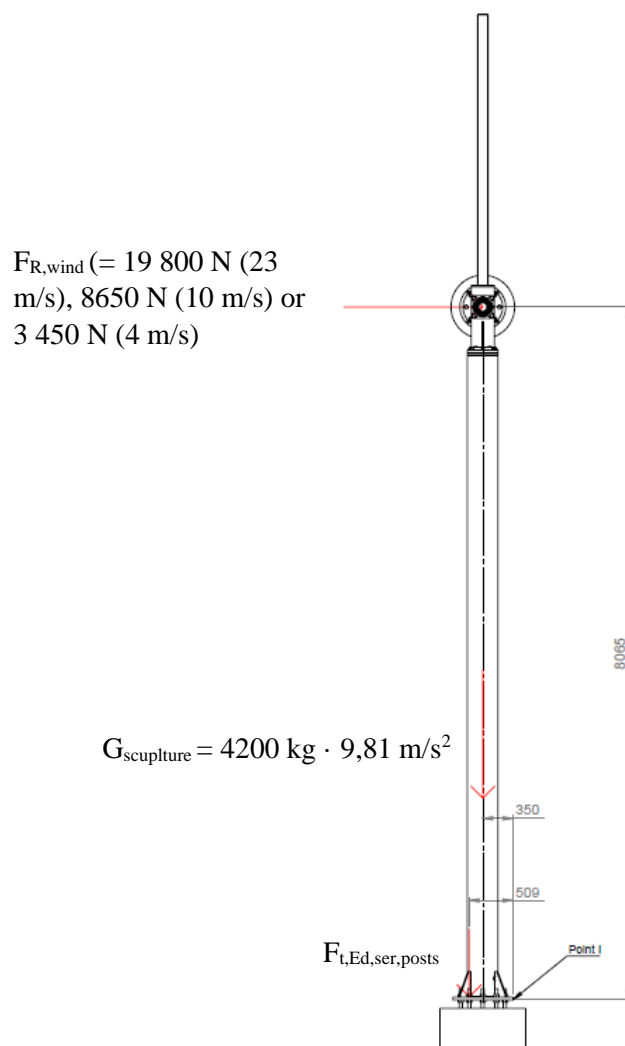
Design tensile and shear forces for shaft carrier's bolts M20 5-8 and M20 9-12 are:

	Tensile force	Shear force
Storm wind 23 m/s	16 350 N	14 295 N
Maximum operating wind 10 m/s	10 395 N	6 250 N
Mean wind velocity in Hämeenlinna 4 m/s, used in fatigue assessment	7 650 N	2 500 N
Snow load in failure mode	13 300 N	-

Design tensile and shear forces for endcap's bolts M20 1-4 and M20 13-16 are:

	Tensile force	Shear force
Storm wind 23 m/s	22 055 N	8778 N
Maximum operating wind 10 m/s	13 050 N	3 840 N
Mean wind velocity in Hämeenlinna 4 m/s, used in fatigue assessment	8 850 N	1 550 N
Snow load in failure mode	13 900 N	-

Tensile force on the foundation bolts (M36 1-10 & M36 11-20):



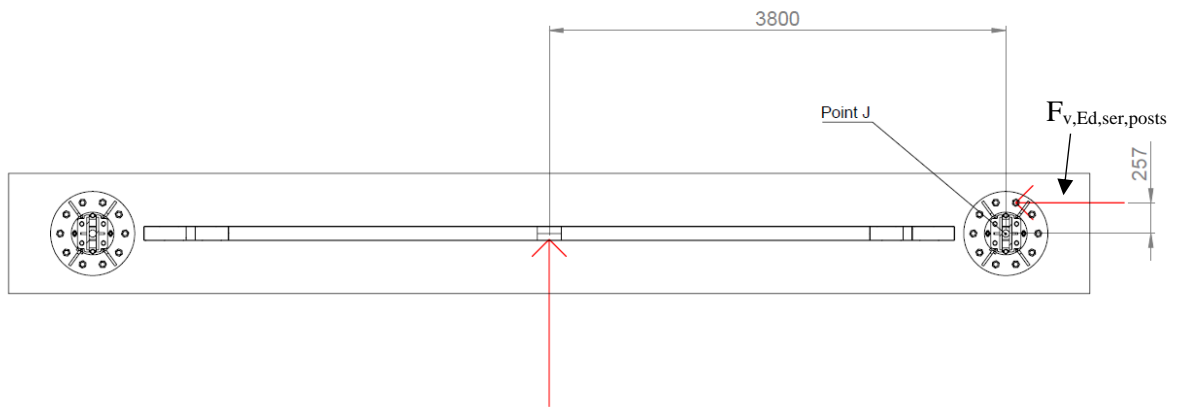
Based on the equilibrium of bending moments in respect of point I:

$$F_{t,Ed,ser,posts} = \frac{\frac{1}{2} \cdot F_{R,wind} \cdot 8065 \text{ mm} - \frac{1}{2} \cdot G_{sculpture} \cdot 350 \text{ mm}}{509 \text{ mm}} \quad (25)$$

It is assumed that only four bolts (4/10) per post carry the tensile load (on the safe side):

$$F_{t,Ed,ser,posts,per \text{ bolt}} = \frac{F_{t,Ed,ser,posts}}{4} \quad (26)$$

Shear force on the foundation bolts (M36 1-10 & M36 11-20):



$F_{R,wind}$ (= 19 800 N (23 m/s), 8650 N (10 m/s) or 3 450 N (4 m/s))

Based on the equilibrium of bending moments in respect of point J:

$$F_{v,Ed,ser,posts} = \frac{\frac{1}{2} \cdot F_{R,wind} \cdot 3800 \text{ mm}}{257 \text{ mm}} \quad (27)$$

It is assumed that only four bolts (4/10) per post carry the shear load (on the safe side):

$$F_{v,Ed,ser,posts,per \text{ bolt}} = \frac{F_{v,Ed,ser,posts}}{4} \quad (28)$$

Design tensile and shear forces for foundation bolts M36 1-10 and M36 11-20 are:

	Tensile force	Shear force
Storm wind 23 m/s	35 680 N	36 600 N
Maximum operating wind 10 m/s	13 600 N	16 000 N
Mean wind velocity in Hämeenlinna 4 m/s, used in fatigue assessment	3 300 N	6 400 N
Snow load in failure mode	-	-

Appendix 5. Bolt forces determined by FE-analysis (23 m/s storm wind)

Study name: Myrskyluuli 23 ms FINAL		toukokuu 26		2022													
Type	X-Component	Y-Component	Z-Component	Resultant	Connector	Type	X-Component	Y-Component	Z-Component	Resultant	Connector	Type	X-Component	Y-Component	Z-Component	Resultant	Connector
Shear Force (N)	-381,5	0	0	381,5	942,64 Foundation Bolt-1	Shear Force (N)	483,39	0	0	483,39	1712,9 Foundation Bolt-11	Shear Force (N)	1643,2	0	0	1643,2	1712,9 Foundation Bolt-11
Axial Force (N)	0	3538,1	0	3538,1	3538,1 Foundation Bolt-1	Axial Force (N)	0	3692	0	3692	3692 Foundation Bolt-11	Axial Force (N)	0	3692	0	3692	3692 Foundation Bolt-11
Bending moment (N.m)	-2,3871	0	25,933	26,043	26,043 Foundation Bolt-1	Bending moment (N.m)	-10,862	0	-25,826	28,018	28,018 Foundation Bolt-11	Bending moment (N.m)	-25,826	0	-25,826	28,018	28,018 Foundation Bolt-11
Shear Force (N)	-1100,9	0	2183,9	2445,7	2445,7 Foundation Bolt-2	Shear Force (N)	820,29	0	2923,8	3036,7	3036,7 Foundation Bolt-12	Shear Force (N)	2923,8	0	2923,8	3036,7	3036,7 Foundation Bolt-12
Axial Force (N)	0	183,69	0	183,69	183,69 Foundation Bolt-2	Axial Force (N)	0	89,571	0	89,571	89,571 Foundation Bolt-12	Axial Force (N)	0	89,571	0	89,571	89,571 Foundation Bolt-12
Bending moment (N.m)	-28,196	0	-14,029	31,493	31,493 Foundation Bolt-2	Bending moment (N.m)	-37,6	0	10,561	39,055	39,055 Foundation Bolt-12	Bending moment (N.m)	-37,6	0	10,561	39,055	39,055 Foundation Bolt-12
Shear Force (N)	-150,39	0	3081,7	3085,4	3085,4 Foundation Bolt-3	Shear Force (N)	-430,19	0	3469,3	3495,9	3495,9 Foundation Bolt-13	Shear Force (N)	3469,3	0	3469,3	3495,9	3495,9 Foundation Bolt-13
Axial Force (N)	0	439,98	0	439,98	439,98 Foundation Bolt-3	Axial Force (N)	0	435,27	0	435,27	435,27 Foundation Bolt-13	Axial Force (N)	0	435,27	0	435,27	435,27 Foundation Bolt-13
Bending moment (N.m)	-37,505	0	-0,96018	37,518	37,518 Foundation Bolt-3	Bending moment (N.m)	-42,229	0	-6,0895	42,666	42,666 Foundation Bolt-13	Bending moment (N.m)	-42,229	0	-6,0895	42,666	42,666 Foundation Bolt-13
Shear Force (N)	2581,9	0	2289,9	3451	3451 Foundation Bolt-4	Shear Force (N)	-3295,1	0	2170,7	3945,9	3945,9 Foundation Bolt-14	Shear Force (N)	2170,7	0	2170,7	3945,9	3945,9 Foundation Bolt-14
Axial Force (N)	0	455,85	0	455,85	455,85 Foundation Bolt-4	Axial Force (N)	0	468,48	0	468,48	468,48 Foundation Bolt-14	Axial Force (N)	0	468,48	0	468,48	468,48 Foundation Bolt-14
Bending moment (N.m)	-28,073	0	30,958	41,791	41,791 Foundation Bolt-4	Bending moment (N.m)	-26,827	0	-39,424	47,686	47,686 Foundation Bolt-14	Bending moment (N.m)	-39,424	0	-39,424	47,686	47,686 Foundation Bolt-14
Shear Force (N)	2631	0	213,93	2639,6	2639,6 Foundation Bolt-5	Shear Force (N)	-3100,2	0	-408,59	3127	3127 Foundation Bolt-15	Shear Force (N)	-408,59	0	-408,59	3127	3127 Foundation Bolt-15
Axial Force (N)	0	316,51	0	316,51	316,51 Foundation Bolt-5	Axial Force (N)	0	279,78	0	279,78	279,78 Foundation Bolt-15	Axial Force (N)	0	279,78	0	279,78	279,78 Foundation Bolt-15
Bending moment (N.m)	-2,4714	0	32,932	33,025	33,025 Foundation Bolt-5	Bending moment (N.m)	5,264	0	-38,841	39,196	39,196 Foundation Bolt-15	Bending moment (N.m)	5,264	0	-38,841	39,196	39,196 Foundation Bolt-15
Shear Force (N)	478,95	0	-1566,2	1637,8	1637,8 Foundation Bolt-6	Shear Force (N)	-414,7	0	-2376,9	2412,8	2412,8 Foundation Bolt-16	Shear Force (N)	-2376,9	0	-2376,9	2412,8	2412,8 Foundation Bolt-16
Axial Force (N)	0	3926,1	0	3926,1	3926,1 Foundation Bolt-6	Axial Force (N)	0	4140,5	0	4140,5	4140,5 Foundation Bolt-16	Axial Force (N)	0	4140,5	0	4140,5	4140,5 Foundation Bolt-16
Bending moment (N.m)	28,306	0	-28,058	39,856	39,856 Foundation Bolt-6	Bending moment (N.m)	38,016	0	31,216	49,19	49,19 Foundation Bolt-16	Bending moment (N.m)	31,216	0	31,216	49,19	49,19 Foundation Bolt-16
Shear Force (N)	-1147	0	25,525	1147,3	1147,3 Foundation Bolt-7	Shear Force (N)	1575,4	0	-345,26	1612,8	1612,8 Foundation Bolt-17	Shear Force (N)	-345,26	0	-345,26	1612,8	1612,8 Foundation Bolt-17
Axial Force (N)	0	8054,4	0	8054,4	8054,4 Foundation Bolt-7	Axial Force (N)	0	8386,1	0	8386,1	8386,1 Foundation Bolt-17	Axial Force (N)	0	8386,1	0	8386,1	8386,1 Foundation Bolt-17
Bending moment (N.m)	59,988	0	-150,12	161,66	161,66 Foundation Bolt-7	Bending moment (N.m)	59,624	0	157,62	168,52	168,52 Foundation Bolt-17	Bending moment (N.m)	59,624	0	157,62	168,52	168,52 Foundation Bolt-17
Shear Force (N)	-2697,4	0	-234,12	2707,6	2707,6 Foundation Bolt-8	Shear Force (N)	3279,2	0	-408,37	3304,6	3304,6 Foundation Bolt-18	Shear Force (N)	-408,37	0	-408,37	3304,6	3304,6 Foundation Bolt-18
Axial Force (N)	0	8952,4	0	8952,4	8952,4 Foundation Bolt-8	Axial Force (N)	0	9737,8	0	9737,8	9737,8 Foundation Bolt-18	Axial Force (N)	0	9737,8	0	9737,8	9737,8 Foundation Bolt-18
Bending moment (N.m)	-145,24	0	20,67	146,7	146,7 Foundation Bolt-8	Bending moment (N.m)	-154,19	0	-28,181	156,74	156,74 Foundation Bolt-18	Bending moment (N.m)	-154,19	0	-28,181	156,74	156,74 Foundation Bolt-18
Shear Force (N)	154,36	0	615,42	634,48	634,48 Foundation Bolt-9	Shear Force (N)	338,77	0	811,24	879,14	879,14 Foundation Bolt-19	Shear Force (N)	811,24	0	811,24	879,14	879,14 Foundation Bolt-19
Axial Force (N)	0	9108,1	0	9108,1	9108,1 Foundation Bolt-9	Axial Force (N)	0	9568,1	0	9568,1	9568,1 Foundation Bolt-19	Axial Force (N)	0	9568,1	0	9568,1	9568,1 Foundation Bolt-19
Bending moment (N.m)	-158,56	0	-61,52	170,08	170,08 Foundation Bolt-9	Bending moment (N.m)	-165,36	0	59,693	175,8	175,8 Foundation Bolt-19	Bending moment (N.m)	-165,36	0	59,693	175,8	175,8 Foundation Bolt-19
Shear Force (N)	-368,88	0	2187,7	2218,6	2218,6 Foundation Bolt-10	Shear Force (N)	743,1	0	2661,2	2763	2763 Foundation Bolt-20	Shear Force (N)	2661,2	0	2661,2	2763	2763 Foundation Bolt-20
Axial Force (N)	0	7578,3	0	7578,3	7578,3 Foundation Bolt-10	Axial Force (N)	0	7718,8	0	7718,8	7718,8 Foundation Bolt-20	Axial Force (N)	0	7718,8	0	7718,8	7718,8 Foundation Bolt-20
Bending moment (N.m)	26,189	0	122,89	125,65	125,65 Foundation Bolt-10	Bending moment (N.m)	31,426	0	-129,31	133,07	133,07 Foundation Bolt-20	Bending moment (N.m)	-129,31	0	-129,31	133,07	133,07 Foundation Bolt-20

8:50 torstai		toukokuu 26		2022													
Study name:Myrskytuuli 23 ms FINAL																	
Type	X-Component	Y-Component	Z-Component	Resultant	Connector	Type	X-Component	Y-Component	Z-Component	Resultant	Connector	Type	X-Component	Y-Component	Z-Component	Resultant	Connector
Shear Force (N)	-3369,4	0	581,55	3419,2	Counterbore Screw-1	Shear Force (N)	-91,189	-9,75E-10	-1166,4	1170	Counterbore Screw-11	Shear Force (N)	-91,189	-9,75E-10	-1166,4	1170	Counterbore Screw-11
Axial Force (N)	0	-638,1	0	-638,1	Counterbore Screw-1	Axial Force (N)	0	619,76	-5,18E-10	619,76	Counterbore Screw-11	Axial Force (N)	0	619,76	-5,18E-10	619,76	Counterbore Screw-11
Bending moment (N.m)	-14,011	0	-79,899	81,118	Counterbore Screw-1	Bending moment (N.m)	32,04	-2,53E-12	-3,0309	32,183	Counterbore Screw-11	Bending moment (N.m)	32,04	-2,53E-12	-3,0309	32,183	Counterbore Screw-11
Shear Force (N)	226,09	-2,93E-09	-3230,6	3238,5	Counterbore Screw-2	Shear Force (N)	-1466,6	0	624,5	1594	Counterbore Screw-12	Shear Force (N)	-1466,6	0	624,5	1594	Counterbore Screw-12
Axial Force (N)	0	632,26	-5,73E-10	632,26	Counterbore Screw-2	Axial Force (N)	0	616,49	0	616,49	Counterbore Screw-12	Axial Force (N)	0	616,49	0	616,49	Counterbore Screw-12
Bending moment (N.m)	83,696	6,37E-12	7,0301	83,991	Counterbore Screw-2	Bending moment (N.m)	-16,59	0	-35,825	39,48	Counterbore Screw-12	Bending moment (N.m)	-16,59	0	-35,825	39,48	Counterbore Screw-12
Shear Force (N)	89,076	3,27E-09	3903,1	3904,1	Counterbore Screw-3	Shear Force (N)	4507,3	0	7932,5	9123,6	Counterbore Screw-13	Shear Force (N)	4507,3	0	7932,5	9123,6	Counterbore Screw-13
Axial Force (N)	0	762,35	-6,38E-10	762,35	Counterbore Screw-3	Axial Force (N)	0	622,86	0	622,86	Counterbore Screw-13	Axial Force (N)	0	622,86	0	622,86	Counterbore Screw-13
Bending moment (N.m)	-90,867	1,47E-12	1,762	90,884	Counterbore Screw-3	Bending moment (N.m)	-167,17	0	94,255	191,91	Counterbore Screw-13	Bending moment (N.m)	-167,17	0	94,255	191,91	Counterbore Screw-13
Shear Force (N)	3477,1	0	749,53	3557	Counterbore Screw-4	Shear Force (N)	-4823,1	0	7560,5	8967,9	Counterbore Screw-14	Shear Force (N)	-4823,1	0	7560,5	8967,9	Counterbore Screw-14
Axial Force (N)	0	623,48	0	623,48	Counterbore Screw-4	Axial Force (N)	0	609,78	0	609,78	Counterbore Screw-14	Axial Force (N)	0	609,78	0	609,78	Counterbore Screw-14
Bending moment (N.m)	-20,16	0	79,539	82,054	Counterbore Screw-4	Bending moment (N.m)	-158,23	0	-91,734	182,9	Counterbore Screw-14	Bending moment (N.m)	-158,23	0	-91,734	182,9	Counterbore Screw-14
Shear Force (N)	-7727	0	-5491,8	9479,7	Counterbore Screw-5	Shear Force (N)	5080	0	-2800,3	5800,7	Counterbore Screw-15	Shear Force (N)	5080	0	-2800,3	5800,7	Counterbore Screw-15
Axial Force (N)	0	590,29	0	590,29	Counterbore Screw-5	Axial Force (N)	0	587,76	0	587,76	Counterbore Screw-15	Axial Force (N)	0	587,76	0	587,76	Counterbore Screw-15
Bending moment (N.m)	122,03	0	-165,97	206	Counterbore Screw-5	Bending moment (N.m)	62,334	0	109,25	125,78	Counterbore Screw-15	Bending moment (N.m)	62,334	0	109,25	125,78	Counterbore Screw-15
Shear Force (N)	-6867,8	0	10825	12819	Counterbore Screw-6	Shear Force (N)	-4764,2	0	-3032,8	5647,6	Counterbore Screw-16	Shear Force (N)	-4764,2	0	-3032,8	5647,6	Counterbore Screw-16
Axial Force (N)	0	270,05	0	270,05	Counterbore Screw-6	Axial Force (N)	0	590,65	0	590,65	Counterbore Screw-16	Axial Force (N)	0	590,65	0	590,65	Counterbore Screw-16
Bending moment (N.m)	-229,73	0	-145,37	271,86	Counterbore Screw-6	Bending moment (N.m)	65,999	0	-112,13	130,11	Counterbore Screw-16	Bending moment (N.m)	65,999	0	-112,13	130,11	Counterbore Screw-16
Shear Force (N)	7374,9	0	-5813,2	9390,6	Counterbore Screw-7	Shear Force (N)	612,14	0	-208,86	417,85	Counterbore with Nut-1	Shear Force (N)	612,14	0	-208,86	417,85	Counterbore with Nut-1
Axial Force (N)	0	567,99	0	567,99	Counterbore Screw-7	Axial Force (N)	0	361,91	0	361,91	Counterbore with Nut-1	Axial Force (N)	0	361,91	0	361,91	Counterbore with Nut-1
Bending moment (N.m)	125,79	0	167,69	209,62	Counterbore Screw-7	Bending moment (N.m)	0	-6,2855	-11,021	12,688	Counterbore with Nut-1	Bending moment (N.m)	0	-6,2855	-11,021	12,688	Counterbore with Nut-1
Shear Force (N)	7219,9	0	10621	12842	Counterbore Screw-8	Shear Force (N)	0	216,74	-141,71	258,95	Counterbore with Nut-2	Shear Force (N)	0	216,74	-141,71	258,95	Counterbore with Nut-2
Axial Force (N)	0	609,34	0	609,34	Counterbore Screw-8	Axial Force (N)	605,87	0	0	605,87	Counterbore with Nut-2	Axial Force (N)	605,87	0	0	605,87	Counterbore with Nut-2
Bending moment (N.m)	-223,27	0	145,01	266,23	Counterbore Screw-8	Bending moment (N.m)	0	-4,3397	-6,4272	7,7551	Counterbore with Nut-2	Bending moment (N.m)	0	-4,3397	-6,4272	7,7551	Counterbore with Nut-2
Shear Force (N)	1498,9	0	519,01	1586,2	Counterbore Screw-9	Shear Force (N)	657,39	0	-197,74	391,11	Counterbore with Nut-3	Shear Force (N)	657,39	0	-197,74	391,11	Counterbore with Nut-3
Axial Force (N)	0	-487,61	0	-487,61	Counterbore Screw-9	Axial Force (N)	657,39	0	0	657,39	Counterbore with Nut-3	Axial Force (N)	657,39	0	0	657,39	Counterbore with Nut-3
Bending moment (N.m)	-12,897	0	36,252	38,477	Counterbore Screw-9	Bending moment (N.m)	0	-9,3392	-9,1594	13,081	Counterbore with Nut-3	Bending moment (N.m)	0	-9,3392	-9,1594	13,081	Counterbore with Nut-3
Shear Force (N)	3,4891	1,54E-09	1703,2	1703,2	Counterbore Screw-10	Shear Force (N)	0	383,99	-175,66	422,27	Counterbore with Nut-4	Shear Force (N)	0	383,99	-175,66	422,27	Counterbore with Nut-4
Axial Force (N)	0	696,86	-6,32E-10	696,86	Counterbore Screw-10	Axial Force (N)	612,78	0	0	612,78	Counterbore with Nut-4	Axial Force (N)	612,78	0	0	612,78	Counterbore with Nut-4
Bending moment (N.m)	-37,104	8,58E-13	0,94589	37,116	Counterbore Screw-10	Bending moment (N.m)	0	-5,3053	-11,47	12,637	Counterbore with Nut-4	Bending moment (N.m)	0	-5,3053	-11,47	12,637	Counterbore with Nut-4

8:50 torstai		toukokuu 26		2022							
Study name:Myrskytuuli 23 ms FINAL											
Type	X-Component	Y-Component	Z-Component	Resultant	Connector	Type	X-Component	Y-Component	Z-Component	Resultant	Connector
Shear Force (N)	0	217,75	-121,34	249,27	Counterbore with Nut-5	Shear Force (N)	22,063	110,96	0	113,13	Counterbore with Nut-15
Axial Force (N)	608,55	0	0	608,55	Counterbore with Nut-5	Axial Force (N)	0	0	-776,76	776,76	Counterbore with Nut-15
Bending moment (N.m)	0	-3,554	-6,5073	7,4146	Counterbore with Nut-5	Bending moment (N.m)	-2,8974	0,53547	0	2,9465	Counterbore with Nut-15
Shear Force (N)	0	323,54	-168,9	364,97	Counterbore with Nut-6	Shear Force (N)	-37,226	112,17	0	118,19	Counterbore with Nut-16
Axial Force (N)	684,52	0	0	684,52	Counterbore with Nut-6	Axial Force (N)	0	0	-779,98	779,98	Counterbore with Nut-16
Bending moment (N.m)	0	-2,4279	-9,3925	9,7012	Counterbore with Nut-6	Bending moment (N.m)	-2,9346	-0,94393	0	3,0827	Counterbore with Nut-16
Shear Force (N)	0	189,91	-36,026	193,29	Counterbore with Nut-7	Shear Force (N)	-119,05	-358,7	0	377,94	Counterbore with Nut-17
Axial Force (N)	-612,09	0	0	612,09	Counterbore with Nut-7	Axial Force (N)	0	0	-775,66	775,66	Counterbore with Nut-17
Bending moment (N.m)	0	0,74692	5,4348	5,4859	Counterbore with Nut-7	Bending moment (N.m)	9,3292	-3,1142	0	9,8352	Counterbore with Nut-17
Shear Force (N)	0	199,26	10,09	199,52	Counterbore with Nut-8	Shear Force (N)	100,52	-356,81	0	370,7	Counterbore with Nut-18
Axial Force (N)	-620,37	0	0	620,37	Counterbore with Nut-8	Axial Force (N)	0	0	-774,33	774,33	Counterbore with Nut-18
Bending moment (N.m)	0	-1,0491	5,846	5,9394	Counterbore with Nut-8	Bending moment (N.m)	9,2647	2,6029	0	9,6234	Counterbore with Nut-18
Shear Force (N)	0	457,19	-44,404	459,34	Counterbore with Nut-9	Shear Force (N)	-102,1	-571,83	0	580,87	Counterbore with Nut-19
Axial Force (N)	-637,69	0	0	637,69	Counterbore with Nut-9	Axial Force (N)	0	0	-784,75	784,75	Counterbore with Nut-19
Bending moment (N.m)	0	-2,5557	13,624	13,861	Counterbore with Nut-9	Bending moment (N.m)	14,935	-2,6186	0	15,163	Counterbore with Nut-19
Shear Force (N)	0	494,63	-65,529	498,95	Counterbore with Nut-10	Shear Force (N)	94,761	-571,94	0	579,73	Counterbore with Nut-20
Axial Force (N)	-612,35	0	0	612,35	Counterbore with Nut-10	Axial Force (N)	0	0	-785,16	785,16	Counterbore with Nut-20
Bending moment (N.m)	0	1,8222	14,735	14,848	Counterbore with Nut-10	Bending moment (N.m)	14,989	2,3495	0	15,172	Counterbore with Nut-20
Shear Force (N)	0	207,09	-7,5158	207,23	Counterbore with Nut-11	Shear Force (N)	39,566	-101,09	0	108,56	Counterbore with Nut-21
Axial Force (N)	-611,31	0	0	611,31	Counterbore with Nut-11	Axial Force (N)	0	0	-782,33	782,33	Counterbore with Nut-21
Bending moment (N.m)	0	0,18402	6,2934	6,2961	Counterbore with Nut-11	Bending moment (N.m)	2,7005	1,0849	0	2,9103	Counterbore with Nut-21
Shear Force (N)	0	157,26	-68,143	171,39	Counterbore with Nut-12	Shear Force (N)	-53,356	-103,03	0	116,03	Counterbore with Nut-22
Axial Force (N)	-725,3	0	0	725,3	Counterbore with Nut-12	Axial Force (N)	0	0	-779,84	779,84	Counterbore with Nut-22
Bending moment (N.m)	0	3,7271	3,9192	5,4085	Counterbore with Nut-12	Bending moment (N.m)	2,8208	-1,5299	0	3,209	Counterbore with Nut-22
Shear Force (N)	-104,3	573,67	0	583,07	Counterbore with Nut-13	Shear Force (N)	-120,27	350,74	0	370,78	Counterbore with Nut-23
Axial Force (N)	0	0	-777,76	777,76	Counterbore with Nut-13	Axial Force (N)	0	0	-781,68	781,68	Counterbore with Nut-23
Bending moment (N.m)	-14,916	-2,7436	0	15,166	Counterbore with Nut-13	Bending moment (N.m)	-9,0751	-3,109	0	9,5929	Counterbore with Nut-23
Shear Force (N)	97,127	575,24	0	583,38	Counterbore with Nut-14	Shear Force (N)	101,22	347,88	0	362,3	Counterbore with Nut-24
Axial Force (N)	0	0	-776,78	776,78	Counterbore with Nut-14	Axial Force (N)	0	0	-782,74	782,74	Counterbore with Nut-24
Bending moment (N.m)	-14,962	2,5336	0	15,175	Counterbore with Nut-14	Bending moment (N.m)	-8,9748	2,5717	0	9,336	Counterbore with Nut-24

Appendix 6. Fatigue assessment for the most critical welded joints

Pilarin juuri:															
	Pilarin vaikutus Pyyntöalumin kuorma (N)	Jännitys 0,4t etäisyydellä alemmalla rajaviivalla:	Jännitys 1,0t etäisyydellä alemmalla rajaviivalla:	Jännitys 0,4t etäisyydellä ylemmällä rajaviivalla:	Jännitys 1,0t etäisyydellä ylemmällä rajaviivalla:	Jännitys 1,0t aiheuttama Hot Spot - jännitys alemmalla rajaviivalla (MPa):	Jännitys 1,0t aiheuttama Hot Spot - jännitys ylemmällä rajaviivalla (MPa):	Pyöretalmin aiheuttama Hot Spot - jännitys alemmalla rajaviivalla (MPa):	Pyöretalmin aiheuttama Hot Spot - jännitys ylemmällä rajaviivalla (MPa):	FAT-luokka	Alemmän rajatilan kestoaika:	Ylemmän rajatilan kestoaika:	Pyöretalmin sytien lukumäärä:	Kesto alempi rajaviiva:	Kesto ylempi rajaviiva:
Femillä laskettu kuorma, josta interpoloitu muut jännitykset															
	204,7	0,4	1,7	3,3	2,6	1,3	3,8	0,4	0,8	90	224 033 487 296	27 231 973 240	210 023 559	124 363	15 116
	291,7	0,5	0,8	1,0	0,8	0,6	1,1	0,6	1,1	90	849 571 410 642	102 049 502 791	243 084 796	34 301	4 246
	387,7	0,6	1,0	1,3	1,0	0,8	1,3	0,8	1,3	90	1 252 738 605 351	152 762 830 108	383 989 723	6 595	1 791
	520,3	1,0	1,7	2,3	1,5	1,1	2,1	1,1	2,1	90	1 944 936 100	2 397 837 233	815 453	24 091	2 328
	1028,1	4,1	3,8	7,4	5,3	4,2	8,5	4,2	8,5	90	215 645 613	26 211 659	1	215 645 613	26 211 659
	10715,1	19,3	17,2	33,4	26,3	18,9	36,2	18,9	36,2	90	92 110 876	22 139 556	0	92 110 876	22 139 556
	12893,9	23,2	21,3	42,6	33,5	24,1	46,8	24,1	46,8	90	194 397 952	12 695 885	0	194 397 952	12 695 885
	14786,3	26,6	24,4	48,7	38,4	27,6	53,6	27,6	53,6	90	354 871 174	8 471 174	0	354 871 174	8 471 174
	23224,3	41,8	39,5	76,6	60,4	43,4	87,5	43,4	87,5	90	17 695 318	2 173 953	0	17 695 318	2 173 953
	34336,2	61,3	58,5	113,5	89,4	64,2	123,6	64,2	123,6	90	5 505 454	869 187	0	5 505 454	869 187
Hämisenännen keskimääräisen tuulenopeuden 15 m/s ilmatieteenlaitos, tuuliautas, aiheuttama Hot Spot -jännitys koko elinkaaren aikana:															
Jännitys 0,4t etäisyydellä alemmalla rajaviivalla:	7,472	Jännitys 0,4t etäisyydellä ylemmällä rajaviivalla:	11,904	Jännitys 1,0t etäisyydellä alemmalla rajaviivalla:	16,22776	Jännitys 1,0t etäisyydellä ylemmällä rajaviivalla:	25,009461	Hot Spot - käyttöä alemmalla rajaviivalla:	341555,318	Hot Spot -käyttöä ylemmällä rajaviivalla:	11579,625	Käyttötuulen vaikutuksen sytlien lukumäärä (2 x kok. kierrokset):	242,67	Kesto alempi rajaviiva:	23,50
Akselin kannakkeen alaosa (ylempi rajaviiva kriittinen):															
Femillä laskettu kuorma, josta interpoloitu muut jännitykset															
	204,7	0,0000	0,0000	1,06	0,47	0,0000	7,1830	0,0000	1,5	90	468 403 762 311	4 000 511 964	210 023 559	124 363	2 221
	291,7	0,0000	0,0000	1,42	1,07	0,0000	3,3	0,0000	3,3	90	849 571 410 642	98 762 830 108	224 162 233	34 301	4 246
	387,7	0,0000	0,0000	2,33	1,29	0,0000	4,0	0,0000	4,0	90	1 252 738 605 351	22 441 573 852	383 989 723	6 595	1 791
	520,3	0,0000	0,0000	3,8	2,29	0,0000	5,3	0,0000	5,3	90	1 944 936 100	350 785 195	815 453	24 091	2 328
	1028,1	0,0000	0,0000	11,70	5,18	0,0000	16,1	0,0000	16,1	90	215 645 613	350 785 195	1	215 645 613	26 211 659
	10715,1	0,0000	0,0000	55,72	24,84	0,0000	72,3	0,0000	72,3	90	92 110 876	3 850 629	0	92 110 876	22 139 556
	12893,9	0,0000	0,0000	70,52	31,19	0,0000	86,9	0,0000	86,9	90	194 397 952	3 251 629	0	194 397 952	12 695 885
	14786,3	0,0000	0,0000	79,52	33,94	0,0000	95,9	0,0000	95,9	90	354 871 174	1 894 022	0	354 871 174	8 471 174
	23224,3	0,0000	0,0000	120,77	53,42	0,0000	165,3	0,0000	165,3	90	17 695 318	1 244 458	0	17 695 318	2 173 953
	34336,2	0,0000	0,0000	176,86	79,11	0,0000	245,7	0,0000	245,7	90	5 505 454	98 307	0	5 505 454	869 187
Hämisenännen keskimääräisen tuulenopeuden 15 m/s ilmatieteenlaitos, tuuliautas, aiheuttama Hot Spot -jännitys koko elinkaaren aikana:															
Jännitys 0,4t etäisyydellä alemmalla rajaviivalla:	0	Jännitys 0,4t etäisyydellä ylemmällä rajaviivalla:	3,8952	Jännitys 1,0t etäisyydellä alemmalla rajaviivalla:	30,743472	Jännitys 1,0t etäisyydellä ylemmällä rajaviivalla:	45,716318	Hot Spot - käyttöä alemmalla rajaviivalla:	50 176,318	Hot Spot -käyttöä ylemmällä rajaviivalla:	11579,625	Käyttötuulen vaikutuksen sytlien lukumäärä (2 x kok. kierrokset):	4,33	Kesto alempi rajaviiva:	4,33

Akselin laippa:												
Pilatin vaikuttava pyörretalimien kuorma (N)	Jännitys 0,4t etäisyydellä alemmalta rajaviivalta:	Jännitys 1,0t etäisyydellä alemmalta rajaviivalta:	Jännitys 0,4t etäisyydellä ylempältä rajaviivalta:	Jännitys 1,0t etäisyydellä ylempältä rajaviivalta:	Pyörretalimien aiheuttama Hot Spot - jännitys ylempällä rajaviivalta (MP-a):	Pyörretalimien aiheuttama Hot Spot - jännitys alemmalla rajaviivalta (MP-a):	FAT-luokka	Alemman rajaviivan kesto:	Ylemmän rajaviivan kesto:	Pyörretalimien syklien lukumäärä:	Kesto ylempi rajaviiva:	Kesto alempi rajaviiva:
1000	0,700	0,400	2,400	2,800	0,901	0,901	90	1 959 348 120 759	150 451 239 459		256 586 057 859	22 316 306 635
3,8	0,003	0,002	0,003	0,011	0,008	0,008	90	36 327 236 452 145 2 100 000	2 747 853 050 600 000 000	12 262 469	84 756 632	4 000 000 000
8,6	0,006	0,004	0,021	0,024	0,008	0,016	90	3 133 319 216 853 570 000	234 572 808 712 740 000	232 340 327	10 701 802 064	807 736 452
10,4	0,007	0,004	0,025	0,029	0,009	0,022	90	1 772 079 220 396 230 000	133 750 651 653 807 000	340 81 880	5 209 051 024	333 962 617
11,4	0,007	0,004	0,029	0,033	0,009	0,022	90	28 091 965 593 933 000	2 120 289 216 469 680	253 109 246	106 417 457	8 182 369
188,2	0,130	0,074	0,447	0,521	0,168	0,387	90	308 776 475 366 469	23 305 417 738 737	42 427	7 277 828 161	549 306 286
197	0,130	0,074	0,447	0,552	0,177	0,420	90	260 726 078 473 733	19 678 738 038 532	20 380	12 733 232 506	965 500 679
237,2	0,166	0,095	0,559	0,664	0,214	0,506	90	149 361 646 054 815	11 273 320 881 369	1 284	116 325 271 071	8 779 844 323
243,4	0,175	0,100	0,599	0,725	0,225	0,532	90	128 497 241 203 238	9 696 544 783 005	551	233 207 334 318	17 801 774 670
271,4	0,190	0,109	0,651	0,780	0,245	0,579	90	99 713 422 067 161	7 526 037 759 907	118	845 029 000 569	63 779 391 074
427	0,239	0,171	0,827	1,196	0,385	0,930	90	25 603 511 113 320	1 532 467 940 374	1	25 603 511 113 320	139 247 940 374
632,4	0,443	0,253	1,516	1,771	0,570	1,348	90	7 881 476 178 706	534 867 632 612	0	#JAKO0!	#JAKO0!

Hämeenlinnan keskimääräisen tuulennopeuden 15 m/s Ilmatieteenlaitos, tuuliatlas) aiheuttama Hot Spot - jännitys koko elinkaaren aikana:												
Jännitys 0,4t etäisyydellä alemmalta rajaviivalta:	Jännitys 1,0t etäisyydellä ylempältä rajaviivalta:	Jännitys 0,4t etäisyydellä ylempältä rajaviivalta:	5 m/s tuulen aiheuttama Hot Spot - jännitys ylempällä rajaviivalta (MP-a):	5 m/s tuulen aiheuttama Hot Spot - jännitys alemmalla rajaviivalta (MP-a):	FAT-luokka	Hot Spot - käyttöikä alemmalla rajaviivalta:	Hot Spot - käyttöikä ylempällä rajaviivalta:	Käyttötuulen vaikutuksen syklien lukumäärä (2 x kok. kierrokset):	Kesto ylempi rajaviiva:	Kesto alempi rajaviiva:		
3,0128	1,7216	10,3236	3,877904	9,176128	90	25 001 517 127	1887 031 435	11579 625	2 159,10	162,96		

Kehän laippa (alempi rajaviiva kritittinen):												
Pilatin vaikuttava pyörretalimien kuorma (N)	Jännitys 0,4t etäisyydellä alemmalta rajaviivalta:	Jännitys 1,0t etäisyydellä alemmalta rajaviivalta:	Jännitys 0,4t etäisyydellä ylempältä rajaviivalta:	Jännitys 1,0t etäisyydellä ylempältä rajaviivalta:	Pyörretalimien aiheuttama Hot Spot - jännitys ylempällä rajaviivalta (MP-a):	Pyörretalimien aiheuttama Hot Spot - jännitys alemmalla rajaviivalta (MP-a):	FAT-luokka	Alemman rajaviivan kesto:	Ylemmän rajaviivan kesto:	Pyörretalimien syklien lukumäärä:	Kesto ylempi rajaviiva:	Kesto alempi rajaviiva:
1000	0,6000	0,4000	0,0000	0,0000	0,7940	0,0000	90	3 686 967 795 808	#JAKO0!	122 852 483	546 933 676 764	#JAKO0!
3,8	0,0023	0,0015	0,0000	0,0000	0,0028	0,0000	90	67 192 152 593 163 400 000	#JAKO0!	189 317 101	63 286 648 632	#JAKO0!
5,8	0,0039	0,0022	0,0000	0,0000	0,0050	0,0000	90	11 861 055 571 804 400 000	#JAKO0!	232 640 327	10 701 802 064	#JAKO0!
8,6	0,0060	0,0034	0,0000	0,0000	0,0077	0,0000	90	3 133 319 216 853 570 000	#JAKO0!	340 191 680	5 209 051 024	#JAKO0!
10,4	0,0073	0,0042	0,0000	0,0000	0,0094	0,0000	90	1 772 079 220 396 230 000	#JAKO0!	253 109 246	7 277 828 161	#JAKO0!
188,2	0,1303	0,0745	0,4470	0,5200	0,1678	0,3870	90	308 776 475 366 469	#JAKO0!	42 427	12 733 232 506	#JAKO0!
197	0,1329	0,0768	0,4470	0,5200	0,1725	0,4200	90	260 726 078 473 733	#JAKO0!	20 380	116 325 271 071	#JAKO0!
237,2	0,1660	0,0949	0,5590	0,6640	0,2137	0,5060	90	149 361 646 054 815	#JAKO0!	1 284	233 207 334 318	#JAKO0!
243,4	0,1746	0,1066	0,5990	0,7240	0,2247	0,5320	90	128 497 241 203 238	#JAKO0!	551	845 029 000 569	#JAKO0!
271,4	0,1900	0,1086	0,6510	0,7800	0,2445	0,5790	90	99 713 422 067 161	#JAKO0!	118	25 603 511 113 320	#JAKO0!
427	0,2389	0,1708	0,8270	1,1960	0,3847	0,9300	90	25 603 511 113 320	#JAKO0!	0	#JAKO0!	#JAKO0!
632,4	0,4427	0,2530	1,5160	1,7710	0,5938	1,3480	90	7 881 476 178 706	#JAKO0!	0	#JAKO0!	#JAKO0!

Hämeenlinnan keskimääräisen tuulennopeuden 15 m/s Ilmatieteenlaitos, tuuliatlas) aiheuttama Hot Spot - jännitys koko elinkaaren aikana:												
Jännitys 0,4t etäisyydellä alemmalta rajaviivalta:	Jännitys 1,0t etäisyydellä ylempältä rajaviivalta:	Jännitys 0,4t etäisyydellä ylempältä rajaviivalta:	5 m/s tuulen aiheuttama Hot Spot - jännitys ylempällä rajaviivalta (MP-a):	5 m/s tuulen aiheuttama Hot Spot - jännitys alemmalla rajaviivalta (MP-a):	FAT-luokka	Hot Spot - käyttöikä alemmalla rajaviivalta:	Hot Spot - käyttöikä ylempällä rajaviivalta:	Käyttötuulen vaikutuksen syklien lukumäärä (2 x kok. kierrokset):	Kesto ylempi rajaviiva:	Kesto alempi rajaviiva:		
2,5824	1,7216	0	3,159196	0	90	46 243 657 394	#JAKO0!	11579 625	3 999,54	#JAKO0!		

Appendix 7. Shear fatigue of bolts

Shear fatigue of bolts according to SFS-EN 1993 - 1 - 9 :

The maximum shear force for M24:

$$F_{v,Ed,ser,M24,max} := 23260 \text{ N}$$

The maximum shear force for M20:

$$F_{v,Ed,ser,M20,max} := 14300 \text{ N}$$

The maximum shear force for M36:

$$F_{v,Ed,ser,M36,max} := 36600 \text{ N}$$

Nominal stress areas:

$$A_{s,M24} := 353 \text{ mm}^2$$

$$A_{s,M20} := 245 \text{ mm}^2$$

$$A_{s,M36} := 817 \text{ mm}^2$$

$$\tau_{max,M24} := \frac{F_{v,Ed,ser,M24,max}}{A_{s,M24}} = 65,8924 \text{ MPa}$$

$$\tau_{max,M20} := \frac{F_{v,Ed,ser,M20,max}}{A_{s,M20}} = 58,3673 \text{ MPa}$$

$$\tau_{max,M36} := \frac{F_{v,Ed,ser,M36,max}}{A_{s,M36}} = 44,798 \text{ MPa}$$

Total cycles (15 years and 12,5 h per day with 1,41 rpm):

$$N_{total} := 15 \cdot 365 \cdot 12,5 \cdot 60 \cdot 1,41 \cdot 2 = 1,158 \cdot 10^7$$

$$m := 5$$

$$\Delta\tau_c := 100 \text{ MPa}$$

$$\Delta\tau_R := \sqrt[m]{\frac{\Delta\tau_c^m \cdot (2 \cdot 10^6)}{N_{total}}} = 70,3829 \text{ MPa}$$

Cut off limit:

$$\Delta\tau_z := 0,457 \cdot \Delta\tau_c = 45,7 \text{ MPa}$$

Appendix 8. Design forces and resistances of welds

Design forces and resistances for welds according to SFS-EN 1993 - 1 - 8:

Resultant force (from bolt forces):

$$F_w := 116450 \text{ N} + 46520 \text{ N}$$

Length of the weld:

$$l_{\text{weld}} := 1380 \text{ mm}$$

Design force per unit length:

$$F_{w,Ed} := \frac{F_w}{l_{\text{weld}}} = 118,0942 \frac{\text{N}}{\text{mm}}$$

Ultimate strength of the weakest material:

$$f_u := 470 \text{ MPa}$$

Correlation factor:

$$\beta_w := 0,9$$

Partial safety factor:

$$\gamma_{M2} := 1,25$$

Throat thickness:

$$a := 4 \text{ mm}$$

Design resistance:

$$f_{vw,d} := \frac{f_u}{\beta_w \cdot \gamma_{M2}} = 241,2041 \text{ MPa}$$

Design resistance per unit length:

$$F_{w,Rd} := f_{vw,d} \cdot a = 964,8164 \frac{\text{N}}{\text{mm}}$$

Usage:

$$\frac{F_{w,Ed}}{F_{w,Rd}} = 0,1224$$